UC Riverside

UC Riverside Electronic Theses and Dissertations

Title

Secrecy Enhancement with Full-Duplex Radio in Wireless Networks

Permalink

https://escholarship.org/uc/item/65r107w6

Author

Zabir, Ishmam

Publication Date

2022

Peer reviewed|Thesis/dissertation

eScholarship.org Powered by the California Digital Library
University of California

UNIVERSITY OF CALIFORNIA
RIVERSIDE

Secrecy Enhancement with Full-Duplex Radio in Wireless Networks

A Dissertation submitted in partial satisfaction
of the requirements for the degree of

Doctor of Philosophy

in

Electrical Engineering

by

Ishmam Zabir

March 2022

Dissertation Committee:

Dr. Yingbo Hua, Chairperson
Dr. Ilya Dumer
Dr. Jiasi Chen

Copyright by
Ishmam Zabir
2022

The Dissertation of Ishmam Zabir is approved:

Committee Chairperson

University of California, Riverside

Acknowledgments

I am grateful to my advisor Dr. Yingbo Hua, who is always being patient to me, teaches me with his erudite knowledge and affects me with his rigorous personality. Without his guidance, I would not have been here.

I would like to thank Dr. Ilya Dumer, Dr. Jiasi Chen for their generous help as being committee members for my dissertation evaluation and defense. The text of this dissertation, in part, is a reprint of the material as it appears in 2019 IEEE Globecom, 2020 IEEE Transaction of information forensic and security. The co-author Dr. Yingbo Hua listed in that publication directed and supervised the research which forms the basis for this dissertation. Also, i would like to thank my other collaborators Dr. Ananthram Swami, Dr. Brian M. Sadler, Dr. Gaojie Chen and Dr. Eric Graves.

To my parents and wife for all the support.

ABSTRACT OF THE DISSERTATION

Secrecy Enhancement with Full-Duplex Radio in Wireless Networks

by

Ishmam Zabir

Doctor of Philosophy, Graduate Program in Electrical Engineering
University of California, Riverside, March 2022
Dr. Yingbo Hua, Chairperson

Physical layer security (PLS) is an approach that provides secrecy based on information-theoretic model which does not account for any computation capability assumption or pre-installed standardized secret key generation algorithm and it is a good additional protection on the top of the existing security scheme. This work includes two different topics for improving PLS with full-duplex radio. In the first topic, we study the secrecy performance of several schemes for multi-antenna transmission to single-antenna users with full-duplex (FD) capability against randomly distributed single-antenna eavesdroppers (EDs). These schemes and related scenarios include transmit antenna selection (TAS), transmit antenna beamforming (TAB), artificial noise (AN) from the transmitter, user selection based their distances to the transmitter, and colluding and non-colluding EDs. The locations of randomly distributed EDs and users are assumed to be distributed as Poisson Point Process (PPP). We derive closed form expressions for the secrecy outage probabilities (SOP) of all these schemes and scenarios. The derived expressions are useful to reveal the impacts of various environmental parameters and user's choices on the SOP, and hence useful for

network design purposes. Furthermore, we have investigated the secrecy performance of the scheme where multiple legitimate users are randomly located. Examples of such numerical results are discussed.

For the second topic, we present a secure downlink communication system where a transmitter sends information to multiple single antenna users under ultra reliable and low-latency communication (uRLLC) system requirement. To meet uRLLC requirement and provide secrecy against multi-antenna eavesdropper (Eve), transmitter adopts a special channel training scheme called anti-eavesdropping channel estimation (ANECE) as well as a standard transmit beamforming to send secret information in short blocklength regime. Using ANECE, two or more cooperative full-duplex radio devices obtain their receive channel state information (CSI) with respect to each other while preventing Eve from obtaining any consistent estimate of its receive CSI, which improves the secrecy of subsequent transmission of information between the devices. We derive the closed form expression of average secrecy throughput (AST) of ANECE assisted transmission. Our closed form expression of approximated AST in terms of blocklength and various controllable parameters provides useful insights to maximize AST under uRLLC requirement. In another chapter, we investigate the uplink communication system where multiple single antenna users send secret information to multi-antenna access point (AP) under ultra reliable and low-latency communication (uRLLC) system requirement. Finally, numerical results are discussed.

Contents

List of Figures

Chapter 1

Introduction

1.1 Physical layer security

1.1.1 Motivations

Since Wyner's work [1], physical layer security has been studied as an alternative or complementary approach to cryptography for information security. This trend of study has accelerated in recent years given its importance for 5G and future wireless networks [2].

Due to the broadcast nature of wireless communications, transmitted information in air is highly vulnerable to eavesdropping unless a positive secrecy rate at the physical layer is achieved. Many prior works for achieving a positive secrecy rate require that the locations and/or channel-state-information (CSI) of eavesdroppers (EDs or Eve) are known to the legitimate users (also referred to as users) [3]-[12]. This requirement is generally difficult to meet in practice.

One way to handle EDs whose locations and CSI are unknown to users is to assume

a statistical model for EDs' CSI where both the small-scale-fading and large-scale-fading of EDs' CSI are statistically modelled. While the small-scale-fading is commonly modelled as Gaussian distributed, the large-scale-fading can be treated by assuming EDs to be randomly distributed according to a Poisson Point Process (PPP) [13]-[24]. This paper will also adopt the PPP model to investigate the impact of random EDs locations on secrecy performance which is useful over a time window within which the EDs' locations change randomly.

We present statistical analyses of SOP for a range of downlink transmission schemes for pairs of multi-antenna base-station (BS) and single-antenna user equipment (UE) in the presence of randomly located EDs, which is illustrated in Fig. 1.3. These schemes include the following scenarios: the BS may or may not apply Tx-AN, the UE may or may not apply Rx-AN or equivalently operate in either FD or HD mode, and the EDs may or may not collude with each other to form a virtual antenna array. For randomly distributed UEs, the BS can have them ordered according to their distances to the BS before a downlink transmission may be applied. Furthermore, the BS may apply a transmit-antenna-selection (TAS) scheme or a transmit-antenna-beamforming (TAB) scheme. The TAB scheme requires full CSI knowledge at BS whereas the TAS scheme is a comparatively low-cost low-complexity method [32]. In particular, we will focus on the SOP for all the schemes listed above (with exception shown in Table 1.1). Note that HD is a special case of FD, and using no Tx-AN is a special case of using Tx-AN. Much of the mathematical details is given in appendices. Section 3.5 shows numerical results to verify the analysis. Section IX summarizes the paper.

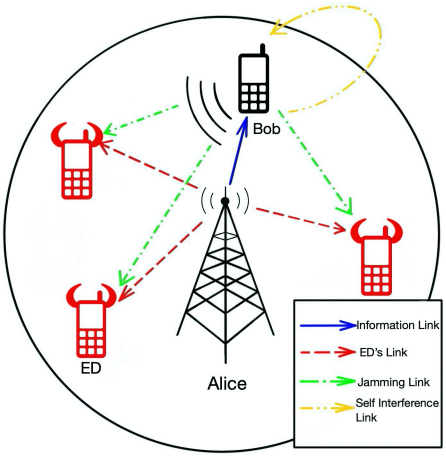

Figure 1.1: Wireless network subject to randomly located eavesdroppers where Alice is BS and UE is Bob.

Table 1.1: Organization of Chapters 2 and 3

	non-colluding EDs			colluding EDs	
	FD UE	HD UE	multi-UE ordering	FD UE	HD UE
TAS	2.2	2.2.1	[35]	3.2	3.2.1
TAB	2.3	2.3.2	2.4	3.3& 3.4	3.3

1.1.2 Related Work

The conventional radio is half-duplex (HD). But full-duplex (FD) radio promises to be available in the near future [25]-[30]. A user equipped with FD capability can receive a desired information while transmitting an artificial noise (AN) to jam nearby EDs [7], [27]-[31]. We will also refer to this AN as Rx-AN which differs from the AN (along with information signal) transmitted by a multi-antenna transmitter. The latter will also be referred to as Tx-AN. Subject to randomly distributed EDs, schemes based on Tx-AN without Rx-AN have been studied in [16]-[20] for non-colluding EDs and in [21]-[24] for colluding EDs. In [16], authors investigated the design of multi-antenna Tx-AN to minimize

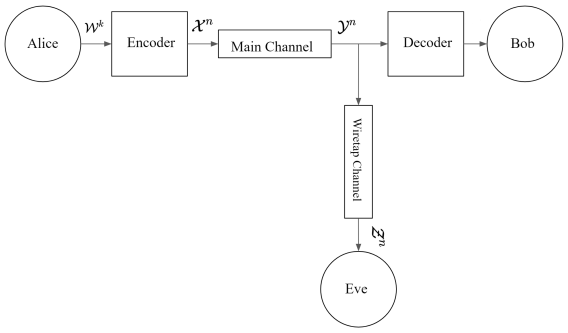

Figure 1.2: The wiretap channel model

the secrecy outage probability (SOP) by ignoring thermal noise at EDs. In [17] and [18], authors derived exact closed-form expressions for optimal Tx-AN allocation to minimize SOP. In [19], authors further investigated secrecy performance under imperfect CSI. The aforementioned studies reveal that Tx-AN (for HD receiver) improves secrecy performance against any EDs' scenarios.

1.1.3 Secrecy Capacity

In the traditional sense of the definition of secrecy [1] the communication channel can be modeled as a broadcast channel followed by a wire-tap channel as shown in Fig. 1.2. Alice broadcasts her message $w^k \in \mathcal{W}^k$ encoded into a codeword $x^n \in \mathcal{X}^n$. Bob and Eve respectively receive $y^n \in \mathcal{Y}^n$ and $z^n \in \mathcal{Z}^n$. The information Eve gains from her received signal is modeled as

$$I(z^n; w^k) = h(w^k) - h(w^k|z^n), \tag{1.1}$$

where $I(a;b)$ is the mutual information between a and b, and h is entropy. Perfect secrecy is then achieved if Eve can not decode any bits of information, i.e.,

$$I(z^n; w^k) = 0 \;\leftrightarrow\; h(w^k) = h(w^k|z^n) \tag{1.2}$$

in other words, the amount of ambiguity about the secret information in Eve is not changed after receiving z^n.

Now let us define P_e as the probability of making an error in estimating the message w^k, and $\hat{w}^k$ as the estimate of w^k, so

$$P_e = \mathcal{P}\{w^k \neq \hat{w}^k\}. \tag{1.3}$$

The rate of ambiguity Eve has about message w^k is called the equivocation rate and is defined as

$$R_e = \frac{1}{n} h(w^k|z^n), \tag{1.4}$$

with $0 \leq R_e \leq h(w^k)/n$. It is evident that if $R_e = h(w^k)/n$, perfect secrecy is achieved, which is associated with a perfect secrecy rate R_s. A certain R_s is said to be achievable if for any $\epsilon > 0$, there is a sequence of $(2^{nR_s}, n)$ codes such that for any $n \geq n(\epsilon)$, we have

$$\begin{cases} P_e < \epsilon \\ R_s - \epsilon < R_e. \end{cases} \tag{1.5}$$

The first condition is the achievable rate constraint. The second constraint is the condition on equivocation rate to guarantee prefect secrecy. Finally, secrecy capacity C_s is the maximum achievable secrecy rate. It is then proven in [1] that C_s is the difference between the capacity of the main channel C_M and the capacity of the wiretap channel C_W, i.e.,

$$C_s = (C_M - C_W)^+, \tag{1.6}$$

where $(.)^+ \triangleq \max(0, .)$ is the positive secrecy rate. While Wyner proved this for the discrete memory-less channel, the principle that secrecy capacity is the difference of capacities of the legitimate and eavesdropper's channels is proven to be true.

1.1.4 Contributions

Part of this work has been included in [34]. The key contributions include the following:

- We derive the closed form expressions of SOP for all the schemes/scenarios listed in Table 1.1. In the context of randomly distributed EDs, the scheme with both Tx-AN and Rx-AN was not studied before, and none of the schemes listed under colluding EDs was before considered either.

- We focus on SOP conditional on user's CSI, which results in a tight lower bound of SOP for both TAS and TAB schemes against randomly located colluding EDs. This is in contrast to [33] where TAS was analyzed based on unconditional SOP and zero thermal noise at EDs. The latter is only valid for scenarios of high jamming noise.

- We extend the analysis shown in [35] from TAS to TAB with Tx-AN for multiple HD users. Comparisons between TAS and TAB are shown analytically and numerically. (The low cost advantage of antenna selection has been exploited for network throughput as well as physical layer security [44]-[47]. But TAS shown in [33] and [35] is the most relevant to this paper.)

- We reveal the existence of a finite optimum Rx-AN power for both TAS and TAB schemes, which can be also computed based on our closed form SOP expressions.

1.1.5 Acknowledgment

This work was supported in part by the Army Research Office under Grant Number W911NF-17-1-0581. The views and conclusions contained in this document are those of the authors and should not be interpreted as representing the official policies, either expressed or implied, of the Army Research Office or the U.S. Government. The U.S. Government is authorized to reproduce and distribute reprints for Government purposes notwithstanding any copyright notation herein.

1.2 Finite Blocklength Secrecy

1.2.1 Motivations

In the emerging ultra reliable and low latency communication (uRLLC) scenarios, relatively short information packets (often called finite blocklength) are transmitted to meet the latency and reliability requirements [60]-[61]. Furthermore, transmitter adopts secrecy coding of finite blocklength (FBL) during information transmission phase to ensure secrecy against eavesdropper (Eve). Prior works in [52]-[53] investigate the average secrecy throughput (AST) as metric to study the secrecy performance in FBL where the channel state information (CSI) anywhere is assumed to be known everywhere. In particular, Eve's receive CSI is assumed to be known to Eve, which is too conservative if anti-eavesdropping channel estimation (ANECE) is applied [30].

In this paper, we study the AST of a downlink FBL communication system where one multi-antenna transmitter sends secret information to a single user against Eve with any number of antennas. To enhance AST, the transmitter adopts transmit antenna beamform-

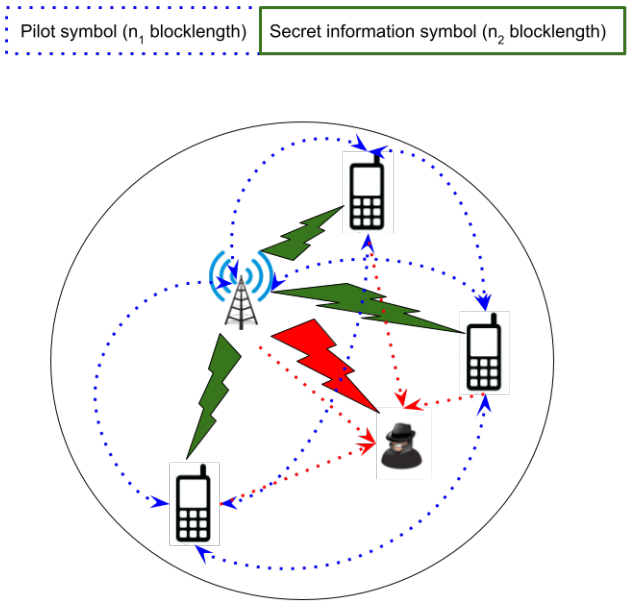

Figure 1.3: Short-packet communication model. $N-1$ single antenna users send secret information to AP with N_A number of full-duplex antenna against one Eve with N_E antenna.

ing as well as ANECE. Proposed in [30], ANECE allows two or more cooperative full-duplex radio devices to obtain consistent estimates of their CSI with respect to each other, and at the same time ANECE prevents Eve from obtaining any consistent estimate of its receive CSI. This property of ANECE is useful to maintain a non-zero secrecy of the subsequent transmissions of information between these devices against Eve with any number of antennas [31]. Moreover, we will apply some of the techniques in [55] to the ANECE assisted case. We also assume that the forced channel estimation error at Eve (due to ANECE) is only treated by Eve as a source of additional noise at Eve. In other words, Eve does not apply advanced methods such as blind detection [31] to mitigate the effect of ANECE.

1.2.2 Related Work

We consider a relatively short or often called finite blocklength (FBL) transmission of information between devices, which is important for applications such as Internet-of-Things (IoT) [49]-[61]. Prior AST analyses of FBL transmissions are available in [51]-[53] where the CSI anywhere is assumed to be known everywhere. In particular, Eve's receive CSI is assumed to be known to Eve. For the ANECE assisted case, Eve no longer knows its receive CSI perfectly, which makes the prior results not applicable.

However, we will apply some of the techniques in [54]-[55] to the ANECE assisted case. We also assume that the forced channel estimation error at Eve (due to ANECE) is only treated by Eve as a source of additional noise at Eve. In other words, Eve does not apply advanced methods such as blind detection [31] to mitigate the effect of ANECE.

1.2.3 Contributions

The key contributions of this paper (a substantial extension of [62]) include the following:

- The average secrecy throughput (AST) of a uplink communication system is studied using the information-theoretic results on finite-blocklength bounds for wiretap channels. We derived the closed-form approximations of secret information transmission scheme for multi-antenna AP to evaluate the AST against multi-antenna Eve.

- We introduce a special channel training scheme called ANECE where all legitimate users apply cooperative channel training to force Eve with inconsistent channel state information (CSI) estimation. We show substantial AST enhancement of the short

packet communication with ANECE and compared it's AST performance with conventional channel training scheme (MMSE estimation without ANECE strategy).

- We studied the impact orthogonal and non-orthogonal transmission of information from cooperative users the AST. Later, we discuss a scenario when Eve utilize prior information knowledge to combat against ANECE scheme.

- We present numerical results to analyze the impact of various parameters, i.e, block-length, training sequence length, transmit power, number of cooperative users, number of antennas at Alice and Eve on the AST. Our results provide useful insights to design the system parameters in terms of the AST maximization under the reliability and latency constraints. Finally, we verify our theoretical results with independent Monte Carlo trials.

1.2.4 Acknowledgment

This work was supported in part by the Army Research Office under Grant Number W911NF-17-1-0581 and the Department of Defense under W911NF-19-S-0013. The views and conclusions contained in this document are those of the authors and should not be interpreted as representing the official policies, either expressed or implied, of the Army Research Office or the U.S. Government. The U.S. Government is authorized to reproduce and distribute reprints for Government purposes notwithstanding any copyright notation herein.

1.3 Notations

Bold-faced lower-case letters, e.g., $\mathbf{x}$, are used for vectors and Bold-faced lower-case letters, e.g., $\mathbf{A}$, are used for matrix. $\mathbf{A}^H$, $\mathbf{A}^T$, and $\mathbf{A}^*$ denote Hermitian transpose, normal transpose and conjugate of a matrix $\mathbf{A}$, respectively. $\|\cdot\|$ stands for the vector's Euclidean norm and $|\cdot|$ stands for the absolute value of a complex/real scalar number. $\mathcal{C}$ and $\mathcal{R}$ denote the set of all complex and real numbers, respectively. The $n \times n$ identity matrix is $\mathbf{I}_n$ or simply $\mathbf{I}$ when its dimension is obvious. The trace, expectation, differential, natural logarithm, base-2 logarithm, determinant and Kronecker product are respectively Tr, $\mathbb{E}$, ∂, ln, $\log_2$, $|\cdot|$ and $\otimes$. All other notations are defined in the context.

The symbols used in this paper are shown in Table 1.2.

Table 1.2: Notation and Symbols

Symbol	Definition
$\mathcal{CN}$	complex Gaussian
Φ	the set of locations of EDs
ρ_E	intensity or density of Φ
α	path loss exponent
ρ	normalized self-interference coefficient
P_T	transmission (signal plus AN) power from Alice
P_J	transmission (jamming) power from Bob
ϵ	fraction of transmission power at Alice for AN
$\mathbb{E}_{\mathbf{v}}$	expectation over v
$[x]^+$	max(0,x)
$B(x,y)$	Beta function, where $B(x,y) = \frac{\Gamma(x)\Gamma(y)}{\Gamma(x+y)}$
$\Gamma(x,y)$	upper incomplete Gamma function
$\gamma(x,y)$	lower incomplete Gamma function
$U(a,b,z)$	Confluent hypergeometric function of second kind
$\mathbf{F}(a,b,c;z)$	Gaussian hypergeometric function
$\mathcal{L}$	Laplace transform
$\mathbf{E_1}(x)$	Exponential integral function
P_i	transmission power from Alice during phase $i \in \{1,2\}$
$\mathbf{P}_A$	$N_A \times n_1$ pilot matrix transmitted by Alice
$\mathbf{P}_U$	$(N-1) \times n_1$ pilot matrix transmitted by all $N-1$ users
$\mathbf{K_{x,y}}$	the correlation matrix between two random vectors $\mathbf{x}$ and $\mathbf{y}$
ϵ	decoding error probability at Rx
δ	the information leakage to Eve
$Q^{-1}(\cdot)$	inverse of the Gaussian-Q function
T_s	average secrecy throughput

Chapter 2

Secrecy performance of TAB and TAS scheme against Non-colluding EDs

2.1 System Model

We consider a base station (BS or Alice) with multiple antennas located at the center of a circle of radius R, which transmits secret information to a single-antenna (omnidirectional) user equipment (UE or Bob). Without loss of generality, we first assume that Bob is located at a unit distance away from Alice. There are randomly located single-antenna (omnidirectional) eavesdroppers (EDs) in the circle, and the random locations of EDs (denoted by Φ) are modeled as a PPP with the intensity ρ_E.

The channel gain vector from Alice to Bob is denoted by $\mathbf{h} \in \mathcal{C}^{M\times 1}$, which has

been normalized to be a complex Gaussian random vector with zero mean and the identity covariance matrix, i.e., $\mathcal{CN}(\mathbf{0}, \mathbf{I})$. We assume Bob is equipped with full-duplex antenna (full-duplex can be implemented with either one Tx and one Rx antenna or even with single antenna via RF circulator [36]) where Bob can transmit and receive at the same time in the same frequency band. The normalized residual instantaneous self-interference channel gain at Bob is $\sqrt{\rho}g_B$ with the distribution $\mathcal{CN}(0, \rho)$ where ρ corresponds to a normalized gain factor (which is relative to the main/user channel gain and should be kept small in application although it can be larger than one if the actual distance between Alice and Bob is relatively large [29]). The channel vector from Alice to the eth ED is $\sqrt{a_e}\mathbf{h}_{AE_e} \in \mathcal{C}^{M\times 1}$ and distributed as $\mathcal{CN}(\mathbf{0}, a_e\mathbf{I})$, and the channel gain from Bob to the eth ED is $\sqrt{b_e}h_{BE_e}$ and distributed as $\mathcal{CN}(0, b_e)$. We also let $a_e = \frac{1}{d^{\alpha}_{AE_e}}$ with d_{AE_e} being the normalized distance between Alice and the eth ED, and $b_e = \frac{1}{d^{\alpha}_{BE_e}}$ with d_{BE_e} being the normalized distance between Bob and the eth ED. Note that a_e and b_e are the large-scale fading parameters as they are dependent on the location of ED while $\mathbf{h}$, g_B, $\mathbf{h}_{AE_e}$ and h_{BE_e} are the small-scale fading parameters. We assume that the channels are all quasi-static where the channel coefficients stay constant during transmission of any given packet.

The secrecy rate of the downlink transmission from Alice to Bob is

$$S_{AB} = [\log_2(1 + SNR_{AB}) - \log_2(1 + SNR_{AE_*})]^+, \tag{2.1}$$

where $SNR_{AE_*} = \mathcal{F}(SNR_{AEe})$. The operator $\mathcal{F}(.)$ takes the location dependent Signal-to-Noise Ratios (SNRs) of EDs as argument. The form of $\mathcal{F}(.)$ is dependent on whether EDs are acting independently or colluding with each other. In the case of non-colluding EDs,

the strongest ED channel is considered and the form of $\mathcal{F}(.)$ is defined as

$$\mathcal{F}(.) = \max_{e \in \Phi}(.). \tag{2.2}$$

In the case of colluding EDs, we assume that all EDs can combine their own SNRs to jointly decode the information bearing signal. We consider passive (distributed) EDs. Since they do not have access to the full CSI between Alice and themselves, they are unable to form a virtual antenna array for colluding. This assumption is the same as in [13]-[24] and [33]-[35]. Thus,

$$\mathcal{F}(.) = \sum_{e \in \Phi}(.). \tag{2.3}$$

For a target secrecy rate R_S, the SOP is defined as

$$P_{out} \triangleq P(S_{AB} \leq R_S) = P\left[\frac{1 + SNR_{AB}}{1 + SNR_{AE_*}} \leq 2^{R_S}\right], \tag{2.4}$$

where $P(\cdot)$ denotes the probability. We will also use $P_{con} \triangleq 1 - P_{out}$.

2.1.1 Transmit Antenna Selection

In the TAS scheme, Alice only transmits via the antenna corresponding to the element in $\mathbf{h}$ that has the largest amplitude. Let $\sqrt{P_T}x_A(k)$ of power P_T be the information signal transmitted from Alice, and h_{i^*} be the element selected from $\mathbf{h} = [h_1, \cdots, h_M]^T$, i.e., $|h_{i^*}| = \max_i |h_i|$. Thus, Bob and Eve receive the following signals respectively:

$$y_B(k) = h_{i^*}\sqrt{P_T}x_A(k) + \sqrt{\rho P_J}g_B\tilde{w}_B(k) + n_B(k), \tag{2.5}$$

$$y_{E_e}(k) = \sqrt{a_e P_T}h_{A_{i^*}E_e}x_A(k) + \sqrt{b_e P_J}h_{BE_e}w_B(k) + n_{E_e}(k), \tag{2.6}$$

where $\sqrt{P_J}w_B(k)$ of power P_J is the jamming noise or Rx-AN from Bob, $n_B(k)$ and $n_E(k)$ are the background Gaussian noises at Bob and Eve each with the unit variance, and the

second term of (2.5) denotes the residual self-interference. Then, the SNR at Bob is

$$SNR_{AB}^{TAS} = \frac{|h_{i^*}|^2 P_T}{1 + \rho |g_B|^2 P_J}, \tag{2.7}$$

and the SNR at the eth Eve is

$$SNR_{AEe}^{TAS} = \frac{a_e |h_{A_{i^*}E_e}|^2 P_T}{1 + b_e |h_{BE_e}|^2 P_J}. \tag{2.8}$$

2.1.2 Transmit Antenna Beamforming

In the TAB scheme, Alice takes the advantage of the complete knowledge of $\mathbf{h}$ by transmitting the following signal:

$$\mathbf{s}(k) = \sqrt{(1-\epsilon)P_T}\mathbf{t}x_A(k) + \sqrt{\frac{\epsilon P_T}{M-1}}\mathbf{W}\mathbf{v}(k), \tag{2.9}$$

where $x_A(k)$ is the message signal of zero mean and unit variance, $\mathbf{t} = \frac{\mathbf{h}^*}{\|\mathbf{h}\|}$, $\mathbf{W} \in \mathcal{C}^{M\times(M-1)}$ has the orthonormal columns that span the left null space of $\mathbf{t}$ (hence $\mathbf{t}\mathbf{t}^H + \mathbf{W}\mathbf{W}^H = \mathbf{I}$), $\mathbf{v} \in \mathcal{C}^{(M-1)\times 1}$ is the Tx-AN $\mathcal{CN}(\mathbf{0}, \mathbf{I})$, and $\epsilon \in \{0, 1\}$ is the power fraction factor that splits the total power P_T between the Tx-AN term and the message term.

Consequently, the received signal at Bob and the eth Eve are:

$$\begin{aligned}
y_B(k) &= \sqrt{(1-\epsilon)P_T}\|\mathbf{h}\|x_A(k) + \sqrt{\rho P_J}g_B\tilde{w}_B(k) + n_B(k), \\
y_{E_e}(k) &= \sqrt{a_e(1-\epsilon)P_T}\frac{\mathbf{h}_{AEe}^T\mathbf{h}^*}{\|\mathbf{h}\|}x_A(k) + \sqrt{b_e P_J}h_{BE_e}w_B(k) \\
&\quad + \sqrt{a_e}\sqrt{\frac{\epsilon P_T}{M-1}}\mathbf{h}_{AEe}^T\mathbf{W}\mathbf{v}(k) + n_{E_e}(k),
\end{aligned}$$

respectively. Then the SNR at Bob is

$$SNR_{AB}^{TAB} = \frac{(1-\epsilon)\|\mathbf{h}\|^2 P_T}{1 + \rho |g_B|^2 P_J}, \tag{2.10}$$

and the SNR at the eth Eve is

$$\begin{aligned} SNR_{AE_e}^{TAB} &= \frac{a_e(1-\epsilon)\frac{|\mathbf{h}_{AE_e}^T\mathbf{h}^*|^2}{\|\mathbf{h}\|^2}P_T}{1+b_e|h_{BE_e}|^2P_J+a_e\frac{\epsilon P_T}{M-1}\mathbb{E}_{\mathbf{v}}\{|\mathbf{h}_{AE_e}^T\mathbf{W}\mathbf{v}|^2\}} \\ &= \frac{a_e(1-\epsilon)\frac{|\mathbf{h}_{AE_e}^T\mathbf{h}^*|^2}{\|\mathbf{h}\|^2}P_T}{1+b_e|h_{BE_e}|^2P_J+a_e\frac{\epsilon P_T}{M-1}\|\mathbf{h}_{AE_e}\|^2(1-\frac{|\mathbf{h}_{AE_e}^T\mathbf{h}^*|^2}{\|\mathbf{h}_{AE_e}\|^2\|\mathbf{h}\|^2})} \\ &= \frac{(1-\epsilon)X_1\Theta P_T}{d_{AE_e}^{\alpha}+\frac{P_Jd_{AE_e}^{\alpha}}{d_{BE_e}^{\alpha}}X_2+\frac{\epsilon P_T}{M-1}X_1(1-\Theta)}, \end{aligned} \tag{2.11}$$

where $\mathbb{E}_{\mathbf{v}}$ denotes the expectation over $\mathbf{v}$ and $\mathbb{E}_{\mathbf{v}}\{|\mathbf{h}_{AE_e}^T\mathbf{W}\mathbf{v}|^2\} = \mathbb{E}_{\mathbf{v}}\{|\mathbf{h}_{AE_e}^T\mathbf{W}\mathbf{v}\mathbf{v}^T\mathbf{W}^T\mathbf{h}_{AE_e}|^2\} = \mathbf{h}_{AE_e}^T(\mathbf{I}-\mathbf{t}\mathbf{t}^H)\mathbf{h}_{AE_e}$, $X_1 = \|\mathbf{h}_{AE_e}\|^2$, $X_2 = |h_{BE_e}|^2$ and $\Theta = \frac{|\mathbf{h}_{AE_e}^T\mathbf{h}^*|^2}{\|\mathbf{h}_{AE_e}\|^2\|\mathbf{h}\|^2}$. Note that X_1, X_2 and Θ are independent of each other.

Furthermore, X_1 has a Chi-squared distribution with $2M$ degrees of freedom (DoF), i.e., its probability density function (PDF) is $f_{X_1}(x) = \frac{x^{M-1}e^{-x}}{\Gamma(M)}$; X_2 has a Chi-squared distribution with 2 DoF (also known as the exponential distribution of the unit mean); and Θ is known to have the beta distribution [30] with parameters $B(1, M-1)$, i.e., $f_{\Theta}(x) = (M-1)(1-x)^{M-2}$. Note that $Beta(a,b)$ distributed random variable X the PDF $f_X(x) = \frac{x^{a-1}(1-x)^{b-1}}{B(a,b)}$.

In order to maintain a data rate R_D from Alice to Bob, we must have $\log_2(1 + SNR_{AB}^{TAB}) > R_D$, i.e., $1-\epsilon > \frac{1+\rho|g_B|^2P_J}{\|\mathbf{h}\|^2P_T}(2^{R_D}-1)$ for the non-negative ϵ.

2.1.3 TAB with User Selection (TAB-US)

In the TAB-US scheme, we assume that Alice (BS) serves multiple single-antenna HD Bobs (UEs) (where $P_J = 0$) based on the user's distance from Alice. The locations of Eves and Bobs are all modeled as spatial PPP, i.e., Φ_E with intensity ρ_E and Φ_U with intensity ρ_U respectively.

Let d_{AB_n} be the distance from Alice to the nth (nearest) Bob. Similar to (2.10), the SNR at the nth Bob is

$$SNR_{AB_n} = \frac{(1-\epsilon)P_T\|\mathbf{h}_{AB_n}\|^2}{d_{AB_n}^{\alpha}}, \tag{2.12}$$

and, similar to (2.11), the SNR at the eth Eve is

$$SNR_{AE_e} = \frac{a_e(1-\epsilon)\|\mathbf{h}_{AE_e}\|^2 \frac{\|\mathbf{h}_{AE_e}^H \mathbf{h}_{AB_n}\|^2}{\|\mathbf{h}_{AE_e}\|^2\|\mathbf{h}_{AB_n}\|^2} P_T}{1 + a_e \frac{\epsilon P_T}{M-1}\|\mathbf{h}_{AE_e}\|^2(1 - \frac{\|\mathbf{h}_{AE_e}^H \mathbf{h}_{AB_n}\|^2}{\|\mathbf{h}_{AE_e}\|^2\|\mathbf{h}_{AB_n}\|^2})}, \tag{2.13}$$

where $X_{2,n} = \|\mathbf{h}_{AB_n}\|^2$ is independent from X_1 and both follow the Chi-squared distribution with $2M$ degrees of freedom, i.e., $f_{X_{2,n}}(x) = f_{X_1}(x) = \frac{x^{M-1}e^{-x}}{\Gamma(M)}$. Also $\Theta = \frac{\|\mathbf{h}_{AE_e}^H \mathbf{h}_{AB_n}\|^2}{\|\mathbf{h}_{AE_e}\|^2\|\mathbf{h}_{AB_n}\|^2}$ follows the $B(1, M-1)$ distribution [30], and $X_4 = \Theta X_1$ is exponentially distributed with mean equal to one. Also, $X_{4,4} = (1-\Theta)X_1$ follows $\Gamma(M-1, 1)$ distribution and most importantly $X_{2,n}$, X_4 and $X_{4,4}$ are independent.

Throughout this section, we study the secrecy performance of both the TAB and TAS schemes against independently acting EDs. Furthermore, we analyze the secrecy performance of the TAB scheme as a function of the ordering index of each Bob (among randomly distributed Bobs) with respect to his distance to Alice.

2.2 Secrecy performance of the TAS Scheme

The performance of the TAS scheme was analyzed in [33] by assuming that the noise at each node is dominated by the interference. A novelty of the following analysis is an insight that there is generally a nonzero optimal P_J. Such an analytical insight would not be possible if the noise is assumed to be negligible from the very beginning of the analysis. Moreover, authors of [33] derived the SOP expression averaged over the distribution of

legitimate channel. Such analysis does not provide useful insights for a given/common realization of the legitimate channel. In this paper, we study the SOP expression conditioned on the legitimate channel CSI. For a large coherence period of the legitimate channel, the SOP averaged over EDs' distribution can be minimized over the jamming power from FD Bob. Thus, this study enables us to find the optimum allocation at Bob. We will also show the overall averaged SOP considering the distribution of the legitimate channel.

We will use the following parameterizations: $\beta \triangleq 2^{R_s}$, $m \triangleq \frac{P_J}{P_T}$ ("a transmit power ratio"), $Y \triangleq SNR_{AB}^{TAS} = \frac{|h_{i^*}|^2}{\frac{1}{P_T}+\rho m|g_B|^2}$ and $Y_0 \triangleq \frac{Y}{\beta}+\frac{1}{\beta}-1$. Note that for any given realization of $\mathbf{h}$ and g_B, Y is a given constant. Hence, $P[S_{AB}^{TAS} > R_s|\Phi, \mathbf{h}, g_B] = P[S_{AB}^{TAS} > R_s|\Phi, Y]$.

Proposition 1 *Conditioned on* $\mathbf{h}$ *and* g_B*, the probability of achieving a secrecy rate strictly larger than* R_s *using the TAS scheme is given by*

$$P_{con,Y} \quad = \quad \exp\left[-\rho_E \int_0^R \int_0^{2\pi} \Psi(Y, r, \theta) r \, d\theta \, dr \right], \tag{2.14}$$

where

$$\Psi(Y, r_e, \theta_e) = \frac{\exp(-\frac{d_{AE_e}^{\alpha}}{P_T} Y_0)}{1 + m(\frac{d_{AE_e}}{d_{BE_e}})^{\alpha} Y_0}, \tag{2.15}$$

and (r_e, θ_e) *are the polar coordinates of the location of the* e*th Eve with the origin at the location of Alice. Also* $d_{AE_e} = r_e$ *and* $d_{BE_e} = \sqrt{r_e^2 + d^2 - 2r_e \cos\theta}$.

The proof is shown in Appendix .1.

Remark 1 *It is obvious that* $P_{con,Y}$ *is a decreasing function of* $\Psi(Y, r, \theta)$*. One can verify the following statements subject to* $P_T > 0$*:*

Table 2.1: Effects of parameters on $\Psi(Y, r, \theta)$ & $P_{con,Y}$ when $R_s = 0$, where $-$, $\uparrow$ and $\downarrow$ denote invariance, increasing and decreasing, respectively.

	P_T	$P_J \to \infty (\rho P_J = a)$	$P_J \uparrow (\leq {P_J}^*)$	$P_J \uparrow (\geq {P_J}^*)$
$\Psi(Y, r, \theta)$	$-$	$\to 0$	$\downarrow$	$\uparrow$
$P_{con,Y}$	$-$	$\to 1$	$\uparrow$	$\downarrow$

- *If $R_s = 0$, then $\Psi(Y, r, \theta)$ is invariant to P_T.*

- *If $R_s = 0$ and the product ρP_J is a fixed constant, then as P_J increases to ∞, $\Psi(Y, r, \theta)$ decreases monotonically to zero and hence $P_{con,Y}$ increases monotonically to one.*

- *If $\rho \ll 1$, then in a region of small P_J, Y and hence Y_0 are approximately invariant to P_J. But in this case, $\Psi(Y, r, \theta)$ decreases as P_J increases (since $Y_0 \left(\frac{d_{AE}}{d_{BE}}\right)^{\alpha}$ is not small) and hence $P_{con,Y}$ increases as P_J increases.*

The aforementioned statements are summarized in Table 2.1 where ${P_J}^*$ is nonzero optimal value of P_J and a is an arbitrary constant. Here $P_J \to \infty$ implies that the jamming power from Bob is large or more precisely $P_J \gg \frac{1}{\rho |g_B|^2}$. The expression (2.14) provides the relationship between the target secrecy rate R_s and different parameters in the network. To obtain $P_{con,Y}$ numerically, the double integrals shown there need to be computed for a given choice of the path loss exponent α. In general, experimentally estimated α results in difficulty for simplification of the double integrals. But for $R_s = 0$ (i.e. $Y_0 = Y$) and $\alpha = 2$, a simplification can be shown to be

$$P_{con,Y} = \exp\Bigg[-\rho_E \Bigg(\frac{\pi P_T}{Y} \big(1 - \exp(-\frac{Y R^2}{P_T})\big) - \pi m Y \times \int_0^{R^2} \frac{\exp(-\frac{Yr}{P_T}) r}{\sqrt{\big((1+mY)r + d^2\big)^2 - 4rd^2}} \mathrm{d}r \Bigg) \Bigg] \tag{2.16}$$

which is shown in Appendix .2.

Then, the unconditional $P_{con} = \mathbb{E}_Y[P_{con,Y}]$ can be obtained by

$$P_{con} = P[S_{AB}^{TAS} > R_s] = \int_{y=0}^{\infty} P_{con,y} f_Y(y) \mathrm{d}y, \tag{2.17}$$

where the distribution of Y due to the random $|h_{i^*}|^2$ and $|g_B|^2$ is given in the following lemma:

Lemma 2 *The cumulative distribution function (CDF) of Y is*

$$F_Y(y) = \sum_{i=0}^{M} C_i^M (-1)^i \frac{e^{-\frac{iy}{P_T}}}{1 + iy\rho m}, \tag{2.18}$$

where $C_i^M = \frac{M!}{(M-i)!i!}$. Hence the PDF of Y is

$$f_Y(y) = \sum_{i=0}^{M} C_i^M (-1)^{i+1} i e^{-\frac{iy}{P_T}} \frac{(\frac{iy\rho m}{P_T} + \frac{1}{P_T} + \rho m)}{(1 + iy\rho m)^2}. \tag{2.19}$$

Next, we consider $P_{con,Y}$ in the two special cases: $P_J = 0$ and $P_J \to \infty$.

2.2.1 The Case of $P_J = 0$

Now we consider the case of $P_J = 0$ thus $m = 0$ and assume that $P_T \gg \frac{1-\beta}{|h_{i^*}|^2}$ thus $Y_0 \approx \frac{P_T |h_{i^*}|^2}{\beta}$. It follows from (.2) that $\Psi(Y; r, \theta) = \exp(-\frac{d_{AEe}^{\alpha}}{P_T} Y_0) = \exp\left(-r^{\alpha} \frac{|h_{i^*}|^2}{\beta}\right)$. Hence

$$\begin{aligned}
\frac{\ln P_{con,Y}}{\rho_E} &= -\int_0^R \int_0^{2\pi} \Psi(Y; r, \theta) r \mathrm{d}\theta \mathrm{d}r \\
&= -2\pi \int_0^R \exp\left(-r^{\alpha} \frac{|h_{i^*}|^2}{\beta}\right) r \mathrm{d}r \\
&= -\frac{2\pi \beta^{\frac{2}{\alpha}}}{\alpha (|h_{i^*}|^2)^{\frac{2}{\alpha}}} \int_0^{\frac{R^{\alpha}(|h_{i^*}|^2}{\beta}} \exp(-z) z^{\frac{2}{\alpha}-1} \mathrm{d}z \\
&= -\frac{2\pi \beta^{\frac{2}{\alpha}}}{\alpha (|h_{i^*}|^2)^{\frac{2}{\alpha}}} \gamma\left(\frac{2}{\alpha}, \frac{|h_{i^*}|^2 R^{\alpha}}{\beta}\right),
\end{aligned} \tag{2.20}$$

where $z = r^\alpha \frac{|h_{i^*}|^2}{\beta}$ and $\gamma(x,y) = \int_0^y z^{x-1}e^{-z}\mathrm{d}z$ is the lower incomplete gamma function which increases monotonically with y. From (2.20), it is clear that $P_{con,Y}$ monotonically decreases as R increases. In particular,

$$\lim_{R\to\infty} \frac{\ln P_{con,Y}}{\rho_E} = -\pi \left(\frac{\beta}{|h_{i^*}|^2}\right)^{\frac{2}{\alpha}} \frac{2}{\alpha}\Gamma\left(\frac{2}{\alpha}\right), \tag{2.21}$$

where $\Gamma(x) = \int_0^\infty z^{x-1}e^{-z}\mathrm{d}z$. It is known that $x\Gamma(x) = \Gamma(x+1)$ for positive x and $\Gamma(x+1)$ decreases to one as x decreases to zero. Then, provided $\frac{\beta}{|h_{i^*}|^2} > 1$, the above limit increases as α increases. The result (2.21) serves as a benchmark corresponding to a HD Bob.

2.2.2 The case of $P_J = \infty$

We now consider the case of $P_J = \infty$ and also assume $R_s = 0$ and $\alpha = 2$. In this case, $Y_0 = Y = 0$ and $mY = \frac{|h_{i^*}|^2}{\rho|g_B|^2}$. Then, following a similar derivation as that in section 1 of the supplement, one can verify that

$$\frac{\ln P_{con,Y}}{\rho_E} = -2\pi \int_{r=0}^{R} \left(1 - \frac{1}{\sqrt{1+\rho\frac{|g_B|^2}{|h_{i^*}|^2}(1+\frac{d}{r})^2}}\right.$$
$$\left. \times \frac{1}{\sqrt{1+\rho\frac{|g_B|^2}{|h_{i^*}|^2}(1-\frac{d}{r})^2}}\right) r\mathrm{d}r, \tag{2.22}$$

where the integrant converges to $\left(1 - \frac{1}{1+\rho\frac{|g_B|^2}{|h_{i^*}|^2}}\right) r$ as r becomes large and the integral goes to ∞ as $R \to \infty$. Hence $\lim_{R\to\infty} P_{con,Y} = 0$. This result suggests that P_J should not be too large. Combining this with a previous result for small P_J implies that there is generally a finite nonzero optimal P_J.

2.3 Secrecy performance of the TAB Scheme

Unlike the TAS scheme, Alice will now use all transmit antennas via beamforming to transmit each information symbol. We will assume that all the channel links from Alice to Bob are independent and identically distributed.

In addition to $m = \frac{P_J}{P_T}$ and $\beta = 2^{R_s}$, we will use $Z = \frac{SNR_{AB}^{TAB}}{(1-\epsilon)} = \frac{\|\mathbf{h}\|^2}{\frac{1}{P_T}+\rho m|g_B|^2}$, $C = \frac{Z}{\beta P_T} - \frac{(1-\frac{1}{\beta})}{(1-\epsilon)P_T}$, $f_e = (\frac{d_{AE_e}}{d_{BE_e}})^\alpha m$ ("a large scale receive power ratio") and $G = \frac{1}{CP_T} = \frac{\beta(1+\rho P_J|g_B|^2)}{P_T\|\mathbf{h}\|^2}$. The random variables Z, C and G are one-to-one related to each other. We will use z, c and g for the realizations of Z, C and G respectively. Unlike f_e, the variables z, c and g are invariant to the locations of Eves but dependent on the small scale fading parameters $\mathbf{h}$ and g_B. For given realization of $\mathbf{h}$ and g_B, z is given. For $m = 0$, $Z = P_T\|\mathbf{h}\|^2$ has obviously a Chi-squared distribution with $2M$ DoF. For $m > 0$, one can prove the following lemma:

Lemma 3 *If $m > 0$, the legitimate channel's SNR_{AB} (which is Z) has the following PDF (shown in Appendix .3)*

$$f_Z(z) = \frac{M\rho m(z\rho m)^{M-1}}{(1+z\rho m)^{M+1}} e^{\frac{1}{\rho P_J}}. \tag{2.23}$$

Proposition 2 *Conditioned on $\mathbf{h}$ and g_B, the probability of achieving a secrecy rate strictly larger than R_s using the TAB scheme is given by*

$$P_{con,\mathbf{h},g_B} = P_{con,z} = \exp\left[-\rho_E \int_0^R r \int_0^{2\pi} \Omega(\frac{1}{g}; r, \theta)\, d\theta\, dr\right], \tag{2.24}$$

and hence $P_{con} = \int_0^\infty P_{con,z} f_Z(z) dz$ where

$$\Omega(\frac{1}{g}; r, \theta) = \frac{e^{\frac{d_{BE}^\alpha}{P_J}}}{(1+\frac{f_e}{g})(1+\frac{\epsilon}{(M-1)g})^{M-1}} \tag{2.25}$$

and all other variables are defined before.

The proof is shown in Appendix .4.

Remark 4 *From* (2.24) *and* (2.25)*, one can also verify the following subject to* $P_T > 0$*:*

- *For* $\epsilon > 0$*,* $P_{con,\mathbf{h},g_B} \to 1$ *as* $P_T \to \infty$*.* $(1 + \frac{\epsilon}{(M-1)g})^{M-1}$ *converges to* $e^{\epsilon/g}$ *as* M *increases. For large* P_T*,* $\frac{1-\frac{1}{\beta}}{(1-\epsilon)P_T} \approx 0$ *so,* $\frac{f_e}{g} = \left(\frac{d_{AEe}}{d_{BEe}}\right)^{\alpha} \frac{\|\mathbf{h}\|^2}{\beta(\frac{1}{P_J}+\rho|g_B|^2)}$ *which is invariant to* P_T *and* $\frac{\epsilon}{g} = \frac{\epsilon P_T \|\mathbf{h}\|^2}{\beta(1+\rho P_J|g_B|^2)}$ *which goes to* ∞ *as* $P_T \to \infty$ *.*

- $P_{con,\mathbf{h},g_B}$ *increases as* ρ *decreases. As* ρ *decreases,* Z *and* c *increase, and hence* g *and* $\Omega(\frac{1}{g}; r, \theta)$ *decrease, and hence* $P_{con,\mathbf{h},g_B}$ *increases.*

- *If* $\rho \to 0$*, then* $P_{con,\mathbf{h},g_B} \to 1$ *as* $P_J \to \infty$*.*

- *If* $\epsilon = 0$*, the optimal* P_J *is* ∞*. If* $\epsilon = 0$ *then it follows from* (2.24) *and* (2.25) *that*

$$P_{con,\mathbf{h},g_B} = \exp\left[-\rho_E \int_0^R r \int_0^{2\pi} \frac{e^{\frac{d_{BEe}^{\alpha}}{P_J}}}{1+\frac{f_e}{g}} d\theta\, dr \right], \tag{2.26}$$

which is independent of P_T *and monotonically increases as* P_J *increases. Thus the optimum* P_J *is* ∞*.*

- *For* $\epsilon > 0$ *and* $P_T > 0$*, the optimal* P_J *is a finite positive number. For* $\epsilon > 0$ *and* $P_T > 0$*,* $\frac{f_e}{g}$ *monotonically increases to* $\frac{\|\mathbf{h}\|^2}{\beta\rho|g_B|^2}$ *as* $P_J \to \infty$ *and* $1 + \frac{d_{BEe}^{\alpha}}{P_J}$ *monotonically decreases to* 1 *as* $P_J \to \infty$*. So,* $\frac{1+\frac{d_{BEe}^{\alpha}}{P_J}}{1+\frac{f_e}{g}}$ *monotonically decreases to* $\frac{1}{(1+\frac{\|\mathbf{h}\|^2}{\beta\rho|g_B|^2})}$ *for* $P_J \to \infty$*. We can also observe that* $\frac{\epsilon}{g}$ *monotonically decreases to* 0 *for* $P_J \to \infty$*, so* $\frac{1}{(1+\frac{\epsilon}{(M-1)g})^{M-1}}$ *monotonically increases to* 1 *as* $P_J \to \infty$*. So, we can conclude that there is a finite positive* P_J *at which* $P_{con,\mathbf{h},g_B}$ *is maximized.*

Table 2.2: Effects of parameters on $\Omega(z,r,\theta)$ & $P_{con,z}$ when $R_s = 0$

	$P_T \to \infty$	$P_J \to \infty$	$P_J \uparrow (\leq {P_J}^*)$	$P_J \uparrow (\geq {P_J}^*)$
$\Omega(z,r,\theta)\|_{\epsilon=0}$	$-$	$\downarrow \to const.$	$\downarrow$	$-$
$P_{con,z}, \epsilon = 0$	$-$	$\uparrow \to const.$	$\uparrow$	$-$
$\Omega(z,r,\theta)\|_{\epsilon\neq 0}$	$\to 0$	$\uparrow \to const.$	$\downarrow$	$\uparrow$
$P_{con,z}, \epsilon \neq 0$	$\to 1$	$\downarrow \to const.$	$\uparrow$	$\downarrow$

- *For $R_s = 0$, $\Omega(\frac{1}{g}; r, \theta)$ is a decreasing function of ϵ which makes the upper bound of ϵ optimal. Furthermore, $\Omega(\frac{1}{g}; r, \theta)$ is rather flat around the optimal P_J, which makes it easy to find a practically optimal P_J.*

The aforementioned observations are summarized in Table 2.2.

As shown in Appendix .5, $\Omega(\frac{1}{g}; r, \theta)$ for any r and θ is a unimodal function with its minimum at a finite positive value of P_J. Therefore, $\int_0^R r \int_0^{2\pi} \Omega(\frac{1}{g}; r, \theta) \mathrm{d}\theta \mathrm{d}r$ must also have its minimum at a finite positive value of P_J, or equivalently $P_{con,z} = \exp(-\rho_E \int_0^R r \int_0^{2\pi} \Omega(\frac{1}{g}; r, \theta) \mathrm{d}\theta \mathrm{d}r)$ has its peak at that value of P_J.

Next, we consider two special cases for which the double integral in (2.24) can be simplified.

2.3.1 Bob in Full Duplex Mode with $\beta = 1$ and $\alpha = 2$

For $\beta = 1$ and $\alpha = 2$, it is shown in Appendix .6 that

$$\int_0^R \int_0^{2\pi} \Omega(z; r, \theta) \mathrm{d}\theta r \mathrm{d}r = \frac{2\pi}{(1 + \frac{z\epsilon}{M-1})^{M-1}} \times \int_0^R \left(1 - \frac{1}{\sqrt{1 + \frac{(r+d)^2}{r^2 zm}} \sqrt{1 + \frac{(r-d)^2}{r^2 zm}}}\right) r \mathrm{d}r. \tag{2.27}$$

And $P_{out} = 1 - P_{con}$ versus P_J and ϵ will be illustrated in Fig. 2.3 from which we will see that for a given ϵ there is an optimal P_J and the optimal P_J is not very sensitive to ϵ.

Furthermore, if $P_J \to \infty$, then $z \to 0$, $zm \to \frac{\|\mathbf{h}\|^2}{\rho|g_B|^2}$ and (2.27) yields

$$\int_0^R \int_0^{2\pi} \Omega(z; r, \theta) d\theta r dr = 2\pi \int_0^R \Bigg(1 - \frac{1}{\sqrt{1 + \rho\frac{|g_B|^2}{\|\mathbf{h}\|^2}(1 + \frac{d}{r})^2}\sqrt{1 + \rho\frac{|g_B|^2}{\|\mathbf{h}\|^2}(1 - \frac{d}{r})^2}}\Bigg) r dr. \tag{2.28}$$

Comparing (2.22) and (2.28), we see a similar structure of the two expressions. Since $\|\mathbf{h}\|^2 \geq \max_{i \in M} |h_i|^2$, the TAB scheme always yields a lower SOP than the TAS scheme.

Also note that if $\epsilon > 0$ and $P_T \to \infty$, then (2.27) implies that the SOP of the TAB scheme becomes one (similar to the case for TAS).

2.3.2 Bob in Half-Duplex Mode

In this case, we have $P_J = 0$ and $z = P_T\|\mathbf{h}\|^2$. Also assuming a large P_T, it is shown in Appendix .7 that

$$\begin{aligned} &\int_0^R \int_0^{2\pi} \Omega(z; r, \theta) \mathrm{d}\theta r \mathrm{d}r \\ &= \frac{2\pi\beta^{\frac{2}{\alpha}}}{\alpha(\|\mathbf{h}\|^2)^{\frac{2}{\alpha}}(1 + \frac{\epsilon P_T}{M-1}\frac{\|\mathbf{h}\|^2}{\beta})^{M-1}} \gamma\big(\frac{2}{\alpha}, \frac{R^\alpha\|\mathbf{h}\|^2}{\beta}\big). \end{aligned} \tag{2.29}$$

Here $\gamma(\frac{2}{\alpha}, \frac{R^\alpha\|\mathbf{h}\|^2}{\beta})$ is the lower incomplete gamma function and increases monotonically as R increases. (2.29) is similar to (2.20) and is independent of P_T when $\epsilon = 0$. Since $\|\mathbf{h}\|^2 \geq \max_{i \in M} |h_i|^2$, the HD-TAB (even without using AN) results in a better secrecy performance than the HD-TAS. Note that the secrecy performance of the HD-TAB depends on P_T when $\epsilon > 0$. Furthermore, the term $\int_0^R \int_0^{2\pi} \Omega(z; r, \theta) \mathrm{d}\theta r \mathrm{d}r$ is inversely proportional

to the factor $\left(1+\frac{\epsilon P_T\|\mathbf{h}\|^2}{(M-1)g}\right)^{M-1}$. Thus, the term $\int_0^R\int_0^{2\pi}\Omega(z;r,\theta)\mathrm{d}\theta r\mathrm{d}r$ and hence SOP decreases as the number of transmit antenna M increases.

2.4 Secrecy performance of the TAB-US Scheme

In [35], a TAS based downlink transmission scheme for multiple ordered half-duplex receivers or "a TAS based User Selection (US) scheme" was considered. In this section, we consider a TAB based counter part of the above scheme, which will be referred to as the TAB-US scheme.

As shown in Appendix .8, we have

Proposition 3 *For $\epsilon \geq 0$, the probability of achieving a secrecy rate strictly larger than R_s conditional on the distance of a selected user is*

$$\begin{aligned} P[S_{AB} > R_s | d_{AB_n}] &= \exp\left[\frac{-2\pi\rho_E}{\alpha}\frac{(\beta d_{AB_n}^{\alpha})^M B(M-\frac{2}{\alpha},\frac{2}{\alpha})}{(\frac{\epsilon P_T}{M-1})^{M-\frac{2}{\alpha}}}\right. \\ &\times \left. U(M-\tfrac{2}{\alpha}, 2-\tfrac{2}{\alpha}, \tfrac{(M-1)\beta d_{AB_n}^{\alpha}}{\epsilon P_T})\right] \end{aligned} \tag{2.30}$$

where d_{AB_n} is the distance between Alice and the nth closest user, and U denotes the confluent hypergeometric function of the second kind [42].

With $P(S_{AB} > R_s|d_{AB_n})$ and $f_{d_{AB_n}}(x)$ from lemma 7 in Appendix .9, one can readily compute the SOP $P(S_{AB} < R_s) = \int_0^{\infty} P(S_{AB} > R_s|x) f_{d_{AB_n}}(x)dx$ for any ϵ. We will show via simulation that the TAB-US scheme outperforms the TAS-US scheme.

As shown in Appendix .9, for the special case of $\epsilon = 0$, $P(S_{AB} < R_s)$ can be

simplified into:

$$P[S_{AB} > R_s] = \frac{1}{\left(1 + \frac{\rho_E}{\rho_U}\frac{2}{\alpha}\beta^{\frac{2}{\alpha}}B(M - \frac{2}{\alpha}, \frac{2}{\alpha})\right)^n}, \tag{2.31}$$

where $\frac{\rho_E}{\rho_U}$ is the ratio of the density of EDs over that of the legitimate receivers.

Furthermore, for $n = 1$ (the nearest Bob), (2.31) reduces to

$$P[S_{AB} < R_s] = 1 - \frac{1}{1 + \frac{\rho_E}{\rho_U}\frac{2}{\alpha}\beta^{\frac{2}{\alpha}}B(M - \frac{2}{\alpha}, \frac{2}{\alpha})}. \tag{2.32}$$

2.5 Simulations

In this section, we illustrate the secrecy outage probabilities (SOP) of the TAS and TAB schemes against randomly located EDs. Most of our simulation results provide comparisons between TAS and TAB schemes. Moreover, we present the secrecy performance enhancement of the TAB scheme using AN.

Throughout the simulations, we will assume unit noise variance, $\alpha = 2$, $P_T = 40$ dB, $R_D = 4$ b/s/Hz, $\rho_E = 1$, $M = 5$, $d = 1$ and $R = 5$. Unless otherwise specified, we let P_J, ρ and ϵ be 40 dB, 0.01 and 0.01 respectively. Since Alice can estimate the legitimate channel and know the self interference channel of Bob, therefore, we will first study the SOP under conditional $\mathbf{h}$ and g_B for the TAB scheme. Considering $R_D = 4$, ϵ can be set between 0 and 0.53 to maintain a nonzero desired data transmission for the above given ρ and P_J.

In Fig. 2.1, the SOP of the TAS and TAB schemes for non-colluding EDs is illustrated under different values of P_J and ρ. For the TAB scheme, $\epsilon = 0$ is chosen. We see that as ρ decreases, the optimum jamming power increases which results in lower

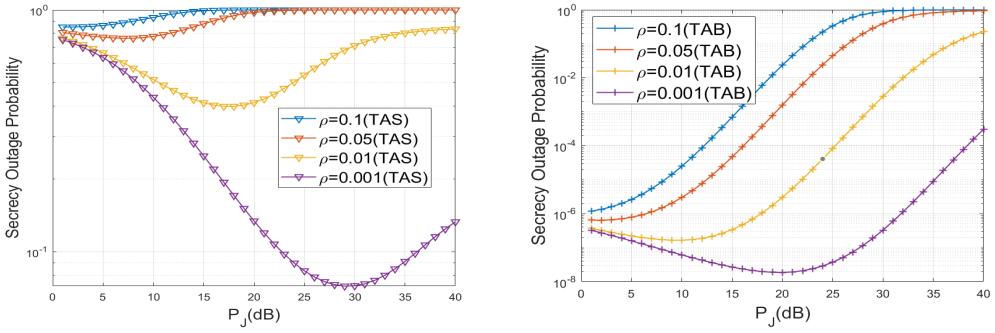

Figure 2.1: Comparison of the TAS and TAB schemes in terms of P_{out} against non-colluding EDs.

SOP for both TAS and TAB schemes. And the TAB scheme outperforms the TAS scheme substantially.

In Fig. 2.2, we compare the Monte Carlo (MC) simulation results (using $N_R = 10^5$ independent runs) with our theoretical results shown in (2.24) where $R = 5$ and $\rho_E = 10$. We observe that the two results match each other very well. This consistency between theory and simulation holds for all other results we have tested under a sufficiently large N_R.

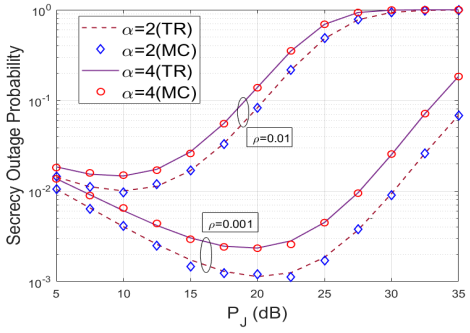

Figure 2.2: Comparison of theoretical results ("TR") and simulation results ("MC") of the TAB scheme in terms of P_{out} versus P_J.

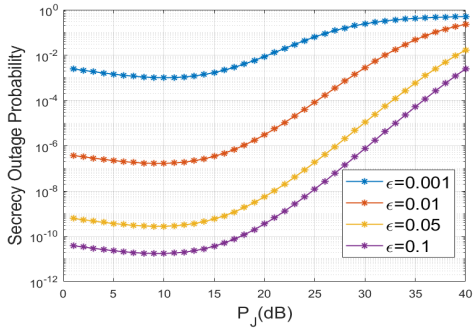

Figure 2.3: Illustration of $P_{out} = 1 - P_{con}$ versus P_J and ϵ for the TAB scheme.

Fig. 2.3 shows the SOP of the TAB scheme with $\epsilon > 0$. We see that the SOP decreases as ϵ increases, the optimal value of P_J is dependent on ϵ but the dependence is rather weak (or not very sensitive).

To illustrate the TAS and TAB schemes with user selection (i.e., TAS-US and TAB-US), we consider $P_T = 50$ dB, $\alpha = 2$, $\beta = 2$, $\epsilon = 0.00001$, $\rho_U = 0.5$ and $\rho_E = 0.1$ unless otherwise specified.

Fig. 2.4 shows the SOP of the TAS-US and TAB schemes for the nearest user. As the number M of transmit antennas increases, the performance gap between TAB-US and TAS-US increases rapidly for $\epsilon > 0$. More importantly, we see that only a small fraction (e.g., $\epsilon = 0.00001$ or $\epsilon P_T = 0$ dB which is at the same level as the noise variance) of the transmit power used for AN makes a huge difference.

Fig. 2.5 illustrates the effects of ED's density ρ_E on the SOP of TAS-US and TAB-US for the nearest user. And Fig. 2.6 illustrates the effects of the users' density ρ_U on the SOP of TAS-US and TAB-US for the nearest user. We see that SOP increases as

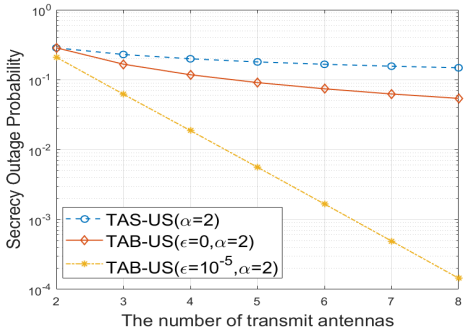

Figure 2.4: SOP of TAS-US and TAB-US for the nearest user vs the number of transmit antennas against non-colluding EDs.

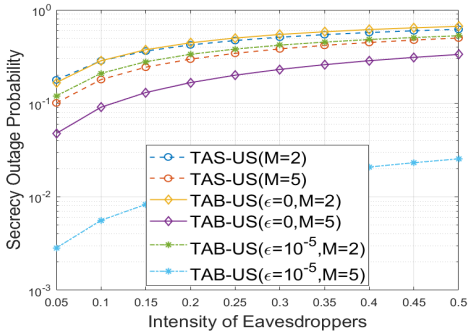

Figure 2.5: SOP vs intensity of eavesdroppers for ordered users against non-colluding EDs.

ρ_E increases but decreases as ρ_U increases. The performance gap between TAS-US and TAB-US remains approximately the same as ρ_E increases but increases as ρ_U increases.

Fig. 2.7 shows the SOP of the TAS-US and TAB-US schemes as functions of the order index (n) of users (from nearest to farthest). We see that the SOP increases as n increases and the performance gap between TAB-US and TAS-US reduces as n increases.

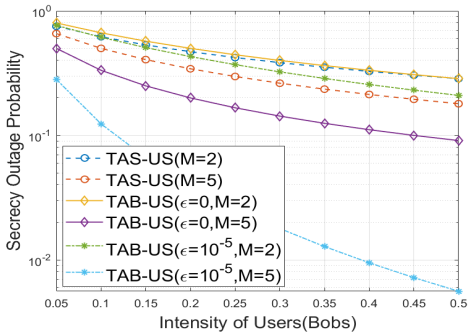

Figure 2.6: SOP vs intensity of users against non-colluding EDs.

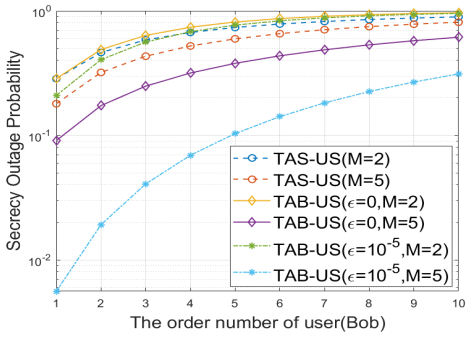

Figure 2.7: SOP vs the order number of user against non-colluding EDs.

Chapter 3

Secrecy Performance Against Colluding Eavesdroppers

3.1 Introduction

In this section, we consider the situation that EDs can share all information to decode the message. Since Alice knows the channel between Alice and Bob, the secrecy performance conditional on $\mathbf{h}$ and g_B is a useful measure. In one coherence period, $\mathbf{h}$ and g_B remains deterministic and study of closed form expression is important to find the optimal resource allocation strategy (i.e., how to choose ϵ and P_J). Considering $\mathbf{h}$ and g_B as deterministic makes the study completely different from that in [33] as the Laplace trick used there can not be directly applied to derive the SOP closed form expression.

3.2 Full-Duplex Bob in the TAS scheme

The SOP against colluding EDs conditional on $\mathbf{h}$ and g_B is

$$\begin{aligned} P[S_{AB}^{TAS} < R_s|\mathbf{h}, g_B] &= P\left[\frac{1+SNR_{AB}^{TAS}}{1+\sum\limits_{e\in\Phi} SNR_{AE_e}^{TAS}} < 2^{R_S}|\mathbf{h}, g_B\right] \\ &= P\left[\sum_{e\in\Phi} \frac{|h_{A_{i^*}E_e}|^2}{\frac{d_{AE_e}^{\alpha}}{P_T} + \frac{d_{AE_e}^{\alpha}}{d_{BE_e}^{\alpha}} mX_2} > y_0\right] \\ &= \int_{y_0}^{\infty} f_{I_e}(x)\mathrm{d}x \end{aligned} \tag{3.1}$$

where $I_e = \sum\limits_{e\in\Phi} SNR_{AE_e}^{TAS} = \sum\limits_{e\in\Phi} \frac{|h_{A_{i^*}E_e}|^2}{\frac{d_{AE_e}^{\alpha}}{P_T} + \frac{d_{AE_e}^{\alpha}}{d_{BE_e}^{\alpha}} mX_2}$ which is the sum of SNRs at all EDs. It is shown in Appendix .10 that the Laplace transform of the PDF of I_e is

$$\mathcal{L}_{I_e}(s) = \exp\Big[-\rho_E \int_0^R \int_0^{2\pi} \frac{s}{f_e} \mathbf{E_1}(K(s)) e^{K(s)} \mathrm{d}\theta r \mathrm{d}r\Big] \tag{3.2}$$

where $\mathbf{E_1}(a) = \int_0^{\infty} \frac{e^{-ax}}{1+x}\mathrm{d}x$ is the so called exponential integral function of a and $K(s) = \frac{s+\frac{d_{AE_e}^{\alpha}}{P_T}}{f_e}$. Note that $\mathbf{E_1}(a)$ is monotonically decreasing function of a, and $K(s)$ is a strictly positive quantity. Later, we will discuss the relationship between $\mathbf{E_1}(K(s))$ and SOP.

We know that

$$\begin{aligned} & P[S_{AB}^{TAS} < R_s|\mathbf{h}, g_B] = P[\frac{I_e}{y_0} > 1] \\ & \lessapprox P[\frac{I_e}{y_0} > l] \\ & = \mathbb{E}\big[1 - \exp(-\frac{aI_e}{y_0})\big]^N \\ & = \mathbb{E}\left[\sum_{n=0}^{N} \binom{N}{n} (-1)^n \exp(-\frac{an}{y_0} I_e)\right] \\ & = \sum_{n=0}^{N} \binom{N}{n} (-1)^n \mathcal{L}_{I_e}(\frac{an}{y_0}), \end{aligned} \tag{3.3}$$

where $\lessapprox$ denotes "less than and asymptotically equal to", and l is a normalized gamma distributed random variable with the shape parameter N, and as $N \to \infty$, l approaches its upper bound equal to 1 [39]-[41]. (Note that the left side of $\lessapprox$ is less than the right side if N is finite, or equals to the right side if $N \to \infty$.) Also $a = \frac{N}{(N!)^{\frac{1}{N}}}$, and y_0 is a realization of Y.

From (3.2) and (3.3), we have

Proposition 4 *For the TAS scheme,*

$$P[S_{AB}^{TAS} < R_s|\mathbf{h}, g_B] \lessapprox \sum_{n=0}^{N} \binom{N}{n} (-1)^n \exp\Bigg[-\rho_E \int_0^R \int_0^{2\pi} \frac{s}{f_e} \mathbf{E_1}(K(s)) e^{K(s)} \, d\theta r \, dr \Bigg]\Bigg|_{s=\frac{an}{y_0}} \tag{3.4}$$

where $s = \frac{an}{y_0}$, $K(s) = K(s)\big|_{s=\frac{an}{y_0}} = K(s)\big|_{s=\frac{an}{\frac{y}{\beta}-1+\frac{1}{\beta}}} = \frac{d_{BEe}^{\alpha}}{P_J} + \frac{s}{f_e} = \frac{d_{BEe}^{\alpha}}{P_J} + \frac{an}{f_e y_0}$. *If* $\beta = 1$, *we have* $y_0 = y$ *and then* $K(s) = \frac{d_{BEe}^{\alpha}}{P_J} + an \frac{d_{BEe}^{\alpha}}{d_{AEe}^{\alpha}} \frac{\frac{1}{P_J} + \rho |g_B|^2}{\max\limits_{i \in M} |h_i|^2}$ *which is independent of* P_T.

Remark 5 *The secrecy performance is dependent on* P_J *throughout the term* $\Xi(s, r, \theta)|_{s=\frac{an}{y_0}} = \frac{s}{f_e} \mathbf{E_1}(K(s)) e^{K(s)}|_{s=\frac{an}{y_0}}$. *One can verify that as* P_J *increases,*

- $\frac{s}{f_e} e^{K(s)}$ *decreases monotonically and saturates to a lower bound.*
- $\mathbf{E_1}(K(s))$ *increases monotonically and saturates to an upper bound.*

These statements indicate that finding the optimal P_J to minimize $\Xi(s, r, \theta)|_{s=\frac{an}{y_0}}$ is similar to that of $\Psi(Y, r, \theta)$ for the non-colluding TAS scheme. A comparison between $\Psi(Y, r, \theta)$ and $\Xi(s, r, \theta)|_{s=\frac{an}{y_0}}$ is shown in Table 3.1. Note that, optimum jamming power $P_J{}^*$ is not necessarily the same for $\Psi(Y, r, \theta)$ and $\Xi(s, r, \theta)|_{s=\frac{an}{y_0}}$. Finally, simulation result

Table 3.1: Comparison between $\Psi(Y,r,\theta)$ and $\Xi(s,r,\theta)|_{s=\frac{an}{y_0}}$ subject to $R_s=0$. The column for $P_J\to\infty$ is subject to a fixed ρP_J.

	P_T	$P_J\to\infty$	$P_J\uparrow(\leq {P_J}^*)$	$P_J\uparrow(\geq {P_J}^*)$
$\Psi(Y,r,\theta)$	$-$	$\to 0$	$\downarrow$	$\uparrow$
$\Xi(s,r,\theta)\|_{s=\frac{an}{y_0}}$	$-$	$\to const.$	$\downarrow$	$\uparrow$

shows that as P_J increases, the conditional SOP in (3.4) achieves its minimum at a finite nonzero P_J.

3.2.1 Half-Duplex Bob in TAS scheme

If Bob is in the HD mode, then the sum of ED's SNR is $I_e^{HD}=\sum\limits_{e\in\Phi}\frac{X_{1,e}^{'}P_T}{d_{AE_e}^{\alpha}}$, where $X_{1,e}^{'}$ is exponentially distributed with unit mean. One can verify that the Laplace transform of the PDF of I_e^{HD} is

$$\begin{aligned}\mathcal{L}_{I_e^{HD}}(s)&=E_\Phi\Big[\prod_{e\in\Phi}\frac{1}{1+\frac{sP_T}{d_{AE_e}^{\alpha}}}\Big]\\&=\exp\Big[-\rho_E\pi R^2\mathbf{F}(1,\frac{2}{\alpha};1+\frac{2}{\alpha};-\frac{R^\alpha}{sP_T})\Big]\end{aligned}\tag{3.5}$$

where $\mathbf{F}(1,\frac{2}{\alpha};1+\frac{2}{\alpha};-\frac{R^\alpha}{sP_T})$ is known as the Gaussian hypergeometric function. Note that α is governed by the environment. So, only the last parameter $\frac{R^\alpha}{sP_T}$ in $\mathbf{F}(1,\frac{2}{\alpha};1+\frac{2}{\alpha};-\frac{R^\alpha}{sP_T})$ is controllable via P_T, which takes real value between 0 to ∞. One can verify that $\frac{R^\alpha}{sP_T}$ is independent of P_T for $\beta=1$, which is similar as non-colluding HD TAS scheme.

Replacing $\mathcal{L}_{I_e}$ in (3.3) by $\mathcal{L}_{I_e^{HD}}$ in (3.5) yields

$$\begin{aligned}P[S_{AB}^{TAS}<R_s|\mathbf{h},g_B]\lessapprox\sum_{n=0}^{N}\binom{N}{n}(-1)^n\exp\Big[-\rho_E\pi R^2\\\mathbf{F}(1,\frac{2}{\alpha};1+\frac{2}{\alpha};-\frac{R^\alpha}{sP_T})\Big]\Big|_{s=\frac{an}{y_0}}\end{aligned}\tag{3.6}$$

where $s = \frac{an}{y_0}$. The result in (3.6) is that in (3.4) with $P_J = 0$ but the former is a much simplified form than the latter.

3.3 Full-Duplex Bob in TAB scheme without AN from Alice

Conditional on $\mathbf{h}$ and g_B, the legitimate channel's SNR is z as previously defined. For $\epsilon = 0$ (i.e., without AN from Alice), the SNR at the eth Eve is (from (2.11)):

$$\begin{aligned} SNR_{AE_e}^{TAB} &= \frac{X_1\Theta}{\frac{d_{AE_e}^{\alpha}}{P_T} + m\frac{d_{AE_e}^{\alpha}}{d_{BE_e}^{\alpha}}X_2} \\ &= \frac{X_4}{\frac{d_{AE_e}^{\alpha}}{P_T} + m\frac{d_{AE_e}^{\alpha}}{d_{BE_e}^{\alpha}}X_2}. \end{aligned} \tag{3.7}$$

Similar to the analysis leading to (3.4), the SOP now is still given by (3.4) but with $s = \frac{an}{\frac{z}{\beta}-1+\frac{1}{\beta}}$. Hence, we have:

Proposition 5 *For the TAB scheme with $\epsilon = 0$,*

$$\begin{aligned} P[S_{AB}^{TAB} < R_s|\mathbf{h}, g_B] \lessapprox \sum_{n=0}^{N} \binom{N}{n} (-1)^n \exp\Bigg[-\rho_E \\ \int_0^R \int_0^{2\pi} \frac{s}{f_e} \mathbf{E_1}(K(s)) e^{K(s)} d\theta r\, dr \Bigg]\Bigg|_{s=\frac{an}{\frac{z}{\beta}-1+\frac{1}{\beta}}}. \end{aligned} \tag{3.8}$$

Since $\|\mathbf{h}\|^2 \geq \max_{i\in M} |h_i|^2$, the TAB scheme always outperforms the TAS scheme.

Bob in Half-Duplex Mode

In this case, we have $P_J = 0$ and $z = P_T\|\mathbf{h}\|^2$. The SOP expression is similar to (3.6) and can be expressed as

$$P[S_{AB}^{TAB} < R_s|\mathbf{h}, g_B] \lessapprox \sum_{n=0}^{N} \binom{N}{n}(-1)^n \exp\Big[- \rho_E \pi R^2 \mathbf{F}(1, \frac{2}{\alpha}; 1+\frac{2}{\alpha}; -\frac{R^\alpha}{sP_T})\Big]\Big|_{s=\frac{an}{\frac{z}{\beta}-1+\frac{1}{\beta}}}. \tag{3.9}$$

3.4 Full-Duplex Bob in TAB scheme with AN from Alice

For the TAB scheme with $\epsilon > 0$, we have

$$\begin{aligned} P[S_{AB}^{TAB} < R_s|\mathbf{h}, g_B] &= P[\frac{1+SNR_{AB}^{TAB}}{1+\sum\limits_{e\in\Phi} SNR_{AE_e}^{TAB}} < 2^{R_S}|\mathbf{h}, g_B] \\ &\overset{(a)}{\lessapprox} P[\sum_{e\in\Phi} \frac{X_4}{\frac{\epsilon}{M-1}X_{4,4}+f_eX_2} > \frac{z}{\beta} + \frac{\frac{1}{\beta}-1}{1-\epsilon}] \\ &\overset{(b)}{\lessapprox} \sum_{n=0}^{N} \binom{N}{n}(-1)^n \mathcal{L}_{\tilde{I}_e}\big(\frac{an}{\frac{z}{\beta}+\frac{\frac{1}{\beta}-1}{1-\epsilon}}\big) \end{aligned} \tag{3.10}$$

where the parameters defined after (2.13) have been applied and $\tilde{I}_e = \sum\limits_{e\in\Phi} \frac{X_4}{\frac{\epsilon}{M-1}X_{4,4}+f_eX_2}$. Here, (a) is due to neglecting the background noise $n_{A,E_e}(k)$ at Eve (but not the noise at Bob), and (b) is due to the application of the normalized gamma random variable as discussed before. Similar to that in Appendix .10, one can verify

$$\mathcal{L}_{\tilde{I}_e}(s) = \exp\Big[- \rho_E s \int_0^R \int_0^{2\pi} \int_{x=0}^{\infty} \frac{e^{-sx}}{(1+f_ex)} \times \frac{1}{(1+\frac{\epsilon}{M-1}x)^{M-1}} \mathrm{d}x\mathrm{d}\theta r\mathrm{d}r\Big]. \tag{3.11}$$

3.5 Simulations

In this section, we consider the TAB and TAS schemes for colluding EDs. Throughout the simulations, we will assume unit noise variance, $\alpha = 2$, $P_T = 40$ dB, $R_D = 4$ b/s/Hz, $\rho_E = 1$, $M = 5$, $d = 1$ and $R = 5$. Unless otherwise specified, we let P_J, ρ and ϵ be 40 dB, 0.01 and 0.01 respectively. Since Alice can estimate the legitimate channel and know the self interference channel of Bob, therefore, we will first study the SOP under conditional $\mathbf{h}$ and g_B for the TAB scheme. We assume that there are two circles of radii R_g and R around Alice, and EDs exist and collude within the two circles. In our experiment, we let $R_g = 0.1$ and $R = 5$. Although the closed form expressions of the SOP in this case are all in series expansions, choosing $N = 20$ (e.g., see (3.4)) provided good approximations.

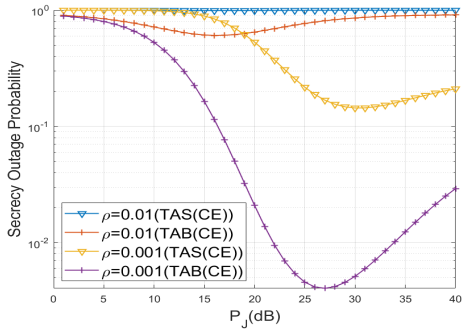

Figure 3.1: Comparison of the TAB and TAS schemes in terms of P_{out} against colluding EDs.

Fig. 3.1 shows the SOP of TAS and TAB schemes for colluding EDs as functions of the self-interference power gain ρ and the jamming power P_J from full-duplex Bob. We see that the optimal P_J increases as the self-interference power gain ρ decreases, and the optimized SOP reduces significantly as ρ decreases.

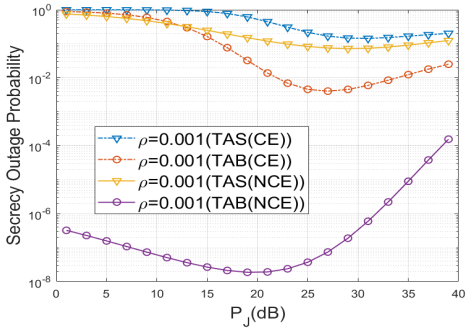

Figure 3.2: Comparison of the TAB and TAS schemes in terms of P_{out} against colluding and non-colluding EDs.

Finally, Fig. 3.2 illustrates the differences of SOP for colluding and non-colluding EDs. We see that the performance gap between colluding and non-colluding is large. But the TAB scheme is consistently better than the TAS scheme in terms of SOP.

Chapter 4

Secrecy Throughput of ANECE Assisted Transmission of Information in Finite Blocklength

4.1 Introduction

This chapter presents a secure uplink communication system where multiple single antenna users send information to a full-duplex multi-antenna access point (AP) under ultra reliable and low-latency communication (uRLLC) system requirement. To meet uRLLC requirement and provide secrecy against multi-antenna Eve, users adopt a special channel training scheme called Anti-eavesdropping channel estimation (ANECE) during pilot transmission phase and later transmit secret information in short blocklength regime. In this ANECE scheme, one or more cooperative users along with one full-duplex AP obtain their

receive channel state information (CSI) with respect to each other while preventing eavesdropper (Eve) from obtaining any consistent estimate of its receive CSI. The relatively improved CSI estimation at legitimate nodes enhances the secrecy of subsequent transmission of information between user and AP. In this paper, we propose an analytical framework to derive the closed form expression of average secrecy throughput (AST) of ANECE assisted transmission of information between users and AP against Eve with multiple antennas. Our closed form expression of approximated AST in terms of blocklegth and various controllable parameters provides useful insights to maximize AST under uRLLC requirement. Furthermore, we showed the performance of the proposed algorithms through extensive simulations under various settings of transmit power budget, number of users, transmission time, number of transmit antennas at the BS and number of transmit antennas at the Eve. Finally, we verify our theoretical results of approximated AST with Monte Carlo simulations and illustrate the impact of the system parameters on the tradeoff between transmission latency and reliability under a secrecy constraint.

4.2 System Model

We consider N single-antenna cooperative full-duplex devices/users subject to a covert/passive eavesdropper (Eve) with N_E antennas in unknown location. To combat eavesdropping, all users apply anti-eavesdropping channel estimation (ANECE) [30] as follows. In phase 1, all users transmit ANECE pilots simultaneously, where the pilot transmitted by user j over n_1 slots is denoted by $p_j(k)$ with $k = 1, \cdots, n_1$ and $n_1 \geq N - 1$. The pilots can be also represented by $\mathbf{p}_j = [p_j(1), .., p_j(n_1)]^T$ for all j and $\mathbf{P} = [\mathbf{p}_1, .., \mathbf{p}_N]^T$. For

ANECE, we need $rank(\mathbf{P}) = rank(\mathbf{P}_{(i)}) = N-1$ for all i where $\mathbf{P}_{(i)}$ results from removing the ith row of $\mathbf{P}$. The reduced-rank condition of $\mathbf{P}$ and the full-rank condition of $\mathbf{P}_{(i)}$ for all i are the required properties of the ANECE pilots. An example of $\mathbf{P}$ is $\mathbf{P} = \mathbf{DQV}$ where $\mathbf{D}$ is a diagonal matrix for power control, $\mathbf{Q}$ is a $N \times (N-1)$ submatrix of the $N \times N$ discrete Fourier transform (DFT) matrix and $\mathbf{V}$ is a $(N-1) \times n_1$ matrix satisfying $\mathbf{V}\mathbf{V}^H = \mathbf{I}_{N-1}$, e.g., see [30], [48]. We will assume that each row of $\mathbf{P}$ has the squared norm equal to $P_1 n_1$.

Then, in phase 1, the $n_1 \times 1$ signal vector received by user i is

$$\mathbf{y}_i = \sum_{j \neq i}^{N} h_{i,j}\mathbf{p}_j + \mathbf{n}_i = \mathbf{P}_{(i)}^T \mathbf{h}_{(i)} + \mathbf{n}_i, \tag{4.1}$$

where $h_{i,j}$ is the complex channel gain from user j to user i, $\mathbf{P}_{(i)}$ is $\mathbf{P}$ without the row $\mathbf{p}_i^T$, $\mathbf{h}_{(i)}$ is the vertical stack of $h_{i,j}$ for all $j \neq i$, and $\mathbf{n}_i$ is the background noise (including residual self-interference of the full-duplex user). We assume that $h_{i,j}$ equals $h_{j,i}$ (reciprocal channels), $h_{i,j}$ is $\mathcal{CN}(0, \sigma_{i,j}^2)$, and $\mathbf{n}_i$ is $\mathcal{CN}(\mathbf{0}, \mathbf{I})$. In phase 1, the $N_E \times n_1$ signal matrix received by Eve can be expressed as

$$\mathbf{Y}_E = \sum_{i=1}^{N} \mathbf{h}_{E,i}\mathbf{p}_i^T + \mathbf{N}_E = \mathbf{H}_E\mathbf{P} + \mathbf{N}_E, \tag{4.2}$$

where $\mathbf{h}_{E,i}$ is the channel vector from user i to Eve, and $\mathbf{H}_E$ (Eve's receive channel matrix or CSI) is the horizontal stack of $\mathbf{h}_{E,i}$ for all i.

As shown next, the ANECE pilots allow every user to have a consistent estimation of their channel gains but do not allow Eve to have a consistent estimation of Eve's receive channel matrix.

4.2.1 Effect of the ANECE Pilots

We will consider minimum-mean-squared-error (MMSE) channel estimation at users and Eve. Let $\mathbf{K}_{\mathbf{x},\mathbf{y}} = \mathcal{E}[\mathbf{x}\mathbf{y}^H]$ denote the correlation matrix between two random vectors $\mathbf{x}$ and $\mathbf{y}$, and $\mathbf{K}_{\mathbf{x},\mathbf{x}} = \mathbf{K}_{\mathbf{x}}$. Then the MMSE estimate of the channel vector $\mathbf{h}_{(i)}$ at user i is

$$\begin{aligned}\hat{\mathbf{h}}_{(i)} &= \mathbf{K}_{\mathbf{h}_{(i)},\mathbf{y}_i}\mathbf{K}_{\mathbf{y}_i}^{-1}\mathbf{y}_i \\ &= \mathbf{\Sigma}_{(i)}^2\mathbf{P}_{(i)}^*(\mathbf{I}_{n_1} + \mathbf{P}_{(i)}^T\mathbf{\Sigma}_{(i)}^2\mathbf{P}_{(i)}^*)^{-1}\mathbf{y}_i \\ &= \mathbf{\Sigma}_{(i)}\big(\mathbf{I}_{N-1} + \mathbf{\Sigma}_{(i)}\mathbf{P}_{(i)}^*\mathbf{P}_{(i)}^T\mathbf{\Sigma}_{(i)}\big)^{-1}\mathbf{\Sigma}_{(i)}\mathbf{P}_{(i)}^*\mathbf{y}_i, \end{aligned} \tag{4.3}$$

where $\mathbf{\Sigma}_{(i)}^2 = diag\{\sigma_{i,1}^2, \cdots, \sigma_{i,i-1}^2, \sigma_{i,i+1}^2, \cdots, \sigma_{i,N}^2\}$. The $(N-1)\times(N-1)$ covariance matrix of the MMSE error vector $\Delta\mathbf{h}_{(i)} = \hat{\mathbf{h}}_{(i)} - \mathbf{h}_{(i)}$ is

$$\begin{aligned}\mathbf{K}_{\Delta\mathbf{h}_{(i)}} &= \mathbf{K}_{\mathbf{h}_{(i)}} - \mathbf{K}_{\mathbf{h}_{(i)},\mathbf{y}_i}\mathbf{K}_{\mathbf{y}_i}^{-1}\mathbf{K}_{\mathbf{y}_i,\mathbf{h}_{(i)}} \\ &= \mathbf{\Sigma}_{(i)}^2 - \mathbf{\Sigma}_{(i)}^2\mathbf{P}_{(i)}^*(\mathbf{I}_{n_1} + \mathbf{P}_{(i)}^T\mathbf{\Sigma}_{(i)}^2\mathbf{P}_{(i)}^*)^{-1}\mathbf{P}_{(i)}^T\mathbf{\Sigma}_{(i)}^2 \\ &= \mathbf{\Sigma}_{(i)}\big(\mathbf{I}_{N-1} + \mathbf{\Sigma}_{(i)}\mathbf{P}_{(i)}^*\mathbf{P}_{(i)}^T\mathbf{\Sigma}_{(i)}\big)^{-1}\mathbf{\Sigma}_{(i)}. \end{aligned} \tag{4.4}$$

Let $\beta_{i,l} = (\mathbf{K}_{\Delta\mathbf{h}_{(i)}})_{l,l}$ be the l-th diagonal element of $\mathbf{K}_{\Delta\mathbf{h}_{(i)}}$, which is the MMSE estimation error variance of the channel between user i and a user $j \neq i$. In Appendix .11, we show that as $n_1P_1 \to \infty$, then $\beta_{i,l} \to 0$ for all i and l.

Assume that Eve also applies MMSE for channel estimation. Let $\mathbf{y}_E = vec(\mathbf{Y}_E)$ and $\mathbf{h}_E = vec(\mathbf{H}_E)$. Then (5.4) becomes

$$\mathbf{y}_E = (\mathbf{P}^T \otimes \mathbf{I}_{N_E})\mathbf{h}_E + \mathbf{n}_E. \tag{4.5}$$

The MMSE estimate of $\mathbf{h}_E$ (assuming $\mathbf{P}$ is also known to Eve) is

$$\begin{aligned}\hat{\mathbf{h}}_E &= \mathbf{K}_{\mathbf{h}_{E,i},\mathbf{y}_E}\mathbf{K}_{\mathbf{y}_E}^{-1}\mathbf{y}_E \\ &= (\mathbf{\Sigma}_E^2\mathbf{P}^*(\mathbf{I}_{n_1}+\mathbf{P}^T\mathbf{\Sigma}_E^2\mathbf{P}^*)^{-1}\otimes\mathbf{I}_{N_E})\mathbf{y}_E, \end{aligned} \tag{4.6}$$

where $\mathbf{\Sigma}_E^2 = diag\{\sigma_{E,1}^2,\cdots,\sigma_{E,N}^2\}$. The covariance matrix of $\Delta\mathbf{h}_E = \hat{\mathbf{h}}_E - \mathbf{h}_E$ is

$$\begin{aligned}\mathbf{K}_{\Delta\mathbf{h}_E} &= \mathbf{\Sigma}_E^2\otimes\mathbf{I}_{N_E} - \mathbf{K}_{\mathbf{h}_E,\mathbf{y}_E}\mathbf{K}_{\mathbf{y}_E}^{-1}\mathbf{K}_{\mathbf{y}_E,\mathbf{h}_E} \\ &= \mathbf{\Sigma}_E^2(\mathbf{I}_{N_E}-\mathbf{P}^*(\mathbf{I}_{n_1}+\mathbf{P}^T\mathbf{\Sigma}_E^2\mathbf{P}^*)^{-1}\mathbf{P}^T\mathbf{\Sigma}_E^2)\otimes\mathbf{I}_{N_E} \\ &= \mathbf{\Sigma}_E(\mathbf{I}_N+\mathbf{\Sigma}_E\mathbf{P}^*\mathbf{P}^T\mathbf{\Sigma}_E)^{-1}\mathbf{\Sigma}_E\otimes\mathbf{I}_{N_E}, \end{aligned} \tag{4.7}$$

where $\beta_{E,i} = (\mathbf{\Sigma}_E(\mathbf{I}_N+\mathbf{\Sigma}_E\mathbf{P}^*\mathbf{P}^T\mathbf{\Sigma}_E)^{-1}\mathbf{\Sigma}_E)_{i,i}$ being the variance of each elements of $\Delta\mathbf{h}_{E,i}$. It is shown in Appendix .11 that as $n_1P_1\to\infty$, we have $\beta_{E,i}\to c_i>0$ where c_i is invariant to n_1P_1.

4.2.2 SNRs at Bob and Eve

In phase 1, ANECE is applied cooperatively by N users as shown previously. We now consider phase 2 where we assume an information transmission between a pair of users. Assume that user i (Alice) transmits the information symbols $x_i(k), k=1,\cdots,n_2$ to user j (Bob) with transmit power P_2. Then the received signal at Bob is

$$y_j(k) = h_{j,i}x_i(k)+n_j(k) = \hat{h}_{j,i}x_i(k)+\Delta h_{j,i}x_i(k)+n_j(k). \tag{4.8}$$

The SNR of $y_j(k)$ is $\gamma_b = \frac{(\sigma_{i,j}^2-\beta_{i,l_j})P_2X_{2,b}}{1+\beta_{i,l_j}P_2X_{1,b}}$ where $X_{1,b} = \frac{|\Delta h_{j,i}|^2}{\beta_{i,l_j}}$ and $X_{2,b} = \frac{|\hat{h}_{j,i}|^2}{\sigma_{i,j}^2-\beta_{i,l_j}}$ are independent exponentially distributed random variables with unit means.

Similarly, in phase 2, Eve receives

$$\mathbf{y}_{E,i}(k) = \hat{\mathbf{h}}_{E,i}x_i(k)+\Delta\mathbf{h}_{E,i}x_i(k)+\mathbf{n}_E(k). \tag{4.9}$$

Since Eve knows $\hat{\mathbf{h}}_{E,i}$, we assume that Eve applies the maximum ratio combining to achieve a maximum SNR equal to

$$\gamma_e = \frac{\|\hat{\mathbf{h}}_{E,i}\|^2 P_2}{1 + \|\frac{\hat{\mathbf{h}}_{E,i}^H}{|\hat{\mathbf{h}}_{E,i}|}\Delta\mathbf{h}_{E,i}\|^2 P_2} = \frac{(\sigma_{E,i}^2 - \beta_{E,i})P_2 X_{2,e}}{1 + \beta_{E,i} P_2 X_{1,e}}, \tag{4.10}$$

where $X_{1,e} = \|\frac{\hat{\mathbf{h}}_{E,i}^H}{|\hat{\mathbf{h}}_{E,i}|}\frac{\Delta\mathbf{h}_{E,i}}{\sqrt{\beta_{E,i}}}\|^2$ is exponentially distributed with unit mean and $X_{2,e} = \frac{\|\hat{\mathbf{h}}_{E,i}\|^2}{\sigma_{E,i}^2 - \beta_{E,i}}$ follows Chi-squared distribution with $2N_E$ degrees of freedom (DoF). We will also assume that Eve applies a conventional method to detect the information transmitted by Alice. In other words, Eve treats $\hat{\mathbf{h}}_{E,i}$ as the true channel vector with respect to user i.

4.2.3 Achievable Secrecy Rate under FBL

For a finite-block-length (FBL) transmission with $n_2 < \infty$, there are decoding errors at both Bob and Eve. The maximal achievable secrecy rate $R(n_2, \epsilon, \delta)$ with the decoding error probability ϵ at Bob and the information leakage δ to Eve can be approximated (according to [56]-[57]) as follows

$$R(n_2, \epsilon, \delta) = \log\left(\frac{1+\gamma_b}{1+\gamma_e}\right) - \sqrt{\frac{V_b}{n_2}}\frac{Q^{-1}(\epsilon)}{\ln 2} - \sqrt{\frac{V_e}{n_2}}\frac{Q^{-1}(\delta)}{\ln 2}, \tag{4.11}$$

where V_b and V_e are the channel dispersions at Bob and Eve respectively, which can be expressed by $V_x = 1 - (1+\gamma_x)^{-2}$ with $x \in \{b, e\}$. It is typical to choose $\delta \in (0, 1/2)$. Let the number of secret information bits transmitted by Alice in every n_2 time slots be n_b. Then, $R(n_2, \epsilon, \delta) = \frac{n_b}{n_2}$, and (5.16) implies

$$\epsilon = Q\left(\sqrt{\frac{n_2}{V_b}}\left(\ln(\frac{1+\gamma_b}{1+\gamma_e}) - \sqrt{\frac{V_e}{n_2}}Q^{-1}(\delta) - \frac{n_b}{n_2}\ln 2\right)\right), \tag{4.12}$$

where the decoding error probability $\epsilon \triangleq \epsilon(\gamma_b, \gamma_e)$ is a function of γ_b and γ_e.

Similar to [55] and [58], we consider an averaged achievable secrecy throughput (in bits per channel use) defined by

$$T_s \triangleq \mathbb{E}_{\gamma_b \geq \gamma_e}\left[\frac{n_b}{n_2}(1-\epsilon_{\gamma_b,\gamma_e})\right] \tag{4.13}$$

where we have excluded the contribution from $\gamma_b < \gamma_e$. Treating γ_b and γ_e as independent random variables, it follows that

$$\begin{aligned} T_s &= \frac{n_b}{n_2}\int_{y=0}^{\infty}\left(\int_{x=y}^{\infty}\big(1-\epsilon(x,y)\big)f_{\gamma_b}(x)\mathrm{d}x\right)f_{\gamma_e}(y)\mathrm{d}y \\ &= \frac{n_b}{n_2}\int_{y=0}^{\infty}\Phi(y)f_{\gamma_e}(y)\mathrm{d}y, \end{aligned} \tag{4.14}$$

where

$$\Phi(y) = \int_{x=y}^{\infty}\big(1-\epsilon(x,y)\big)f_{\gamma_b}(x)\mathrm{d}x. \tag{4.15}$$

The rest of the paper focuses on the computational simplification of T_s and the numerical investigation of the tradeoffs among n_1, n_2, n_b, N, N_E on T_s.

4.3 Averaged Secrecy Throughput

To compute the averaged secrecy throughput T_s, we need to compute (5.20) first where $\epsilon(x,y)$ makes the integral an intractable task. Like [54]-[55], we will use the following approximation of $\epsilon(x,y)$:

$$\epsilon(x,y) \approx \begin{cases} 1, & x < x_0 + \frac{1}{2k} \\ \frac{1}{2} + k(x-x_0), & x_0 + \frac{1}{2k} \leq x \leq x_0 - \frac{1}{2k} \\ 0, & x > x_0 - \frac{1}{2k} \end{cases} \tag{4.16}$$

where x_0 is such that $\epsilon(x_0, y) = 0.5$, i.e., $x_0 = \exp\left(\sqrt{\frac{V_e}{n_2}}Q^{-1}(\delta) + \frac{n_b}{n_2}\ln 2\right)(1+y) - 1$, and $k = \frac{d\epsilon(x,y)}{dx}|_{x=x_0} = -\sqrt{\frac{n_2}{2\pi x_0(x_0+2)}}$. This approximation holds well if $|k|$ is large. Assuming a large $|k|$, it follows from (5.21) and (5.20) that

$$\begin{aligned}\Phi(y) &\approx \int_{x_0+\frac{1}{2k}}^{\infty}(1-\epsilon(x,y))f_{\gamma_b}(x)\mathrm{d}x \\ &= 1 - F_{\gamma_b}\left(x_0+\frac{1}{2k}\right) - \int_{x_0+\frac{1}{2k}}^{x_0-\frac{1}{2k}}\left(\frac{1}{2}+k(x-x_0)\right) \\ &\quad \times f_{\gamma_b}(x)\mathrm{d}x \\ &= 1 + k\int_{x_0+\frac{1}{2k}}^{x_0-\frac{1}{2k}} F_{\gamma_b}(x)\mathrm{d}x, \end{aligned} \tag{4.17}$$

where $F_{\gamma_b}(x)$ is the CDF of γ_b. Since $|k|$ is large, we have $\int_{x_0+\frac{1}{2k}}^{x_0-\frac{1}{2k}} F_{\gamma_b}(x)dx \approx \frac{-1}{k}F_{\gamma_b}(x_0)$ and hence

$$\Phi(y) \approx 1 - F_{\gamma_b}(x_0). \tag{4.18}$$

where $x_0 \stackrel{\Delta}{=} x_0(y)$ is a function of y.

From Appendix .12, we have $F_{\gamma_b}(x) = 1 - \frac{a_j}{a_j+x}e^{-\frac{b_j}{a_j}x}$ where $a_j = \frac{\sigma_{j,i}^2}{\beta_{j,i}} - 1$ and $b_j = \frac{1}{\beta_{j,i}P_2}$. Thus, (5.22) becomes

$$\Phi(y) \approx \frac{a_j}{a_j + x_0(y)}e^{-\frac{b_j}{a_j}x_0(y)}. \tag{4.19}$$

From (5.19), for any $\gamma_1 > 0$, we have

$$T_s = \underbrace{\frac{n_b}{n_2}\int_{y=0}^{\gamma_1}\Phi(y)f_{\gamma_e}(y)\mathrm{d}y}_{T_1} + \underbrace{\frac{n_b}{n_2}\int_{y=\gamma_1}^{\infty}\Phi(y)f_{\gamma_e}(y)\mathrm{d}y}_{T_2}. \tag{4.20}$$

To compute T_1, we let $g(y) = \Phi(y)f_{\gamma_e}(y)$. Then using the Gaussian-Chebyshev quadrature method [59], it follows that

$$T_1 \approx \frac{n_b}{n_2}\frac{\gamma_1}{2}\sum_{n=1}^{M}\left(\frac{\pi}{M}g\big(\frac{\gamma_1}{2}(t_n+1)\big)\sqrt{1-t_n^2}\right), \tag{4.21}$$

where $t_n \triangleq cos(\frac{2n-1}{2M}\pi)$ and the parameter M determines the complexity and accuracy trade-off.

To compute T_2, we simplify $x_0(y)$ by choosing γ_1 sufficiently large such that $V_e = 1-(1+y)^{-2} \approx 1$ for $y \geq \gamma_1$, which implies $x_0(y) \approx \alpha(1+y)-1$ with constant $\alpha = \exp\left(\frac{Q^{-1}(\delta)}{\sqrt{n_2}} + \ln 2\frac{n_b}{n_2}\right)$. Then, it follows that

$$T_2 \approx \frac{n_b}{n_2} e^{-\frac{b_j}{a_j}(\alpha-1)} \int_{y=\gamma_1}^{\infty} \frac{a_j e^{-\frac{b_j}{a_j}\alpha y}}{\alpha y + \alpha - 1 + a_j} f_{\gamma_e}(y)\mathrm{d}y. \tag{4.22}$$

To further simplify T_2, we will consider two special cases: Case 1 is for $\beta_{E,i}P_2 \ll 1$, and Case 2 is for $\beta_{E,i}P_2 \gg 1$. Case 1 applies when ANECE is not applied, and Case 2 applies when ANECE is applied. In both cases, we will use $\gamma = \alpha\gamma_1 + \alpha - 1$ to simplify equations.

4.3.1 Case 1

In this case, $\beta_{E,i}P_2 \ll 1$ and Eve mainly suffers from the channel background noise. Using $b_x = b_e \to \infty$ in Appendix .12, the PDF of γ_e is $f_{\gamma_e}(x) = \frac{\mathrm{d}F_{X_2}(\frac{x}{(\sigma^2_{E,i}-\beta_{E,i})P_2})}{dx} = (\frac{b_e}{a_e})^{N_E}\frac{x^{N_E-1}e^{-\frac{b_e}{a_e}x}}{\Gamma(N_E)}$ where $a_e = \frac{\sigma^2_{E,i}}{\beta_{E,i}} - 1$ and $b_e = \frac{1}{\beta_{E,i}P_2}$. Then the integral in (4.22) can be expressed in terms of Γ functions and, as shown in Appendix .13, (4.22) becomes

$$\begin{aligned} T_2 \approx a_j \frac{n_b}{n_2} (\frac{b_e}{\alpha a_e})^{N_E} e^{b_j + \frac{b_e}{\alpha a_e}(\alpha - 1 + a_j)} \sum_{n=0}^{N_E-1} \frac{(\gamma + a_j)^n}{\Gamma(N_E - n)} \\ \times (\alpha\gamma_1)^{N_E-1-n} \Gamma\big(-n, (\frac{b_j}{a_j} + \frac{b_e}{\alpha a_e})(\gamma + a_j)\big). \end{aligned} \tag{4.23}$$

4.3.2 Case 2

In this case, $\beta_{E,i}P_2 \gg 1$ and hence we can ignore the channel background noise at Eve. Thus,

$$\gamma_e = \frac{(\sigma^2_{E,i} - \beta_{E,i})P_2 X_{2,e}}{1 + \beta_{E,i}P_2 X_{1,e}} \approx a_e \frac{X_{2,e}}{X_{1,e}}, \tag{4.24}$$

and hence $f_{\gamma_e}(x) = \frac{N_E a_e x^{N_E-1}}{(a_e+x)^{N_E+1}}$ (which also follows from Appendix .12). Then T_2 in (4.22) becomes

$$\begin{aligned} T_2 &\approx \frac{n_b}{n_2}\frac{a_j a_e}{\alpha} N_E \int_{y=\gamma_1}^{\infty} \frac{e^{-\frac{b_j}{a_j}(\alpha y+\alpha-1)} y^{N_E-1}}{(y+\frac{\alpha-1+a_j}{\alpha})(a_e+y)^{N_E+1}} \mathrm{d}y \\ &= \frac{n_b}{n_2}\frac{a_j a_e e^{-\frac{b_j}{a_j}(\alpha-1)}}{\alpha-1+a_j} N_E \Bigg[\int_{y=\gamma_1}^{\infty} \frac{e^{-\frac{b_j}{a_j}\alpha y} y^{N_E-1}}{(a_e+y)^{N_E+1}} \mathrm{d}y \\ &\quad - \int_{y=\gamma_1}^{\infty} \frac{e^{-\frac{b_j}{a_j}\alpha y} y^{N_E}}{(y+\frac{\alpha-1+a_j}{\alpha})(a_e+y)^{N_E+1}} \mathrm{d}y \Bigg], \end{aligned} \tag{4.25}$$

after applying the change of variable $x = \frac{1}{y}$ in (4.25), we get

$$\begin{aligned} T_2 &= \frac{n_b}{n_2}\frac{a_j a_e e^{-\frac{b_j}{a_j}(\alpha-1)}}{\alpha-1+a_j} N_E \Bigg[\underbrace{\int_{y=\gamma_1}^{\infty} \frac{e^{-\frac{b_j}{a_j}\alpha y} y^{N_E-1}}{(a_e+y)^{N_E+1}} \mathrm{d}y}_{\Omega(\gamma_1)} \\ &\quad - \int_{x=0}^{\frac{1}{\gamma_1}} \underbrace{\frac{e^{-\frac{b_j}{a_j}\frac{\alpha}{x}}}{(1+\frac{\alpha-1+a_j}{\alpha}x)(1+a_e x)^{N_E+1}}}_{h(x)} \mathrm{d}x \Bigg] \\ &\approx \frac{n_b}{n_2}\frac{a_j a_e e^{-\frac{b_j}{a_j}(\alpha-1)}}{\alpha-1+a_j} N_E \Omega(\gamma_1) - \frac{n_b}{n_2}\frac{a_j a_e e^{-\frac{b_j}{a_j}(\alpha-1)}}{\alpha-1+a_j} \\ &\quad \times \frac{N_E}{2\gamma_1} \sum_{n=1}^{M} \left(\frac{\pi}{M} h\big(\frac{1}{2\gamma_1}(t_n+1)\big)\sqrt{1-t_n^2} \right), \end{aligned} \tag{4.26}$$

where we applied Gaussian-Chebyshev quadrature method on the function denoted as $h(x)$. Furthermore, $\Omega(\gamma_1)$ in (4.26) is shown in Appendix .14 to be

$$\begin{aligned} \Omega(\gamma_1) &= e^{-\frac{b_j}{a_j}\alpha\gamma_1}\Gamma(N_E) \sum_{n=0}^{N_E-1} \frac{1}{\Gamma(N_E-n)} \frac{\gamma_1^{N_E-1-n}}{(a_e+\gamma_1)^{N_E-n}} \\ &\quad \times U\left(n+1, n+1-N_E, \frac{b_j}{a_j}\alpha(a_e+\gamma_1)\right). \end{aligned} \tag{4.27}$$

4.4 Numerical Results

In this section, we show numerical results of the averaged secrecy throughput T_s of secret information transmission from user 1 to user 2 among $N \geq 2$ cooperative single-antenna full-duplex users for which $\sigma_{i,j} = 1$ for all i and $j \neq i$. Unless otherwise specified, we use $P_1 = P_2 = 25$dB, $\delta = 0.001$, $N_E = 4$, $\sigma_E = 1$, $n_1 = 4$, $n_2 = 300$, and $n_b = 200$. To compute T_1 and T_2 in (4.20), we use $\gamma_1 = 10$ and $M = 16$. To verify our theoretical results (TR), we also conducted the 10^4-run Monte Carlo (MC) simulation to compute the expectation in (5.18).

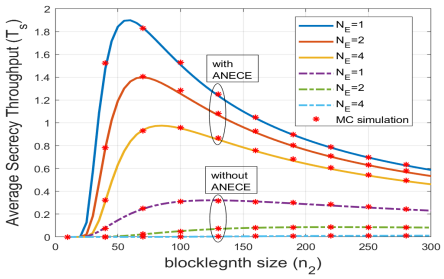

Figure 4.1: T_s versus n_2 for $N_E = 1, 2, 4$ and $N = 4$.

In Fig. 4.1, we show T_s versus n_2 for different N_E, which also compares the cases of "with ANECE" (under ideal full-duplex) and "without ANECE". The case of "with ANECE" is based on $N = 4$ cooperative users in phase 1, but only user 1 transmits secret information to user 2 in phase 2. For the case of "without ANECE", only user 1 sends a pilot in phase 1 which allows both user 2 and Eve to obtain consistent channel estimates. We see a significant gap of T_s between the cases of "with ANECE" and "without ANECE". We also see that as n_2 increases, T_s increases initially and then decreases.

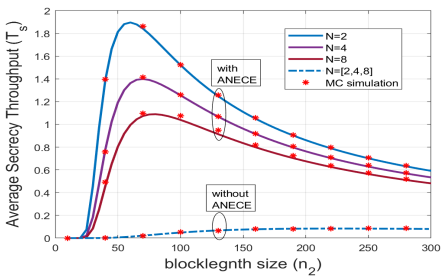

Figure 4.2: T_s versus n_2 for $N_E = 2$ and $N = 2, 4, 8$.

In Fig. 4.2, we show T_s versus n_2 for $N_E = 2$ and $N = 2, 4, 8$. We observe that with ANECE, the averaged secrecy throughput T_s from user 1 to user 2 is maximum when only users 1 and 2 (i.e., $N = 2$) perform ANECE cooperatively. However, we should note that using $N > 2$ cooperative users for ANECE, multiple pairs of users can then transmit secret information to each other without the need for additional phases of channel training. The sum of pair-wise secrecy throughput of all users can scale up linearly with the number of pairs if Eve only applies the conventional methods for channel estimation and information detection.

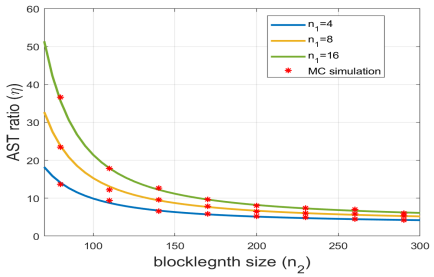

Figure 4.3: η vs n_2 for $n_1 = 4, 8, 16$, $N_E = 2$ and $N = 4$.

In Fig. 4.3, we present the ratio $\eta \triangleq \frac{T_s^{(withANECE)}}{T_s^{(withoutANECE)}}$ versus n_2 for $n_1 = 4, 8, 16$, $N_E = 2$ and $N = 4$. We observe that η is an increasing function of n_1, and $\eta > 1$ for all n_1

and n_2.

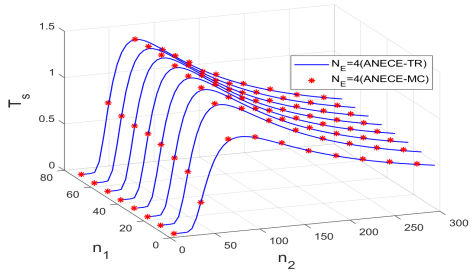

Figure 4.4: T_s vs n_1 and n_2 for the ANECE-assisted case.

In Fig. 4.4, we show T_s vs n_1 and n_2 for the ANECE-assisted case with $N = 4$, $P_1 = P_2 = 25$dB and $N_E = 4$. We see that T_s is an increasing function of n_1. Fig. 5.4 depicts the ANECE-assisted T_s versus n_2 and n_b (the number of secret bits transmitted per block). Here we also observe the quasi-concave nature of T_s with respect to n_2 for each fixed n_b. Thus, the theoretical results can be used to accurately find the optimal n_2. Furthermore, the optimal n_2 increases with n_b.

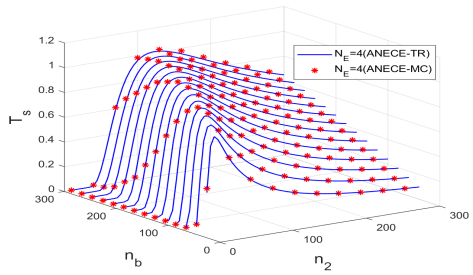

Figure 4.5: T_s vs n_2 and n_b for $N = 4$ and $N_E = 4$.

Chapter 5

Secrecy Throughput Enhancement with ANECE and Multi-Antenna AP in Finite Blocklength

5.1 System Model and Preliminaries

We consider a downlink scenario where a transmitter (Alice) equipped with N_A (≥ 1) antennas needs to transmit secret information to $N-1$ cooperative single-antenna users subject to covert/passive eavesdroppers (Eve) each with N_E antennas at unknown locations. The N nodes (Alice and users) are all full-duplex and apply anti-eavesdropping channel estimation (ANECE) [30] as follows. In phase 1, all nodes transmit ANECE pilots simultaneously, where the pilot transmitted by user $j \in (1, N-1)$ over n_1 slots is denoted by $p_j(k)$ with $k = 1, \cdots, n_1$ and $n_1 \geq N_A + N - 1$. The pilots transmitted by user j is also

represented by $\mathbf{p}_j = [p_j(1), .., p_j(n_1)]^T$ for all j, and $\mathbf{P}_U = [\mathbf{p}_1, .., \mathbf{p}_{N-1}]^T$ denotes the pilot matrix transmitted by all $N-1$ users. The $N_A \times n_1$ pilot matrix transmitted by Alice is represented by $\mathbf{P}_A$. We use $\mathbf{P} = \begin{bmatrix} \mathbf{P}_A \\ \mathbf{P}_U \end{bmatrix}$ to represent pilot matrix jointly transmitted by Alice and all users.

For ANECE pilots, there are special rank constraints. Let $\mathbf{P}_{U,(i)}$ result from removing the ith row of $\mathbf{P}_U$, and $\mathbf{P}_{(i)} = \begin{bmatrix} \mathbf{P}_A \\ \mathbf{P}_{U,(i)} \end{bmatrix}$. To ensure that each user can obtain a consistent channel estimation, we need $\mathbf{P}_{(i)}$ to have the full row rank $N_A + N - 2$ for all $i \in (1, N-1)$. To ensure that Alice can obtain a consistent channel estimation, we need $\mathbf{P}_U$ to have the full row rank $N-1$. To ensure that no Eve is able to obtain a consistent channel estimation, we need $\mathbf{P}$ to have a reduced rank $N_A + N - 2$, i.e., the $N_A + N - 1$ rows of $\mathbf{P}$ are linearly dependent on each other. An example of $\mathbf{P}$ is $\mathbf{P} = \mathbf{DQV}$ where $\mathbf{D}$ is a diagonal matrix for power control, $\mathbf{Q}$ is any $(N_A + N - 1) \times (N_A + N - 2)$ block of the $(N_A + N - 1) \times (N_A + N - 1)$ discrete Fourier transform (DFT) matrix and $\mathbf{V}$ is a $(N_A + N - 2) \times n_1$ matrix satisfying $\mathbf{V}\mathbf{V}^H = \mathbf{I}_{N_A+N-2}$, e.g., see [30], [48]. We will assume that each row of $\mathbf{P}$ has the squared norm equal to $P_1 n_1$.

In phase 1, the $n_1 \times 1$ signal vector received by user i is

$$\begin{aligned} \mathbf{y}_i &= \mathbf{P}_A^T \mathbf{h}_{i,A} + \sum_{j \neq i}^{N-1} h_{i,j} \mathbf{p}_j + \mathbf{n}_i \\ &= \begin{bmatrix} \mathbf{P}_A \\ \mathbf{P}_{U,(i)} \end{bmatrix}^T \begin{bmatrix} \mathbf{h}_{i,A} \\ \mathbf{h}_{U,(i)} \end{bmatrix} + \mathbf{n}_i = \mathbf{P}_{(i)}^T \mathbf{h}_{(i)} + \mathbf{n}_i, \end{aligned} \tag{5.1}$$

where $h_{i,j}$ is the complex channel gain from user j to user i, $\mathbf{h}_{i,A}$ is the complex channel gain from Alice to user i, $\mathbf{h}_{U,(i)}$ is the vertical stack of $h_{i,j}$ for all $j \neq i$, and $\mathbf{n}_i$ is the

background noise (including residual self-interference of the full-duplex user). We assume that $h_{i,j}$ equals $h_{j,i}$ (reciprocal channels), $h_{i,j}$ is $\mathcal{CN}(0, \sigma_{i,j}^2)$, and $\mathbf{n}_i$ is $\mathcal{CN}(\mathbf{0}, \mathbf{I})$. Also in phase 1, the $N_A \times n_1$ signal matrix received by Alice can be expressed as

$$\mathbf{Y}_A = \sum_{i=1}^{N-1} \mathbf{h}_{A,i}\mathbf{p}_i^T + \mathbf{N}_A = \mathbf{H}_A\mathbf{P}_U + \mathbf{N}_A, \tag{5.2}$$

where $\mathbf{H}_A$ is is the horizontal stack of $\mathbf{h}_{A,i}$ for all i. Let $\mathbf{y}_A = vec(\mathbf{Y}_A)$ and $\mathbf{h}_A = vec(\mathbf{H}_A)$. Then (5.2) becomes

$$\mathbf{y}_A = (\mathbf{P}_U^T \otimes \mathbf{I}_{N_A})\mathbf{h}_A + \mathbf{n}_A. \tag{5.3}$$

Furthermore, in phase 1, the $N_E \times n_1$ signal matrix received by Eve can be expressed as

$$\mathbf{Y}_E = \mathbf{H}_{E,A}\mathbf{P}_A + \sum_{i=1}^{N-1} \mathbf{h}_{E,i}\mathbf{p}_i^T + \mathbf{N}_E = \mathbf{H}_E\mathbf{P} + \mathbf{N}_E, \tag{5.4}$$

where $\mathbf{h}_{E,i}$ is the channel vector from user i to Eve, $\mathbf{H}_{E,A}$ is the $N_E \times N_A$ channel matrix from Alice to Eve, and $\mathbf{H}_E$ is Eve's total receive channel matrix (a horizontal stack of $\mathbf{H}_{E,A}$ and $\mathbf{h}_{E,i}$ for all i). Let $\mathbf{y}_E = vec(\mathbf{Y}_E)$ and $\mathbf{h}_E = vec(\mathbf{H}_E)$. Then (5.4) becomes

$$\mathbf{y}_E = (\mathbf{P}^T \otimes \mathbf{I}_{N_E})\mathbf{h}_E + \mathbf{n}_E. \tag{5.5}$$

As shown next, the ANECE pilots allow every user to have a consistent estimation of their channel gains but do not allow Eve to have a consistent estimation of Eve's receive channel matrix.

5.1.1 Effect of the ANECE Pilots

We will consider minimum-mean-squared-error (MMSE) channel estimation at Alice, $N-1$ users and Eve. Let $\mathbf{K}_{\mathbf{x},\mathbf{y}} = \mathcal{E}[\mathbf{x}\mathbf{y}^H]$ denote the correlation matrix between two

random vectors $\mathbf{x}$ and $\mathbf{y}$, and $\mathbf{K}_{\mathbf{x}} = \mathbf{K}_{\mathbf{x},\mathbf{x}}$. Then the MMSE estimate of the channel vector $\mathbf{h}_A$ at Alice is

$$\begin{aligned}\hat{\mathbf{h}}_A &= \mathbf{K}_{\mathbf{h}_A,\mathbf{y}_A}\mathbf{K}_{\mathbf{y}_A}^{-1}\mathbf{y}_A \\ &= (\mathbf{\Sigma}_U^2\mathbf{P}_U^*(\mathbf{I}_{n_1} + \mathbf{P}_U^T\mathbf{\Sigma}_U^2\mathbf{P}_U^*)^{-1} \otimes \mathbf{I}_{N_A})\mathbf{y}_A, \end{aligned} \tag{5.6}$$

where $\mathbf{\Sigma}_U^2 = diag\{\sigma_{A,1}^2, \cdots, \sigma_{A,N-1}^2\}$.

The covariance matrix of the MMSE error vector $\Delta\mathbf{h}_A = \hat{\mathbf{h}}_A - \mathbf{h}_A$ is

$$\begin{aligned}\mathbf{K}_{\Delta\mathbf{h}_A} &= \mathbf{K}_{\mathbf{h}_A} - \mathbf{K}_{\mathbf{h}_A,\mathbf{y}_A}\mathbf{K}_{\mathbf{y}_A}^{-1}\mathbf{K}_{\mathbf{y}_A,\mathbf{h}_A} \\ &= \mathbf{\Sigma}_U^2(\mathbf{I}_{N_A} - \mathbf{P}_U^*(\mathbf{I}_{n_1} + \mathbf{P}_U^T\mathbf{\Sigma}_U^2\mathbf{P}_U^*)^{-1}\mathbf{P}_U^T\mathbf{\Sigma}_U^2) \otimes \mathbf{I}_{N_A} \\ &= \mathbf{\Sigma}_U(\mathbf{I}_{N-1} + \mathbf{\Sigma}_U\mathbf{P}_U^*\mathbf{P}_U^T\mathbf{\Sigma}_U)^{-1}\mathbf{\Sigma}_U \otimes \mathbf{I}_{N_A}. \end{aligned} \tag{5.7}$$

Let $\beta_{A,i} = (\mathbf{\Sigma}_U(\mathbf{I}_{N-1} + \mathbf{\Sigma}_U\mathbf{P}_U^*\mathbf{P}_U^T\mathbf{\Sigma}_U)^{-1}\mathbf{\Sigma}_U)_{i,i}$ which is the MMSE estimation error variance of the channel between Alice and user i. As $n_1P_1 \to \infty$, then $\beta_{A,i} \to 0$ for all i and l [62]. Similarly, user i also estimates $\hat{\mathbf{h}}_{i,A}$.

The MMSE estimate of $\mathbf{h}_E$ (assuming $\mathbf{P}$ is also known to Eve) is

$$\begin{aligned}\hat{\mathbf{h}}_E &= \mathbf{K}_{\mathbf{h}_{E,i},\mathbf{y}_E}\mathbf{K}_{\mathbf{y}_E}^{-1}\mathbf{y}_E \\ &= (\mathbf{\Sigma}_E^2\mathbf{P}^*(\mathbf{I}_{n_1} + \mathbf{P}^T\mathbf{\Sigma}_E^2\mathbf{P}^*)^{-1} \otimes \mathbf{I}_{N_E})\mathbf{y}_E, \end{aligned} \tag{5.8}$$

where $\mathbf{\Sigma}_E^2 = \begin{bmatrix} \sigma_{E,A}^2\mathbf{I}_{N_A} & \mathbf{0} \\ \mathbf{0} & \mathbf{\Sigma}_{E,U}^2 \end{bmatrix}$ and $\mathbf{\Sigma}_{E,U}^2 = diag\{\sigma_{E,1}^2, \cdots, \sigma_{E,N-1}^2\}$. The covariance

matrix of $\Delta\mathbf{h}_E = \hat{\mathbf{h}}_E - \mathbf{h}_E$ is

$$\begin{aligned}\mathbf{K}_{\Delta\mathbf{h}_E} &= \mathbf{\Sigma}_E^2 \otimes \mathbf{I}_{N_E} - \mathbf{K}_{\mathbf{h}_E,\mathbf{y}_E}\mathbf{K}_{\mathbf{y}_E}^{-1}\mathbf{K}_{\mathbf{y}_E,\mathbf{h}_E} \\ &= \mathbf{\Sigma}_E^2(\mathbf{I}_{N_E} - \mathbf{P}^*(\mathbf{I}_{n_1} + \mathbf{P}^T\mathbf{\Sigma}_E^2\mathbf{P}^*)^{-1}\mathbf{P}^T\mathbf{\Sigma}_E^2) \otimes \mathbf{I}_{N_E} \\ &= \mathbf{\Sigma}_E(\mathbf{I}_{N_A+N-1} + \mathbf{\Sigma}_E\mathbf{P}^*\mathbf{P}^T\mathbf{\Sigma}_E)^{-1}\mathbf{\Sigma}_E \otimes \mathbf{I}_{N_E}. \end{aligned} \tag{5.9}$$

Let $\beta_{E,i} = (\mathbf{\Sigma}_E(\mathbf{I}_{N_A+N-1} + \mathbf{\Sigma}_E\mathbf{P}^*\mathbf{P}^T\mathbf{\Sigma}_E)^{-1}\mathbf{\Sigma}_E)_{i,i}$ the variance of each element of $\Delta\mathbf{h}_{E,i}$. As $n_1P_1 \to \infty$, we have $\beta_{E,i} \to c_i > 0$ where c_i is invariant to n_1P_1 [62].

5.1.2 SNRs at User and Eve

In phase 2, Alice transmits the information symbols $s_i(k), k = 1, \cdots, n_2$ to one of the users (i.e., user i and also referred to as Bob) with the transmit power P_2. Here, $\mathbf{h}_{A,i} = \hat{\mathbf{h}}_{A,i} + \Delta\mathbf{h}_{A,i} \in \mathcal{C}^{N_A \times 1}$ is the channel vector between Alice and i-th user. To maximize the SNR for the legitimate channel, Alice adopts the maximum ratio transmission (MRT) and transmits $\mathbf{x}_i(k) = \frac{\hat{\mathbf{h}}_{A,i}}{\|\hat{\mathbf{h}}_{A,i}\|}s_i(k)$ where $\hat{\mathbf{h}}_{A,i} \sim \mathcal{CN}(0, (\sigma_{A,i}^2 - \beta_{A,i})\mathbf{I}_{N_A})$ is the imperfect CSI estimation available at Alice. Then the received signal at user i is

$$\begin{aligned} y_{i,A}(k) &= \mathbf{h}_{A,i}^H\mathbf{x}_i(k) + n_i(k) \\ &= \|\hat{\mathbf{h}}_{A,i}\|s_i(k) + \frac{\Delta\mathbf{h}_{A,i}^H\hat{\mathbf{h}}_{A,i}}{\|\hat{\mathbf{h}}_{A,j}\|}s_i(k) + n_i(k) \end{aligned} \tag{5.10}$$

and the SNR at the i-th user is

$$\gamma_b = \frac{\|\hat{\mathbf{h}}_{A,i}\|^2P_2}{1 + \|\frac{\hat{\mathbf{h}}_{A,i}^H}{|\hat{\mathbf{h}}_{A,i}|}\Delta\mathbf{h}_{A,i}\|^2P_2} = \frac{(\sigma_{A,i}^2 - \beta_{A,i})P_2X_{2,b}}{1 + \beta_{A,i}P_2X_{1,b}} \tag{5.11}$$

where $X_{1,b} = \|\frac{\hat{\mathbf{h}}_{A,i}^H}{|\hat{\mathbf{h}}_{A,i}|}\frac{\Delta\mathbf{h}_{A,i}}{\sqrt{\beta_{A,i}}}\|^2$ is exponentially distributed with unit mean [63] and $X_{2,b} = \frac{\|\hat{\mathbf{h}}_{A,i}\|^2}{\sigma_{A,i}^2 - \beta_{A,i}}$ follows the Chi-squared distribution with $2N_A$ degrees of freedom (DoF). Note

that $X_{1,b}$ and $X_{2,b}$ are statistically independent (the norm and direction of a white circular complex Gaussian random vector are independent of each other).

Similarly, in phase 2, Eve receives

$$\begin{aligned}\mathbf{y}_{E,A}(k) &= \mathbf{H}_{E,A}\mathbf{x}_i(k) + \mathbf{n}_E(k) \\ &= \frac{\hat{\mathbf{H}}_{E,A}\hat{\mathbf{h}}_{A,i}}{\|\hat{\mathbf{h}}_{A,i}\|}s_i(k) + \frac{\Delta\mathbf{H}_{E,A}\hat{\mathbf{h}}_{A,i}}{\|\hat{\mathbf{h}}_{A,i}\|}s_i(k) + \mathbf{n}_E(k) \\ &= \hat{\mathbf{h}}_{E,A}s_i(k) + \Delta\mathbf{h}_{E,A}s_i(k) + \mathbf{n}_E(k), \end{aligned} \tag{5.12}$$

where $\hat{\mathbf{h}}_{E,A} = \frac{\hat{\mathbf{H}}_{E,A}\hat{\mathbf{h}}_{A,i}}{\|\hat{\mathbf{h}}_{A,i}\|}$, $\Delta\mathbf{h}_{E,A} = \frac{\Delta\mathbf{H}_{E,A}\hat{\mathbf{h}}_{A,i}}{\|\hat{\mathbf{h}}_{A,i}\|}$ and $\mathbf{n}_E \sim \mathcal{CN}(\mathbf{0}, \mathbf{I}_{N_E})$ is the background noise at Eve. Each elements of $\hat{\mathbf{h}}_{E,A}$ follows $\sim \mathcal{CN}(\mathbf{0}, (\sigma^2_{E,A} - \beta_{E,A})\mathbf{I}_{N_E})$ and $\Delta\mathbf{h}_{E,A}$ follows $\sim \mathcal{CN}(\mathbf{0}, \beta_{E,A}\mathbf{I}_{N_E})$. Assume that Eve equipped with N_E antennas applies MMSE estimation of $s_i(k)$. Then the received SINR at Eve is

$$\gamma_e = \hat{\mathbf{h}}^H_{E,A}(\Delta\mathbf{h}_{E,A}\Delta\mathbf{h}^H_{E,A} + \frac{1}{P_2}\mathbf{I})^{-1}\hat{\mathbf{h}}_{E,A}. \tag{5.13}$$

We will also assume that Eve treats $\hat{\mathbf{h}}_{E,A}$ as the true channel vector with respect to Alice. Now, the CDF of γ_e can be represented according to the results in [65] as

$$\begin{aligned} F_{\gamma_e}(z) &= 1 - e^{-\frac{z}{(\sigma^2_{E,A} - \beta_{E,A})P_2}} \\ &\quad \times \sum_{m=1}^{N_E} \frac{A_m(z)}{(m-1)!}\left(\frac{z}{(\sigma^2_{E,A} - \beta_{E,A})P_2}\right)^{m-1} \\ &= 1 - e^{-\frac{b_e}{a_e}z}\sum_{m=1}^{N_E}\frac{A_m(z)}{(m-1)!}(\frac{b_e}{a_e}z)^{m-1}, \end{aligned} \tag{5.14}$$

where $a_e = \frac{\sigma^2_{E,A}}{\beta_{E,A}} - 1$, $b_e = \frac{1}{\beta_{E,A}P_2}$ with $\sigma^2_{E,A}$ being the large scale fading between Alice and Eve, and

$$A_m(z) = \begin{cases} 1, & m \le N_E - 1 \\ \frac{1}{1+\frac{\beta_{E,A}}{\sigma^2_{E,A} - \beta_{E,A}}z} = \frac{1}{1+\frac{z}{a_e}}, & m = N_E \end{cases} \tag{5.15}$$

5.1.3 Achievable Secrecy Rate under FBL

In conventional communication system over a wiretap channel, maximal secure transmission rate is achieved by mapping the data to sufficiently long codewords which results in both small error probability at decoder and small information leakage at Eve. However, the error probability at Bob is non-negligible in FBL information transmission. The maximal achievable secrecy rate $R(n_2, \epsilon, \delta)$ with the decoding error probability ϵ at Bob and the information leakage δ to Eve can be approximated (according to [56]-[57]) as follows

$$R(n_2, \epsilon, \delta) = \log\left(\frac{1+\gamma_b}{1+\gamma_e}\right) - \sqrt{\frac{V_b}{n_2}}\frac{Q^{-1}(\epsilon)}{\ln 2} - \sqrt{\frac{V_e}{n_2}}\frac{Q^{-1}(\delta)}{\ln 2}, \tag{5.16}$$

where the channel dispersions of the legitimate and eavesdropping channels are denoted by V_b and V_e respectively, which can be expressed by $V_x = 1-(1+\gamma_x)^{-2}$ with $x \in \{b, e\}$. Here, $Q(x) = \frac{1}{\sqrt{2\pi}}\int_x^\infty e^{-\frac{t^2}{2}}\mathrm{d}t$ and $Q^{-1}(x)$ is the inverse function of $Q(x)$.

Let the number of secret information bits transmitted by Alice in every n_2 time slots be n_b. Then, subject to some ϵ and δ, $R(n_2, \epsilon, \delta) = \frac{n_b}{n2}$ [56]. In other words, given $R(n_2, \epsilon, \delta) = \frac{n_b}{n2}$ along with random γ_b and γ_e, ϵ is also random as governed by (5.16), or equivalently

$$\epsilon = Q\left(\sqrt{\frac{n_2}{V_b}}\left(\ln(\frac{1+\gamma_b}{1+\gamma_e}) - \sqrt{\frac{V_e}{n_2}}Q^{-1}(\delta) - \frac{n_b}{n_2}\ln 2\right)\right), \tag{5.17}$$

which is dependent on γ_b and γ_e. When $\gamma_b < \gamma_e$, secrecy outage occurs (regardless of n_2 and δ). Even if $\epsilon < 1$ in (5.17) for $\gamma_b < \gamma_e$, the decoded secret information at Bob is compromised. To handle this trivial case, we set $\epsilon = 1$. Therefore, the averaged achievable

secrecy throughput (in bits per channel use) can be defined as follows

$$T_s \triangleq \mathbb{E}\left[\frac{n_b}{n_2}(1-\epsilon_{\gamma_b,\gamma_e})\right] = \mathbb{E}_{\gamma_b \geq \gamma_e}\left[\frac{n_b}{n_2}(1-\epsilon_{\gamma_b,\gamma_e})\right]. \tag{5.18}$$

5.2 Averaged Secrecy Throughput of Downlink Transmission

In this section, we discuss the framework to derive closed form expression of AST and investigate the impact of N_A, n_2 and ANECE on the AST defined in (5.18). Here, γ_b and γ_e are independent random variables and T_s in (5.18) can be rewritten as follows

$$\begin{aligned} T_s &= \frac{n_b}{n_2}\int_{y=0}^{\infty}\left(\int_{x=y}^{\infty}\big(1-\epsilon(x,y)\big)f_{\gamma_b}(x)\mathrm{d}x\right)f_{\gamma_e}(y)\mathrm{d}y \\ &= \frac{n_b}{n_2}\int_{y=0}^{\infty}\Phi(y)f_{\gamma_e}(y)\mathrm{d}y, \end{aligned} \tag{5.19}$$

where

$$\Phi(y) = \int_{x=y}^{\infty}\big(1-\epsilon(x,y)\big)f_{\gamma_b}(x)\mathrm{d}x. \tag{5.20}$$

To compute the averaged secrecy throughput T_s, we need to compute (5.20) first where $\epsilon(x,y)$ makes the integral an intractable task. Similar to [55], we will use the following approximation of $\epsilon(x,y)$:

$$\epsilon(x,y) \approx \begin{cases} 1, & x < x_0 + \frac{1}{2k} \\ \frac{1}{2} + k(x-x_0), & x_0 + \frac{1}{2k} \leq x \leq x_0 - \frac{1}{2k} \\ 0, & x > x_0 - \frac{1}{2k} \end{cases} \tag{5.21}$$

where x_0 is such that $\epsilon(x_0,y) = \frac{1}{2}$, i.e., $x_0 = \exp\left(\sqrt{\frac{V_e}{n_2}}Q^{-1}(\delta) + \frac{n_b}{n_2}\ln 2\right)(1+y) - 1$, and $k = \frac{d\epsilon(x,y)}{dx}|_{x=x_0} = -\sqrt{\frac{n_2}{2\pi x_0(x_0+2)}}$. In moderate blocklength range where $10 \leq n_2 \leq 1000$, $|k|$

becomes large and approximation holds fairly well under that scenario. Assuming a large $|k|$, it follows from (5.21) and (5.20) that

$$\begin{aligned}\Phi(y) &\approx \int_{x_0+\frac{1}{2k}}^{\infty} (1-\epsilon(x,y)) f_{\gamma_b}(x)\mathrm{d}x \\ &= 1 - F_{\gamma_b}\left(x_0+\frac{1}{2k}\right) - \int_{x_0+\frac{1}{2k}}^{x_0-\frac{1}{2k}} \left(\frac{1}{2}+k(x-x_0)\right) \\ &\quad \times f_{\gamma_b}(x)\mathrm{d}x \\ &= 1 + k\int_{x_0+\frac{1}{2k}}^{x_0-\frac{1}{2k}} F_{\gamma_b}(x)\mathrm{d}x \approx 1 - F_{\gamma_b}(x_0), \end{aligned} \tag{5.22}$$

where $x_0 \triangleq x_0(y)$ is a function of y and $F_{\gamma_b}(x)$ is the CDF of γ_b. Now, from (5.19) and (5.22), we define the average secrecy throughput between Alice and i-th user as follows

$$\begin{aligned} T_s &= \frac{n_b}{n_2}\int_{y=0}^{\infty} (1-F_{\gamma_b}(x_0(y))) f_{\gamma_e}(y)\mathrm{d}y \\ &= \frac{n_b}{n_2}\int_{y=0}^{\infty} f_{\gamma_b}(x_0(y)) F_{\gamma_e}(y) x_0'(y)\mathrm{d}y \\ &= \underbrace{\frac{n_b}{n_2}\int_{y=0}^{\gamma_1} f_{\gamma_b}(x_0(y)) F_{\gamma_e}(y) x_0'(y)\mathrm{d}y}_{T_1} \\ &\quad + \underbrace{\frac{n_b}{n_2}\int_{y=\gamma_1}^{\infty} f_{\gamma_b}(x_0(y)) F_{\gamma_e}(y) x_0'(y)\mathrm{d}y}_{T_2}, \end{aligned} \tag{5.23}$$

where $x_0'(y) \triangleq \frac{\mathrm{d}x_0(y)}{\mathrm{d}y}$ and γ_1 is sufficiently large SNR such that $V_e \approx 1$, i.e., $x_0(y) = \exp\left(\frac{Q^{-1}(\delta)}{\sqrt{n_2}} + \ln 2\frac{n_b}{n_2}\right)(1+y) - 1 = \alpha(1+y) - 1$ with constant $\alpha = \exp\left(\frac{Q^{-1}(\delta)}{\sqrt{n_2}} + \ln 2\frac{n_b}{n_2}\right)$ when $y \geq \gamma_1$.

To evaluate T_1 and T_2 in (5.23), we require the knowledge of the distribution of γ_b and γ_e. The PDF of γ_b directly follows from [62] as

$$f_{\gamma_b}(z) = \frac{a_a e^{b_a}}{\Gamma(N_A)} \frac{z^{N_A-1}}{(z+a_a)^{N_A+1}} \Gamma(N_A+1, \frac{b_a}{a_a}z + b_a), \tag{5.24}$$

where $a_a = \frac{\sigma_{A,i}^2}{\beta_{A,i}} - 1$ and $b_a = \frac{1}{\beta_{A,i} P_2}$. Now, T_1 from (5.23) can be written as

$$T_1 = \frac{n_b a_a e^{b_a}}{n_2 \Gamma(N_A)} \int_{y=0}^{\gamma_1} \frac{x_0(y)^{N_A-1}}{(x_0(y)+a_a)^{N_A+1}} \times \Gamma(N_A+1, \frac{b_a}{a_a} x_0(y) + b_a) F_{\gamma_e}(y) x_0'(y) \mathrm{d}y. \tag{5.25}$$

Here the integral representation of right hand side term in (5.25) doesn't yield any further simpler form. Thus, (5.25) is approximated by leveraging Gaussian-Chebyshev quadrature [59] as follows

$$T_1 \approx \frac{n_b a_a e^{b_a}}{n_2 \Gamma(N_A)} \frac{\gamma_1}{2} \sum_{n=1}^{M} \Big(\frac{\pi}{M} g\big(\frac{\gamma_1}{2}(t_n+1)\big) \sqrt{1-t_n^2} \Big), \tag{5.26}$$

where $g(y) \triangleq \frac{x_0(y)^{N_A-1}}{(x_0(y)+a_a)^{N_A+1}} \Gamma(N_A+1, \frac{b_a}{a_a} x_0(y) + b_a) F_{\gamma_e}(y) x_0'(y)$ and $t_n \triangleq cos(\frac{2n-1}{2M}\pi)$. Here, the parameter M determines the complexity and accuracy trade-off. Now, the second term T_2 can be written as follows

$$\begin{aligned} T_2 &= \alpha \frac{n_b a_a e^{b_a}}{n_2 \Gamma(N_A)} \int_{y=\gamma_1}^{\infty} \frac{x_0(y)^{N_A-1}}{(x_0(y)+a_a)^{N_A+1}} \Gamma\big(N_A+1, \frac{b_a}{a_a} \\ &\quad \times x_0(y) + b_a\big) \Big[1 - e^{-\frac{b_e}{a_e} y} \sum_{m=1}^{N_E} \frac{A_m(y)}{(m-1)!} \big(\frac{b_e}{a_e} y\big)^{m-1} \Big] \mathrm{d}y \\ &= \alpha a_a N_A \frac{n_b}{n_2} \int_{y=\gamma_1}^{\infty} \frac{x_0(y)^{N_A-1}}{(x_0(y)+a_a)^{N_A+1}} e^{-\frac{b_a}{a_a} x_0(y)} \sum_{k=0}^{N_A} \\ &\quad \frac{(\frac{b_a}{a_a} x_0(y) + b_a)^k}{k!} \Big[1 - e^{-\frac{b_e}{a_e} y} \sum_{m=1}^{N_E} \frac{A_m(y)}{(m-1)!} \big(\frac{b_e}{a_e} y\big)^{m-1} \Big] \mathrm{d}y \\ &= T_{2,1} - T_{2,2}. \end{aligned} \tag{5.27}$$

The details steps are shown in Appendix .15 where we defined a constant term $\gamma = \alpha\gamma_1 + \alpha - 1$ to simplify equations. After combining the results from (5.26) and (5.27), we obtain the approximated closed from expression of T_s which is shown in the top of the

$$T_s \approx \frac{n_b}{n_2}\frac{a_a e^{b_a}}{\Gamma(N_A)}\frac{\gamma_1}{2}\sum_{n=1}^{M}\Big(\frac{\pi}{M}g\big(\frac{\gamma_1}{2}(t_n+1)\big)\sqrt{1-t_n^2}\Big) + a_a\Gamma(N_A+1)\frac{n_b}{n_2}e^{-\frac{b_a}{a_a}\gamma}\sum_{k=0}^{N_A}\frac{(\frac{b_a}{a_a})^k}{k!}$$
$$\times\sum_{l=0}^{N_A-1}\frac{1}{\Gamma(N_A-l)}\frac{\gamma^{N_A-1-l}}{(\gamma+a_a)^{N_A-k-l}}\Xi(k,l,\gamma_1,N_E) - \alpha a_a\frac{n_b}{n_2}\frac{N_A}{\Gamma(N_E)}\frac{1}{2\gamma_1}$$
$$\times\sum_{n=1}^{M}\left(\frac{\pi}{M}h\big(\frac{1}{2\gamma_1}(t_n+1)\big)\sqrt{1-t_n^2}\right). \tag{5.28}$$

where $\Xi(k,l,\gamma_1,N_E) \triangleq U\big(l+1, l+1+k-N_A, \frac{b_a}{a_a}(\gamma+a_a)\big) - e^{-\frac{b_e}{a_e}\gamma_1}\sum_{m=1}^{N_E-1}(\frac{b_e}{a_e}\gamma_1)^{m-1}\sum_{n=0}^{m-1}\frac{(\frac{\gamma+a_a}{\alpha\gamma_1})^n}{\Gamma(m-n)}\frac{\Gamma(l+n+1)}{\Gamma(l+1)\Gamma(n+1)}U\big(l+n+1, l+n+1+k-N_A, (\frac{b_a}{a_a}+\frac{1}{\alpha}\frac{b_e}{a_e})(\gamma+a_a)\big)$.

---

next page. The closed form expression of T_s in (5.28) reveals the impact of n_1, n_2, N_A and N_E on the AST.

5.3 Secrecy Enhancement with Multi-antenna Receiver

In this section, we study the average secrecy throughput of the uplink transmission of information where $N-1$ single antenna users send their secret information to AP equipped with N_A antenna against Eve equipped with N_E antenna. We study two scenarios. In case 1, we consider $N-1$ single antenna users transmit secret information to AP in orthogonal resource blocks. In case 2, we consider non-orthogonal transmission from $K(\leq N-1)$ users forming virtual MIMO.

5.3.1 case 1

In phase 2, all $N-1$ users transmit their secret information in different resource blocks. Without loss of generality, we refer user i as Bob and study the average uplink secrecy throughput, $T_s^{(u)}$ between AP and Bob. To evaluate $T_s^{(u)}$ in (5.23), we require the knowledge of the distribution of γ_a and γ_e.

Now, the CDF of γ_a and γ_e can be obtained from [65]. Then, by taking the derivative, the PDF of γ_a can be represented as follows

$$f_{\gamma_a}(z) = \frac{e^{-\frac{b_a}{a_a}z}}{\Gamma(N_A)} \frac{(\frac{b_a}{a_a}z)^{N_A-1}}{z+a_a}(N_A - 1 + b_a + \frac{a_a}{a_a+z}), \tag{5.29}$$

where $a_a = \frac{\sigma_{A,i}^2}{\beta_{A,i}} - 1$ and $b_a = \frac{1}{\beta_{A,i}P_2}$.

Now, the CDF of γ_e can be represented from [65] as follows

$$\begin{aligned} F_{\gamma_e}(z) &= 1 - e^{-\frac{z}{(\sigma_{E,i}^2 - \beta_{E,i})P_2}} \\ &\quad \times \sum_{m=1}^{N_E} \frac{A_m(z)}{(m-1)!} \left(\frac{z}{(\sigma_{E,i}^2 - \beta_{E,i})P_2} \right)^{m-1} \\ &= 1 - e^{-\frac{b_e}{a_e}z} \sum_{m=1}^{N_E} \frac{A_m(z)}{(m-1)!} (\frac{b_e}{a_e}z)^{m-1}, \end{aligned} \tag{5.30}$$

where $a_e = \frac{\sigma_{E,i}^2}{\beta_{E,i}} - 1$, $b_e = \frac{1}{\beta_{E,i}P_2}$ with $\sigma_{E,i}^2$ being the large scale fading between user i and Eve, and

$$A_m(z) = \begin{cases} 1, & m \leq N_E - 1 \\ \frac{1}{1+\frac{\beta_{E,i}}{\sigma_{E,i}^2 - \beta_{E,i}}z} = \frac{1}{1+\frac{z}{a_e}}, & m = N_E \end{cases} \tag{5.31}$$

Given the PDF of γ_a and CDF of γ_e, we obtain the average uplink secrecy through-

put, $T_s^{(u)}$ as follows

$$T_s^{(u)} = \underbrace{\frac{n_b}{n_2}\int_{y=0}^{\gamma_1} f_{\gamma_a}(x_0(y))F_{\gamma_e}(y)x_0'(y)\mathrm{d}y}_{T_1^{(u)}} + \underbrace{\frac{n_b}{n_2}\int_{y=\gamma_1}^{\infty} f_{\gamma_a}(x_0(y))F_{\gamma_e}(y)x_0'(y)\mathrm{d}y}_{T_2^{(u)}}, \tag{5.32}$$

where

$$T_1^{(u)} = \frac{n_b}{n_2}\frac{(\frac{b_a}{a_a})^{N_A-1}}{\Gamma(N_A)}\int_{y=0}^{\gamma_1}\frac{e^{-\frac{b_a}{a_a}x_0(y)}x_0(y)^{N_A-1}}{(x_0(y)+a_a)}(N_A-1 + b_a + \frac{a_a}{a_a+x_0(y)})F_{\gamma_e}(y)x_0'(y)\mathrm{d}y. \tag{5.33}$$

Here the integral representation of right hand side term in (5.33) doesn't yield any further simpler form. We apply Gaussian-Chebyshev quadrature method used in (5.34) to approximate the integral of right hand side term in (5.33) and $T_1^{(u)}$ can be represented as follows

$$T_1^{(u)} \approx \frac{n_b}{n_2}\frac{(\frac{b_a}{a_a})^{N_A-1}}{\Gamma(N_A)}\frac{\gamma_1}{2}\sum_{n=1}^{M}\Big(\frac{\pi}{M}g_u\big(\frac{\gamma_1}{2}(t_n+1)\big)\sqrt{1-t_n^2}\Big), \tag{5.34}$$

where $g_u(y) \triangleq \frac{e^{-\frac{b_a}{a_a}x_0(y)}x_0(y)^{N_A-1}}{(x_0(y)+a_a)}(N_A-1+b_a+\frac{a_a}{a_a+x_0(y)})F_{\gamma_e}(y)x_0'(y)$ and $t_n \triangleq cos(\frac{2n-1}{2M}\pi)$. Here, the parameter M determines the complexity and accuracy trade-off. Now, the second term $T_2^{(u)}$ can be written as follows

$$\begin{aligned} T_2^{(u)} &= \alpha\frac{n_b}{n_2}\frac{(\frac{b_a}{a_a})^{N_A-1}}{\Gamma(N_A)}\int_{y=\gamma_1}^{\infty}\frac{e^{-\frac{b_a}{a_a}(\alpha+\alpha y-1)}(\alpha+\alpha y-1)^{N_A-1}}{(\alpha+\alpha y-1+a_a)} \\ &\times (N_A-1+b_a+\frac{a_a}{a_a+\alpha+\alpha y-1})\Bigg[1-e^{-\frac{b_e}{a_e}y} \\ &\times \sum_{m=1}^{N_E-1}\frac{\big(\frac{b_e}{a_e}y\big)^{m-1}}{(m-1)!} - \frac{e^{-\frac{b_e}{a_e}y}\big(\frac{b_e}{a_e}y\big)^{N_E-1}}{\Gamma(N_E)}\frac{a_e}{a_e+y}\Bigg]\mathrm{d}y \\ &= T_{2,1}^{(u)} - T_{2,2}^{(u)}. \end{aligned} \tag{5.35}$$

$$T_s^{(u)} \approx \frac{n_b}{n_2}\frac{(\frac{b_a}{a_a})^{N_A-1}}{\Gamma(N_A)}\frac{\gamma_1}{2}\sum_{n=1}^{M}\Big(\frac{\pi}{M}g_u\big(\frac{\gamma_1}{2}(t_n+1)\big)\sqrt{1-t_n^2}\Big) + \frac{n_b}{n_2}e^{-\frac{b_a}{a_a}\gamma}(\frac{b_a}{a_a}\gamma)^{N_A-1}\sum_{l=0}^{N_A-1}\frac{(\frac{a_a+\gamma}{\gamma})^l}{\Gamma(N_A-l)}$$
$$\times\Bigg[\Psi_1(l,\gamma_1,\frac{b_a}{a_a}) - e^{-\frac{b_e}{a_e}\gamma_1}\sum_{m=1}^{N_E-1}(\frac{b_e}{a_e}\gamma_1)^{m-1}\sum_{n=0}^{m-1}\frac{(\frac{a_a+\gamma}{\alpha\gamma_1})^n}{\Gamma(m-n)}\frac{\Gamma(l+n+1)}{\Gamma(l+1)\Gamma(n+1)}\Psi_1(l+n,\gamma_1,\frac{b_a}{a_a}$$
$$+\frac{b_e}{\alpha a_e})\Bigg] - \frac{n_b}{n_2}\frac{(\frac{b_a}{a_a})^{N_A-1}(\frac{b_e}{a_e}\gamma_1)^{N_E-1}}{\Gamma(N_A)}\frac{e^{-\frac{b_a}{a_a}\gamma-\frac{b_e}{a_e}\gamma_1}\alpha a_e}{\alpha(a_e-1)-a_a+1}\sum_{l=0}^{N_E-1}\frac{(\frac{\gamma+a_a}{\alpha\gamma_1})^l}{\Gamma(N_E-l)}\Psi_2(l,\gamma_1) \tag{5.36}$$

where $\Psi_1(l,\gamma_1,c) \triangleq (N_A-1+b_a)U\big(l+1,l+1,c(\gamma+a_a)\big) + \frac{a_a}{a_a+\gamma}U\big(l+1,l,c(\gamma+a_a)\big)$ and $\Psi_2(l,\gamma_1) \triangleq (N_A-1+b_a-\frac{a_a}{\alpha(a_e-1)-a_a+1})\Big(U\big(l+1,l+1,(\frac{b_a}{a_a}+\frac{b_e}{\alpha a_e})(\gamma+a_a)\big)+\alpha^l(\frac{a_e+\gamma_1}{\gamma+a_a})^l U\big(l+1,l+1,(\frac{b_a}{a_a}+\frac{b_e}{\alpha a_e})\alpha(a_e+\gamma_1)\big)\Big) + \frac{a_a}{\gamma+a_a}U\big(l+1,l,(\frac{b_a}{a_a}+\frac{b_e}{\alpha a_e})(\gamma+a_a)\big)$.

The details steps to derive the analytical form of $T_{2,1}^{(u)}$ and $T_{2,2}^{(u)}$ are shown in Appendix .16. Here, we have used a constant term $\gamma = \alpha\gamma_1 + \alpha - 1$ to simplify equations. After combining the results from (5.34) and (5.35), we obtain the approximated closed from expression of $T_s^{(u)}$ which is shown in the top of this page. The closed form expression of $T_s^{(u)}$ in (5.36) reveals the impact of the parameters i.e., n_1, n_2, N_A, N_E, N and P_2 on AST. Later in Section 5.5, we will present numerical results to illustrate the impact.

5.3.2 case 2

We consider $K(\leq N-1)$ number of users are located in same location, i.e., the large scale channel gains between AP and the users are equal. Therefore, a group consists K number of users can from virtual MIMO and transmits secret information simultaneously.

The AP receives the following signal

$$\begin{aligned}\mathbf{y}_A(k) &= \sum_{i=1}^{K} \mathbf{h}_{A,i} s_i(k) + \mathbf{n}_A(k) \\ &= \sum_{i=1}^{K} \hat{\mathbf{h}}_{A,i} s_i(k) + \underbrace{\sum_{i=1}^{K} \Delta\mathbf{h}_{A,i} s_i(k) + \mathbf{n}_A(k)}_{\mathbf{w}_A(k)} \\ &= \hat{\mathbf{h}}_{A,i} s_i(k) + \sum_{j\neq i}^{K} \hat{\mathbf{h}}_{A,j} s_j(k) + \mathbf{w}_A(k), \end{aligned} \tag{5.37}$$

where $\sum_{j\neq i}^{K} \mathbf{h}_{A,j} s_j(k)$ is interfering the i-th stream and $\mathbf{w}_A(k) \sim \mathcal{CN}(0, (1+K\beta_{A,i}P_2)\mathbf{I}_{N_A})$ is the overall noise received at AP respectively. We assume, users apply MMSE for information symbol detection. Then, the SINR at AP from i-th stream of information can be written as follows

$$\gamma_a = \hat{\mathbf{h}}_{A,i}^H (\sum_{j\neq i}^{K} \hat{\mathbf{h}}_{A,j} \hat{\mathbf{h}}_{A,j}^H + \frac{1+K\beta_{A,i}P_2}{P_2} \mathbf{I}_{N_A})^{-1} \hat{\mathbf{h}}_{A,i}. \tag{5.38}$$

The PDF of γ_a can be found in [66] (eqn.(30)) and written as follows

$$\begin{aligned} f_{\gamma_a}(z) = \frac{e^{-\frac{z}{\rho_a}} z^{N_A-1}}{\Gamma(N_A)(1+z)^K \rho_a^{N_A}} \Bigg[&\sum_{l=0}^{K-1} \binom{K-1}{l} \frac{N_A!}{(N_A-l)!} \rho_a^l \\ &+ z \sum_{l=0}^{K-1} \binom{K-1}{l} \frac{(N_A-1)!}{(N_A-l-1)!} \rho_a^l \Bigg], \end{aligned} \tag{5.39}$$

where $\rho_a = \frac{(\sigma_{A,i}^2 - \beta_{A,i})P_2}{1+K\beta_{A,i}P_2}$ is the average SNR at AP from i-th stream of information.

Similarly, the CDF of γ_e can be written as follows

$$\begin{aligned} F_{\gamma_e}(z) = 1 - e^{-\frac{z}{\rho_e}} \Bigg[&\sum_{m=1}^{N_E-k+1} \frac{(\frac{z}{\rho_e})^{m-1}}{(m-1)!} \\ &+ \sum_{m=N_E-K+2}^{N_E} \frac{(\frac{z}{\rho_e})^{m-1}}{(m-1)!} \sum_{i=0}^{K-2} \binom{K-2}{i} \frac{z^i}{(1+z)^{K-1}}, \end{aligned} \tag{5.40}$$

where $\rho_e = \frac{(\sigma_{E,i}^2 - \beta_{E,i})P_2}{1+K\beta_{E,i}P_2}$ is the average SNR at Eve from i-th stream of information.

5.4 Eve's ability to combat ANECE

In this section, we consider Eve has an advantage of having prior knowledge about few transmitted symbols. During information transmission in n_2 blocklength, we assume Eve knows l ($< n_2$) number of information symbols. Therefore, Eve utilize this l number of correctly guessed observation to further reduce the CSI estimation error. Furthermore, Eve can substantially improve the SNR and decrease the average secrecy throughput (AST) of the communication system. We aim to investigate the decrease of AST against Eve's ability to guess the information symbol. Thus, Eve stack the observations horizontally with (5.4) as follows

$$\begin{aligned} \mathbf{Y}_{E,i} &= [\mathbf{Y}_E, \tilde{\mathbf{Y}}_{E,i}] \\ vec(\mathbf{Y}_{E,i}) = \mathbf{y}_{E,i} &= \begin{bmatrix} \sum_{i=1}^{N} (\mathbf{P}_i^T \otimes \mathbf{I}_{N_E}) \\ \mathbf{x}_i^* \otimes \mathbf{I}_{N_E} \end{bmatrix} \mathbf{h}_{E,i} + \begin{bmatrix} \mathbf{n}_E \\ \tilde{\mathbf{n}}_{E,i} \end{bmatrix} \end{aligned} \tag{5.41}$$

where $\mathbf{x}_i \in \mathcal{C}^{l\times 1}$ is the information symbol revealed to Eve. Now, the improved CSI estimation error variance of Eve is $var(\Delta\tilde{\mathbf{h}}_{E,i}) = \mathbf{K}_{\mathbf{h}_{E,i},\bar{\mathbf{y}}_{E,i}} \mathbf{K}_{\bar{\mathbf{y}}_{E,i}}^{-1} \mathbf{K}_{\bar{\mathbf{y}}_{E,i},\mathbf{h}_{E,i}}$, where $\mathbf{K}_{\bar{\mathbf{y}}_{E,i}} = \begin{bmatrix} \mathbf{K}_{\mathbf{y}_{E,i}} & \mathbf{K}_{\mathbf{y}_{E,i},\tilde{\mathbf{y}}_{E,i}} \\ \mathbf{K}_{\tilde{\mathbf{y}}_{E,i},\mathbf{y}_{E,i}} & \mathbf{K}_{\tilde{\mathbf{y}}_{E,i}} \end{bmatrix} = \begin{bmatrix} \bar{\mathbf{P}}^{\mathbf{T}} \Sigma_E \bar{\mathbf{P}}^* & \sigma_{E,i}^2 \mathbf{p}_i \mathbf{x}_i^H \\ \sigma_{E,i}^2 \mathbf{x}_i \mathbf{p}_i^H & \sigma_{E,i}^2 \mathbf{x}_i \mathbf{x}_i^H \end{bmatrix} \otimes \mathbf{I} + \mathbf{I}$ and $\mathbf{K}_{\mathbf{h}_{E,i},\bar{\mathbf{y}}_{E,i}} = \sigma_{E,i}^2 \begin{bmatrix} \mathbf{s}_i^T \bar{\mathbf{P}}^* & \mathbf{x}_i^H \end{bmatrix} \otimes \mathbf{I}$.

Now,

$$
\begin{aligned}
& var(\Delta\tilde{\mathbf{h}}_{E,i}) \\
&= \sigma^2_{E,i}\mathbf{I}_{N_E} - \mathbf{K}_{\mathbf{h}_{E,i},\bar{\mathbf{y}}_{E,i}}\mathbf{K}^{-1}_{\bar{\mathbf{y}}_{E,i}}\mathbf{K}_{\bar{\mathbf{y}}_{E,i},\mathbf{h}_{E,i}} \\
&= \sigma^2_{E,i}\mathbf{I} - \sigma^4_{E,i}\begin{bmatrix}\mathbf{s}_i^T\bar{\mathbf{P}}^* & \mathbf{x}_i^H\end{bmatrix}\left(\begin{bmatrix}\bar{\mathbf{P}}^{\mathbf{T}}\Sigma_E\bar{\mathbf{P}}^* & \sigma^2_{E,i}\mathbf{p}_i\mathbf{x}_i^H \\ \sigma^2_{E,i}\mathbf{x}_i\mathbf{p}_i^H & \sigma^2_{E,i}\mathbf{x}_i\mathbf{x}_i^H\end{bmatrix} + \mathbf{I}\right)^{-1} \\
&\quad \times \begin{bmatrix}\bar{\mathbf{P}}^{\mathbf{T}}\mathbf{s}_i \\ \mathbf{x}_i\end{bmatrix} \otimes \mathbf{I} \\
&= \sigma^2_{E,i}\left(\mathbf{I} - \sigma^2_{E,i}\begin{bmatrix}B_1 & B_2\end{bmatrix}\left(\begin{bmatrix}A_{11} & A_{12} \\ A_{21} & A_{22}\end{bmatrix}\right)^{-1}\begin{bmatrix}B_1^H \\ B_2^H\end{bmatrix}\right) \otimes \mathbf{I}_{N_E} \qquad (5.42)
\end{aligned}
$$

To invert $\begin{bmatrix}A_{11} & A_{12} \\ A_{21} & A_{22}\end{bmatrix}$, we apply Schur complement [67] as follows

$$
\begin{aligned}
\left(\begin{bmatrix}A_{11} & A_{12} \\ A_{21} & A_{22}\end{bmatrix}\right)^{-1} &= \begin{bmatrix}I & 0 \\ -A_{22}^{-1}A_{21} & I\end{bmatrix} \\
&\times \begin{bmatrix}(A_{11} - A_{12}A_{22}^{-1}A_{21})^{-1} & 0 \\ 0 & A_{22}^{-1}\end{bmatrix}\begin{bmatrix}I & -A_{12}A_{22}^{-1} \\ 0 & I\end{bmatrix} \qquad (5.43)
\end{aligned}
$$

We can rewrite (5.42) as follows

$$
\begin{aligned}
&var(\Delta\tilde{\mathbf{h}}_{E,i}) \\
&= \sigma^2_{E,i}\mathbf{I} - \sigma^4_{E,i}\begin{bmatrix} B_1 & B_2 \end{bmatrix}\left(\begin{bmatrix} A_{11} & A_{12} \\ A_{21} & A_{22} \end{bmatrix}\right)^{-1}\begin{bmatrix} B_1^H \\ B_2^H \end{bmatrix} \otimes \mathbf{I} \\
&= \sigma^2_{E,i}\mathbf{I} - \sigma^4_{E,i}\Big((B_1 - B_2A_{22}^{-1}A_{21})(A_{11} - A_{12}A_{22}^{-1}A_{21})^{-1} \\
&\quad \times (B_1 - B_2A_{22}^{-1}A_{21})^H + B_2A_{22}^{-1}B_2^H\Big) \otimes \mathbf{I} \qquad (5.44)
\end{aligned}
$$

where one can easily verify that $A_{22}^{-1} = \mathbf{I} - \mathbf{x}_i(\frac{1}{\sigma^2_{E,i}} + \mathbf{x}_i^H\mathbf{x}_i)^{-1}\mathbf{x}_i^H$, $B_2A_{22}^{-1}B_2^H = \frac{\mathbf{x}_i^H\mathbf{x}_i}{1+\sigma^2_{E,i}\mathbf{x}_i^H\mathbf{x}_i}$, $B_1 - B_2A_{22}^{-1}A_{21} = \frac{\mathbf{s}_i^T\bar{\mathbf{P}}^*}{1+\sigma^2_{E,i}\mathbf{x}_i^H\mathbf{x}_i}$ and $A_{12}A_{22}^{-1}A_{21} = \sigma^4_{E,i}\frac{\mathbf{x}_i^H\mathbf{x}_i}{1+\sigma^2_{E,i}\mathbf{x}_i^H\mathbf{x}_i}\mathbf{p}_i\mathbf{p}_i^H$. Therefore,

$$
A_{11} - A_{12}A_{22}^{-1}A_{21} = \mathbf{I} + \bar{\mathbf{P}}^{\mathbf{T}}\Sigma_E\bar{\mathbf{P}}^* - \sigma^4_{E,i}\frac{\mathbf{x}_i^H\mathbf{x}_i}{1+\sigma^2_{E,i}\mathbf{x}_i^H\mathbf{x}_i}\mathbf{p}_i\mathbf{p}_i^H = \mathbf{I} + \bar{\mathbf{P}}^{\mathbf{T}}\Sigma_{E,i}\bar{\mathbf{P}}^*. \qquad (5.45)
$$

where $\Sigma_{E,i} = diag(\sigma^2_{E,1}, \cdots, \frac{\sigma^2_{E,i}}{1+\sigma^2_{E,i}\mathbf{x}_i^H\mathbf{x}_i}, \cdots, \sigma^2_{E,M}) = \Sigma_E\tilde{\Sigma}_{E,i}$

and $\tilde{\Sigma}_{E,i} = diag(1, \cdots, \frac{1}{1+\sigma^2_{E,i}\mathbf{x}_i^H\mathbf{x}_i}, \cdots, 1)$. Finally, (5.44) can be simplified as follows

$$
\begin{aligned}
&var(\Delta\tilde{\mathbf{h}}_{E,i}) \\
&= \left(\frac{\sigma^2_{E,i} - \sigma^4_{E,i}\mathbf{s}_i^T(\Sigma_E + \tilde{\Sigma}_{E,i}^{-1}(\bar{\mathbf{P}}^*\bar{\mathbf{P}}^{\mathbf{T}})^{-1})^{-1}\mathbf{s}_i}{1+\sigma^2_{E,i}\mathbf{x}_i^H\mathbf{x}_i}\right) \otimes \mathbf{I}_{N_E} \\
&= \mathbf{s}_i^T\left(\Sigma_{E,i}^{-1} + \bar{\mathbf{P}}^*\bar{\mathbf{P}}^{\mathbf{T}}\right)^{-1}\mathbf{s}_i \otimes \mathbf{I}_{N_E} \\
&= \beta_{E,i}(l)(\sigma^2_{E,i} - \Delta\beta_{E,i}(n_t,l)) \otimes \mathbf{I}_{N_E} = \beta_{E,i}(n_t,l) \otimes \mathbf{I}_{N_E} \qquad (5.46)
\end{aligned}
$$

where $\beta_{E,i}(l)$ is decreasing with l and $\beta_{E,i}(n_t,l)$ is increasing with l. Therefore, Eve improves it's CSI estimation by correctly guessing l number of transmitted information symbol from AP as $var(\Delta\tilde{\mathbf{h}}_{E,i})$ decreases as l increases.

5.5 Numerical Results

In this section, we present numerical results of the averaged secrecy throughput T_s of secret information transmission from Alice equipped with N_A to a single antenna user after the application of ANECE participated by Alice and $N-1$ collaborative single-antenna users. Here, we set $\sigma_{A,i}=1$ and $\sigma_{E,i}=1$ for all i. Unless otherwise specified, we use $P_1=P_2=25$dB, $\delta=0.001$, $N=4$, $N_A=2$, $N_E=2$, $\sigma_{E,A}=1$, $n_1=6$, $n_2=300$, and $n_b=200$. To compute $T_s^{(d)}$ in (5.23), we use $\gamma_1=15$ (here $V_e(15)=0.996$ and for any $y\geq 15$, monotonically increasing function $V_e(y)\approx 1$ holds fairly) and $M=16$. We also compare our theoretical results (TR) with 10^4-run Monte Carlo (MC) simulation results.

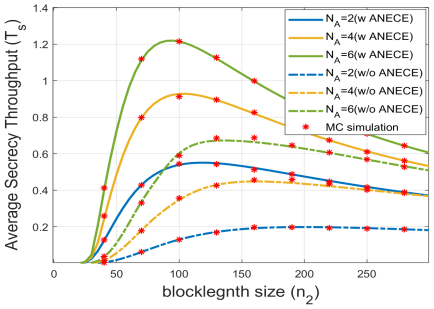

Figure 5.1: T_s versus n_2 for $N_A=2,4,6$, $N_E=2$, $M=25$ and $N=4$.

Fig. 5.1 depicts the relation between T_s and the blocklength n_2 for different N_A. We observe that T_s increases as the number of transmit antenna N_A increases for the two cases: "with ANECE" and "without ANECE". Here, we see a significant gap of T_s between the two cases, i.e., a significant AST enhancement "with ANECE". Furthermore, we see that as n_2 increases, T_s increases initially and then decreases. The maximum point of T_s

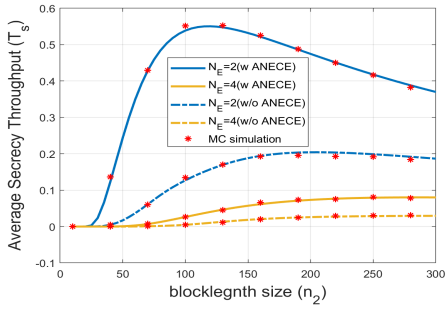

Figure 5.2: T_s versus n_2 for $N_A = 2$, $N_E = 2, 4$ and $N = 4$.

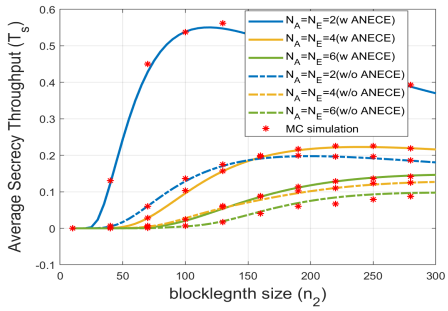

Figure 5.3: T_s versus n_2 for $N_A = N_E = 2, 4, 6$ and $N = 4$.

"with ANECE" is less sensitive to n_2 for different N_A.

In Fig. 5.2, we show T_s versus n_2 for different N_E, which also compares the cases of "with ANECE" and "without ANECE". As N_E increases, T_s decreases significantly for all n_2. We also observe that the optimum n_2 to maximize T_s is heavily dependent on N_E. To enhance the secrecy against multi-antenna Eve, Alice requires a larger number of antennas ($N_A \geq N_E$). In Fig. 5.3, we present the case when $N_A = N_E = [2, 4, 6]$.

Fig. 5.4 depicts the ANECE-assisted T_s versus n_2 and n_b (the number of secret bits transmitted per block). Here we also observe the quasi-concave nature of T_s with respect to n_2 for each fixed n_b. Thus, the theoretical results can be used to accurately find

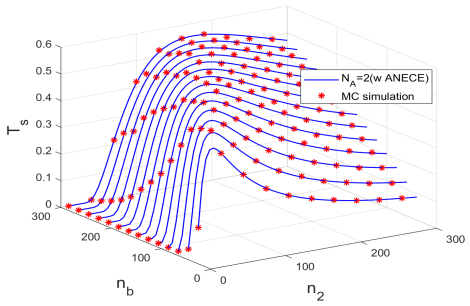

Figure 5.4: T_s vs n_2 and n_b for $N_A = 2$, $N_E = 2$ and $N = 4$.

the optimal n_2. Furthermore, the optimal n_2 increases with n_b.

Chapter 6

Conclusions

In this work, we investigate the techniques that improve physical layer security in wireless networks.

In chapter 2 and 3, we presented closed form expressions of secrecy outage probabilities (SOP) of several schemes for multi-antenna downlink transmissions against randomly located eavesdroppers (EDs). We considered both transmit antenna selection (TAS) and transmit antenna beamforming (TAB) schemes, full-duplex (FD) and half-duplex (HD) receivers/users, colluding and non-colluding EDs, the use of artificial noise (AN) from transmitter, and user selection based on their distances to the transmitter. For all these schemes and scenarios, we assume that EDs are distributed as the Poisson Point Process (PPP). For user selection, we also assume the PPP model for users' locations. The closed-form expressions of SOP are useful for numerical computations needed for network design purposes. We provided numerical examples to illustrate the usefulness of these expressions, which also revealed important observations such as the optimal jamming power from FD users and the

impacts of several other parameters on SOP.

In chapter 4, We have analysed AST of ANECE assisted transmission between single-antenna full-duplex devices against Eve with multiple antennas. The resulting expressions of AST are easy to compute and consistent with the results from costly Monte Carlo simulations. This analysis once again reveals a large gain of secrecy achievable from ANECE. Furthermore, this analysis is done in the context of finite blocklength, which is important for latency sensitive applications.

In chapter 5, we have analyzed the AST of ANECE assisted downlink transmission with transmit antenna beamforming against Eve with multiple antennas. The resulting expressions of AST are useful to analyze the impact of various parameters (i.e, block-length, training sequence length, numbers of antennas at Alice and Eve) on the AST. The numerical results are consistent with the results from costly Monte Carlo simulations. Furthermore, this analysis reveals a large gain of secrecy achievable from ANECE and transmit antenna beamforming under the reliability and latency constraints.

Chapter 7

Appendix

.1 Proof of (2.14)

It follows from (2.1), (2.7) and (2.8) that

$$\begin{aligned} P_{con,\Phi,Y} &\triangleq P[S_{AB}^{TAS} > R_s|\Phi, Y] \\ &= P\left[\left.\frac{1+SNR_{AB}^{TAS}}{1+\max\limits_{e\in\Phi} SNR_{AE_e}^{TAS}} > 2^{R_S}\right|\Phi, Y\right] \\ &= P\left[\left.\max_{e\in\Phi} SNR_{AE_e}^{TAS} < Y_0\right|\Phi, Y\right] \\ &= \prod_{e\in\Phi} P\left[\left.\frac{|h_{A_{i^*}E_e}|^2}{\frac{d_{AE_e}^{\alpha}}{P_T}+\frac{d_{AE_e}^{\alpha}}{d_{BE_e}^{\alpha}}m|h_{BE_e}|^2} < Y_0\right|\Phi, Y\right] \\ &= \prod_{e\in\Phi}\big(1-\Psi(Y, r_e, \theta_e)\big), \end{aligned} \tag{.1}$$

where (due to the lemma shown next)

$$\Psi(Y, r_e, \theta_e) = \frac{\exp(-\frac{d_{AE_e}^{\alpha}}{P_T}Y_0)}{1+m(\frac{d_{AE_e}}{d_{BE_e}})^{\alpha}Y_0}$$

We have applied the following lemma.

Lemma 6 *If A and B (like $|h_{A_{i^*}E_e}|^2$ and $|h_{BE_e}|^2$) are two independent random variables with the exponential distribution of unit mean, then $P(\frac{A}{a+bB} < c) = 1 - \frac{e^{-ac}}{1+bc}$.*

Note that we are only interested in such R_s that $\log_2(1 + SNR_{AB}) \geq R_s$, which implies $Y_0 \geq 0$.

Let $P_{con,Y}$ be P_{con} conditional only on Y. Applying the Campbell's theorem [38] to (.1) yields:

$$\begin{aligned} P_{con,Y} &= \mathbb{E}_\Phi\{P[SNR_{AB}^{TAS} > R_s|\Phi, Y]\} \\ &= \exp\bigg[-\rho_E \int_0^R \int_0^{2\pi} \Psi(Y, r, \theta) r \mathrm{d}\theta \mathrm{d}r\bigg]. \end{aligned}$$

.2 A simplification of the double integral in (2.14)

Assume $R_s = 0$ and $\alpha = 2$. Then, $\beta = 1$ and $Y_0 = Y$. Let the distance between Alice and Bob be d. Then, $\frac{d_{AE}^\alpha}{d_{BE}^\alpha} = \frac{d_{AE}^2}{d_{BE}^2} = \frac{r^2}{r^2+d^2-2rd\cos\theta}$, and furthermore

$$\begin{aligned} & \int_0^R \int_0^{2\pi} \Psi(Y, r, \theta) r \mathrm{d}\theta \mathrm{d}r \\ = & \int_0^R \int_0^{2\pi} \frac{\exp(-\frac{Yr^2}{P_T})}{1 + mY\frac{r^2}{r^2+d^2-2rd\cos\theta}} r \mathrm{d}\theta \mathrm{d}r \\ = & \int_0^R \int_0^{2\pi} \exp(-\frac{Yr^2}{P_T}) \\ & \times \frac{\big((1+mY)r^2 + d^2 - 2rd\cos\theta\big) - mYr^2}{(1+mY)r^2 + d^2 - 2rd\cos\theta} r \mathrm{d}\theta \mathrm{d}r \\ = & 2\pi \int_0^R \exp(-\frac{Yr^2}{P_T}) r \mathrm{d}r \\ & - \int_0^R \int_0^{2\pi} \frac{mYr^3 \exp(-\frac{Yr^2}{P_T})}{(1+mY)r^2 + d^2 - 2rd\cos\theta} \mathrm{d}\theta \mathrm{d}r, \end{aligned} \tag{.2}$$

where the first term can be obviously reduced. The second term in (.2), can be

simplified by applying $\int_0^{2\pi} \frac{1}{a-b\cos\theta}\mathrm{d}\theta = \frac{2\pi}{\sqrt{a^2-b^2}}$ identity. Then, (.2) yields

$$\begin{aligned}
&\int_0^R \int_0^{2\pi} \Psi(Y,r,\theta) r \mathrm{d}\theta \mathrm{d}r \\
= \;& \frac{\pi P_T}{Y}\left(1-\exp\left(-\frac{YR^2}{P_T}\right)\right) - 2\pi mY \\
& \times \int_0^R \frac{r^3 \exp(-\frac{Yr^2}{P_T})}{\sqrt{\left((1+mY)r^2+d^2\right)^2 - 4r^2d^2}}\mathrm{d}r \\
= \;& \frac{\pi P_T}{Y}\left(1-\exp\left(-\frac{YR^2}{P_T}\right)\right) - \pi mY \\
& \times \int_0^{R^2} \frac{\exp\left(-\frac{Yr}{P_T}\right) r}{\sqrt{\left((1+mY)r+d^2\right)^2 - 4rd^2}}\mathrm{d}r. \qquad (.3)
\end{aligned}$$

which is a much simplified expression of the double integral in (2.14).

.3 Proof of Lemma 3

Here, $Z = \frac{\|\mathbf{h}\|^2}{\frac{1}{P_T}+\rho m|g_B|^2}$. Lets consider, $Y_3 = \|\mathbf{h}\|^2$, $Y_2 = \frac{1}{P_T} + \rho m|g_B|^2$ and $Z = \frac{Y_3}{Y_2}$. Note that $f_{Y_3}(x) = \frac{1}{\Gamma(M)}x^{M-1}e^{-x}$ and $f_{Y_2}(x) = \frac{1}{\rho m}exp(-\frac{x-\frac{1}{P_T}}{\rho m}), x > \frac{1}{P_T}$.

$$\begin{aligned}
F_Z(z) &= P[\frac{Y_3}{Y_1} < z] \\
&= P[|g_B|^2 > \frac{Y_3 - \frac{z}{P_T}}{z\rho m}] \\
&= \int_{y=0}^{\infty} f_{Y_3}(y)dy \int_{x=\frac{y-\frac{z}{P_T}}{z\rho m}}^{\infty} e^{-x}dx \\
&= \frac{1}{\Gamma(M)}\int_{y=0}^{\infty} y^{M-1}e^{-y}e^{-\frac{y-\frac{z}{P_T}}{z\rho m}}dy \\
&= \frac{e^{\frac{1}{\rho P_J}}}{\Gamma(M)(1+\frac{1}{z\rho m})^M}\int_{y=0}^{\infty}\big(y(1+\frac{1}{z\rho m})\big)^{M-1} \\
&\quad \times e^{-y(1+\frac{1}{z\rho m})}d\big(y(1+\frac{1}{z\rho m})\big) \\
&= \frac{e^{\frac{1}{\rho P_J}}}{(1+\frac{1}{z\rho m})^M}. \qquad (.4)
\end{aligned}$$

If $m > 0$ then, $f_Z(z) = e^{\frac{1}{\rho P_J}} M\rho m \frac{z\rho m^{M-1}}{(1+z\rho m)^{M+1}}$. Ror $m = 0$, Z follows scaled CHI squared distribution.

.4 Proof of (2.24)

The secrecy of the TAB scheme can be analyzed as follows.

$$
\begin{aligned}
& P_{con,\Phi,\mathbf{h},g_B} \stackrel{\Delta}{=} P[S_{AB} > R_S|\Phi,\mathbf{h},g_B] \\
= \;& P[S_{AB} > R_S|\Phi,z] \\
= \;& P\left[\max_{e\in\Phi} SNR_{AE_e}^{TAB} < \frac{SNR_{AB}}{\beta} - (1-\frac{1}{\beta})\middle|\Phi,z\right] \\
= \;& P\Bigg[\max_{e\in\Phi} \frac{X_1\Theta}{d_{AE}^{\alpha} + \frac{P_J d_{AE_e}^{\alpha}}{d_{BE_e}^{\alpha}} X_2 + \frac{\epsilon P_T}{M-1} X_1(1-\Theta)} \\
& \qquad < \frac{\|\mathbf{h}\|^2}{\beta(1+\rho|g_B|^2 P_J)} - \frac{1-\frac{1}{\beta}}{(1-\epsilon)P_T}\Bigg|\Phi,z\Bigg] \\
= \;& \prod_{e\in\Phi} P\Bigg[\frac{X_1\Theta}{\frac{P_J d_{AE_e}^{\alpha}}{d_{BE_e}^{\alpha}}\left(X_2 + \frac{d_{BE}^{\alpha}}{P_J}\right) + \frac{\epsilon P_T}{M-1} X_1(1-\Theta)} \\
& \qquad < c\Bigg|\Phi,z\Bigg] \\
= \;& \prod_{e\in\Phi} P\left[\Theta < \frac{\frac{\epsilon}{M-1} + f_e \frac{X_3}{X_1}}{\frac{\epsilon}{M-1} + g}\middle|\Phi,z\right], \qquad (.5)
\end{aligned}
$$

where $X_3 = X_2 + \frac{d_{BE}^{\alpha}}{P_J}$, and X_1, X_2 and $\mathbf{\Theta}$ are independent variables as defined previously (after (2.11)). It is easy to verify that $f_{\frac{X_2}{X_1}}(x) = M(1+x)^{-(M+1)}$, which is similar to the $F(2,2M)$ distribution [37]. When large scale channel gain of jamming signal at ED is higher than noise level, i.e., $\frac{P_J}{d_{BE}^{\alpha}} \gg 1$, the shift between X_3 and X_2 becomes smaller. Furthermore, one can verify that $f_{\frac{X_3}{X_1}}(x) \approx e^{\frac{d_{BE}^{\alpha}}{P_J}} M(1+x)^{-(M+1)}$. It follows from the PDF $f_\Theta(x)$ shown earlier that the CDF of Θ is $F_\Theta(x) = 1-(1-x)^{M-1}$. Then, it is shown in Appendix .4.1

that

$$P\left[\Theta > \frac{\frac{\epsilon}{M-1} + f_e \frac{X_3}{X_1}}{\frac{\epsilon}{M-1} + g} | \Phi, z\right] = \frac{e^{\frac{d_{BE}^{\alpha}}{P_J}}}{(1 + \frac{f_e}{g})(1 + \frac{\epsilon}{(M-1)g})^{M-1}}, \tag{.6}$$

where g is a function of Z as defined before. Averaging over the PPP distribution of the locations of the Eves, one can verify (using the Campbell's theorem) that

$$\begin{aligned}
P_{con,\mathbf{h},g_B} = P_{con,z} &\stackrel{\Delta}{=} \mathbb{E}_{\Phi}\{P[S_{AB} > R_S | \Phi, \mathbf{h}, g_B]\} \\
&= \mathbb{E}_{\Phi}\left[\prod_{e \in \Phi}\left(1 - P\left[\Theta > \frac{\frac{\epsilon}{M-1} + f_e \frac{X_3}{X_1}}{\frac{\epsilon}{M-1} + g} | \Phi, z\right]\right)\right] \\
&= \mathbb{E}_{\Phi}\left[\prod_{e \in \Phi}\left(1 - \frac{e^{\frac{d_{BE}^{\alpha}}{P_J}}}{(1 + \frac{f_e}{g})(1 + \frac{\epsilon}{(M-1)g})^{M-1}}\right)\right] \\
&= \exp\left[-\rho_E \int_0^R r \int_0^{2\pi} \Omega(\frac{1}{g}; r, \theta) \mathrm{d}\theta \mathrm{d}r\right],
\end{aligned}$$

where z is a realization of Z, g is a function of z, and

$$\Omega(\frac{1}{g}; r, \theta) = \frac{e^{\frac{d_{BE}^{\alpha}}{P_J}}}{(1 + \frac{f_e}{g})(1 + \frac{\epsilon}{(M-1)g})^{M-1}}.$$

.4.1 Proof of (.6)

The complement of (.6) is

$$\begin{aligned}
& P[\Theta < \frac{\frac{\epsilon}{M-1} + f_e \frac{X_3}{X_1}}{\frac{\epsilon}{M-1} + g} | \Phi, z] \\
= & \int_0^{\infty} F_{\Theta}\left(\frac{\frac{\epsilon}{M-1} + f_e x}{\frac{\epsilon}{M-1} + g}\right) f_{\frac{X_3}{X_1}}(x) \mathrm{d}x \\
= & \int_0^{\frac{g}{f_e}} F_{\Theta}\left(\frac{\frac{\epsilon}{M-1} + f_e x}{\frac{\epsilon}{M-1} + g}\right) f_{\frac{X_3}{X_1}}(x) \mathrm{d}x \\
& + \int_{\frac{g}{f_e}}^{\infty} F_{\Theta}\left(\frac{\frac{\epsilon}{M-1} + f_e x}{\frac{\epsilon}{M-1} + g}\right) f_{\frac{X_3}{X_1}}(x) \mathrm{d}x.
\end{aligned} \tag{.7}$$

Here, $F_{\Theta}(y) = 1$ for $y \geq 1$, so $F_{\Theta}\left(\frac{\frac{\epsilon}{M-1} + f_e x}{\frac{\epsilon}{M-1} + g}\right) = 1$ for $x \geq \frac{g}{f_e}$. Then (.7) continues

as follows:

$$\begin{aligned}
&\int_0^{\frac{g}{f_e}} F_\Theta\left(\frac{\frac{\epsilon}{M-1}+f_e x}{\frac{\epsilon}{M-1}+g}\right) f_{\frac{X_3}{X_1}}(x)\mathrm{d}x + \int_{\frac{g}{f_e}}^{\infty} f_{\frac{X_3}{X_1}}(x)\mathrm{d}x \\
&= \int_0^{\frac{g}{f_e}} \left[1-\left(1-\frac{\frac{\epsilon}{M-1}+f_e x}{\frac{\epsilon}{M-1}+g}\right)^{M-1}\right] f_{\frac{X_3}{X_1}}(x)\mathrm{d}x \\
&\quad + 1 - \int_{x=0}^{\frac{g}{f_e}} f_{\frac{X_3}{X_1}}(x)\mathrm{d}x \\
&= 1 - \frac{M e^{\frac{d_{BE_e}^{\alpha}}{P_J}} g^{M-1}}{(\frac{\epsilon}{M-1}+g)^{M-1}} \int_0^{\frac{g}{f_e}} \left(\frac{1-\frac{f_e}{g}x}{1+x}\right)^{M-1} \frac{\mathrm{d}x}{(1+x)^2}.
\end{aligned} \tag{.8}$$

Let $k=\frac{f_e}{g}$ and $z=\frac{1}{1+x}$. Then $(\frac{1-kx}{1+x})^{M-1} = k^{M-1}\big(-1+z\frac{k+1}{k}\big)^{M-1}$. The above leads to

$$\begin{aligned}
&P[\Theta < \frac{\frac{\epsilon}{M-1}+f_e\frac{X_3}{X_1}}{\frac{\epsilon}{M-1}+g}|\Phi, z] \\
&= 1 - \frac{M e^{\frac{d_{BE_e}^{\alpha}}{P_J}} (gk)^{M-1}}{(\frac{\epsilon}{M-1}+g)^{M-1}} \int_{\frac{k}{k+1}}^{1} \big(-1+z(\frac{k+1}{k})\big)^{M-1}\mathrm{d}z.
\end{aligned} \tag{.9}$$

Now, using $y=z(\frac{k+1}{k})-1$, we have

$$\begin{aligned}
&P[\Theta < \frac{\frac{\epsilon}{M-1}+f_e\frac{X_3}{X_1}}{\frac{\epsilon}{M-1}+g}|\Phi, \mathbf{h}, g_B] \\
&= 1 - \frac{M e^{\frac{d_{BE_e}^{\alpha}}{P_J}} k^M}{(1+k)(1+\frac{\epsilon}{(M-1)g})^{M-1}} \int_{y=0}^{y=\frac{1}{k}} y^{M-1}\mathrm{d}y \\
&= 1 - \frac{e^{\frac{d_{BE_e}^{\alpha}}{P_J}}}{(1+\frac{f_e}{g})(1+\frac{\epsilon}{(M-1)g})^{M-1}}.
\end{aligned} \tag{.10}$$

.5 Unimodality of Ω

From (2.25), we have

$$\Omega(\frac{1}{g}; r, \theta) = \underbrace{\frac{e^{\frac{d_{BE_e}^{\alpha}}{P_J}}}{\left(1+\frac{f_e}{g}\right)}}_{\Omega_1(P_J)} \underbrace{\frac{1}{\left(1+\frac{\epsilon}{(M-1)g}\right)^{M-1}}}_{\Omega_2(P_J)}, \tag{.11}$$

where $\Omega_1(P_J)$ and $\Omega_2(P_J)$ are shown below to be positive and strictly monotonically decreasing and increasing functions, respectively, w.r.t. P_J, i.e., $\Omega_1^{'}(P_J) < 0$ and $\Omega_2^{'}(P_J) > 0$ for any $P_J \geq 0$. We will apply $x = \frac{1}{P_J}$ where $x \in (0, \infty)$ as $P_J \in (0, \infty)$. Now, recall $f_e = (\frac{d_{AE_e}}{d_{BE_e}})^{\alpha} \frac{P_J}{P_T}$ and $g = \frac{\beta(1+\rho P_J |g_B|^2)}{P_T \|\mathbf{h}\|^2}$. Then, it follows that

$$\begin{aligned} \Omega_1(x) &= e^{x d_{BE_e}^{\alpha}} \left(1 - \frac{k_e}{x + k_e + \rho|g_B|^2}\right) \\ \Omega_1^{'}(x) &= \Omega_1(x) \left(d_{BE_e}^{\alpha} + \frac{k_e}{(x + k_e + \rho|g_B|^2)(x + \rho|g_B|^2)}\right), \end{aligned} \tag{.12}$$

where $k_e = \left(\frac{d_{AEe}}{d_{BEe}}\right)^{\alpha} \frac{\|\mathbf{h}\|^2}{\beta}$, and $\Omega_1(x)$ and $\Omega_1^{'}(x)$ are strictly positive. Also,

$$\begin{aligned} \Omega_2(x) &= \frac{1}{\left(1 + \frac{kx}{x+\rho|g_B|^2}\right)^{M-1}} \\ \Omega_2^{'}(x) &= -\Omega_2(x) \frac{(M-1)k\rho|g_B|^2}{(x + kx + \rho|g_B|^2)(x + \rho|g_B|^2)}, \end{aligned} \tag{.13}$$

where $k = \frac{\epsilon P_T ||\mathbf{h}||^2}{(M-1)\beta}$, and $\Omega_2(x)$ and $\Omega_2^{'}(x)$ are strictly positive and negative respectively.

Next, we will show that $\Omega(x) = \Omega_1(x)\Omega_2(x)$ is a unimodal function with minimum at a finite nonzero x. Consider the following stationary condition on x $\Omega^{'}(x) = \Omega_1(x)\Omega_2^{'}(x) + \Omega_2(x)\Omega_1^{'}(x) = 0$ or equivalently $\frac{\Omega_2^{'}(x)}{\Omega_2(x)} = -\frac{\Omega_1^{'}(x)}{\Omega_1(x)}$ which can be further reduced to

$$\begin{aligned} \frac{\Omega_2^{'}(x)}{\Omega_2(x)} &= -\frac{\Omega_1^{'}(x)}{\Omega_1(x)} \\ d_{BE_e}^{\alpha} + \frac{M}{x + \rho|g_B|^2} &= \frac{1}{x + k_e + \rho|g_B|^2} + \frac{M-1}{x + \frac{\rho|g_B|^2}{k+1}}. \end{aligned} \tag{.14}$$

Using $y = x + \rho|g_B|^2$ in (.14) and after some algebraic manipulations, we get

$$y^3 + \left(k_e - \frac{k\rho|g_B|^2}{k+1}\right) y^2 + \left(\frac{k_e}{d^{\alpha}_{BE_e}} - \frac{k\rho|g_B|^2}{k+1}(k_e + \frac{M-1}{d^{\alpha}_{BE_e}})\right) y - \frac{Mk_e k\rho|g_B|^2}{d^{\alpha}_{BE_e}(k+1)} = 0, \tag{.15}$$

which is a cubic polynomial equation. Based on the characteristics of cubic polynomials, (.15) has one, two or three roots and one inflection point [43]. Furthermore, a cubic function is anti-symmetric around its inflection point. To show that (.15) has only one positive solution, we just need to show that the inflection point is negative. The inflection point is where the second-order derivative of the cubic function is zero, i.e., $6y - 2(k_e - \frac{k\rho|g_B|^2}{k+1}) = 0$, or equivalently $x = -\frac{2k+3}{3(k+1)}\rho|g_B|^2 - \frac{k_e}{3}$, which in this case is indeed negative.

Finally, it is easy to verify that $\Omega(\frac{1}{g}; r, \theta)$ is a decreasing function of P_J at $P_J = 0$. Therefore, we have shown that $\Omega(\frac{1}{g}; r, \theta)$ for any r and θ has its minimum at a positive finite P_J.

.6 Proof of (2.27)

Assume $\alpha = 2$ and $\beta = 1$. Then, $g = 1/z$, and

$$\begin{aligned}
&\int_0^R \int_0^{2\pi} \Omega(z; r, \theta) \mathrm{d}\theta r \mathrm{d}r \\
&= \frac{1}{(1 + \frac{z\epsilon}{M-1})^{M-1}} \int_0^R \int_0^{2\pi} \frac{1}{1 + zm\frac{r^2}{r^2 + d^2 - 2rdcos\theta}} \mathrm{d}\theta r \mathrm{d}r \\
&= \frac{1}{(1 + \frac{z\epsilon}{M-1})^{M-1}} \int_0^R \int_0^{2\pi} \Big(1 - \\
&\quad \frac{zmr^2}{(1+zm)r^2 + d^2 - 2rdcos\theta}\Big) \mathrm{d}\theta r \mathrm{d}r,
\end{aligned} \tag{.16}$$

where

$$\int_0^{2\pi} \big(1 - \frac{zmr^2}{(1+zm)r^2 + d^2 - 2rdcos\theta}\big)\mathrm{d}\theta$$
$$= 2\pi\bigg(1 - \frac{1}{\sqrt{1+\frac{(r+d)^2}{r^2zm}}\sqrt{1+\frac{(r-d)^2}{r^2zm}}}\bigg). \tag{.17}$$

Combining (.16) and (.17) yields (27).

.7 Proof of (2.29)

Assuming $P_J = 0$ and a large P_T, it follows that $c = \frac{\|\mathbf{h}\|^2}{\beta} - \frac{1-\frac{1}{\beta}}{(1-\epsilon)P_T} \approx \frac{\|\mathbf{h}\|^2}{\beta}$ and $z = P_T\|\mathbf{h}\|^2$. And from (.5), we have

$$\begin{aligned} & P[S_{AB} > R_S|\Phi, \mathbf{h}, g_B] \\ = & \prod_{e\in\Phi} P\big[\frac{X_1\Theta}{d_{AE_e}^{\alpha} + \frac{\epsilon P_T}{M-1}X_1(1-\Theta)} < c|\Phi, \mathbf{h}, g_B\big] \\ = & \prod_{e\in\Phi} P\big[\frac{X_4}{d_{AE_e}^{\alpha} + \frac{\epsilon P_T}{M-1}X_{4,4}} < \frac{\|\mathbf{h}\|^2}{\beta}|\Phi, \mathbf{h}, g_B\big], \end{aligned} \tag{.18}$$

where $X_4 = \Theta X_1$ is exponentially distributed with mean =1 and $X_{4,4} = (1-\Theta)X_1$ is independent of X_4 and has the $\Gamma(M-1, 1)$ distribution. Then,

$$
\begin{aligned}
&P\big[\frac{X_4}{d_{AE_e}^{\alpha}+\frac{\epsilon P_T}{M-1}X_{4,4}}<\frac{\|\mathbf{h}\|^2}{\beta}|\Phi,\mathbf{h},g_B\big]\\
&=P\big[X_4<\left(\frac{\|\mathbf{h}\|^2}{\beta}d_{AE_e}^{\alpha}+\frac{\|\mathbf{h}\|^2}{\beta}\frac{\epsilon P_T y}{M-1}\right)|\Phi,\mathbf{h},g_B\big]\\
&=\int_0^{\infty}F_{X_4}\left(\frac{\|\mathbf{h}\|^2}{\beta}d_{AE_e}^{\alpha}+\frac{\|\mathbf{h}\|^2}{\beta}\frac{\epsilon P_T y}{M-1}\right)f_{X_{4,4}}(y)\mathrm{d}y\\
&=\int_0^{\infty}\left[1-\exp\left\{-\left(\frac{\|\mathbf{h}\|^2}{\beta}d_{AE_e}^{\alpha}+\frac{\|\mathbf{h}\|^2}{\beta}\frac{\epsilon P_T y}{M-1}\right)\right\}\right]\\
&\times f_{X_{4,4}}(y)\mathrm{d}y\\
&=1-\int_0^{\infty}\exp\left\{-\left(\frac{\|\mathbf{h}\|^2}{\beta}d_{AE_e}^{\alpha}+\frac{\|\mathbf{h}\|^2}{\beta}\frac{\epsilon P_T y}{M-1}\right)\right\}\\
&\times\frac{y^{M-2}e^{-y}}{\Gamma(M-1)}\mathrm{d}y\\
&=1-\frac{e^{-\frac{\|\mathbf{h}\|^2}{\beta}d_{AE_e}^{\alpha}}}{\Gamma(M-1)}\int_0^{\infty}e^{-(1+\frac{\|\mathbf{h}\|^2}{\beta}\frac{\epsilon P_T}{M-1})y}y^{M-2}\mathrm{d}y\\
&=1-\frac{e^{-\frac{z}{\beta}\frac{d_{AE_e}^{\alpha}}{P_T}}}{(1+\frac{z}{\beta}\frac{\epsilon}{M-1})^{M-1}} \qquad (.19)\\
&=1-\Omega(z;r,\theta), \qquad (.20)
\end{aligned}
$$

And then

$$
\begin{aligned}
&\int_0^R\int_0^{2\pi}\Omega(z;r,\theta)d\theta r\mathrm{d}r=\frac{2\pi}{(1+\frac{\epsilon z}{\beta(M-1)})^{M-1}}\int_0^R e^{-\frac{zr^{\alpha}}{\beta P_T}}r\mathrm{d}r\\
&=\frac{2\pi\beta^{\frac{2}{\alpha}}}{\alpha(\|\mathbf{h}\|^2)^{\frac{2}{\alpha}}(1+\frac{\epsilon P_T}{M-1}\frac{\|\mathbf{h}\|^2}{\beta})^{M-1}}\int_0^{\frac{R^{\alpha}\|\mathbf{h}\|^2}{\beta}}e^{-y}y^{\frac{2}{\alpha}-1}y\mathrm{d}y\\
&=\frac{2\pi\beta^{\frac{2}{\alpha}}}{\alpha(\|\mathbf{h}\|^2)^{\frac{2}{\alpha}}(1+\frac{\epsilon P_T}{M-1}\frac{\|\mathbf{h}\|^2}{\beta})^{M-1}}\gamma(\frac{2}{\alpha},\frac{R^{\alpha}\|\mathbf{h}\|^2}{\beta}). \qquad (.21)
\end{aligned}
$$

which is (2.29).

.8 Proof of (2.30)

$$
\begin{aligned}
&P[S_{AB_n} > R_s | d_{AB_n}, \Phi_E] \\
&= P[\max_{e\in\Phi_E} SNR_{AE_e} < \frac{SNR_{AB_n}}{\beta} + (\frac{1}{\beta} - 1)] \\
&= P[\max_{e\in\Phi_E} \frac{(1-\epsilon)P_T X_4}{d^\alpha_{AE_e} + \frac{\epsilon P_T}{M-1} X_{4,4}} < \frac{(1-\epsilon)P_T X_{2,n}}{\beta d^\alpha_{AB_n}} + (\frac{1}{\beta} - 1)] \\
&\approx P[\max_{e\in\Phi_E} \frac{X_4}{d^\alpha_{AE_e} + \frac{\epsilon P_T}{M-1} X_{4,4}} < \frac{X_{2,n}}{\beta d^\alpha_{AB_n}}] \quad \text{(for large } P_T\text{)}
\end{aligned}
$$

And then

$$
\begin{aligned}
&P[\max_{e\in\Phi_E} \frac{X_4}{d^\alpha_{AE_e} + \frac{\epsilon P_T}{M-1} X_{4,4}} < \frac{X_{2,n}}{\beta d^\alpha_{AB_n}}] \\
&= \prod_{e\in\Phi_E} P[\frac{X_4}{X_{2,n}} < \frac{d^\alpha_{AE_e} + \frac{\epsilon P_T}{M-1} X_{4,4}}{\beta d^\alpha_{AB_n}}] \\
&= \prod_{e\in\Phi_E} \int_0^\infty f_{X_{4,4}}(x) F_{\frac{X_4}{X_{2,n}}} \left(\frac{d^\alpha_{AE_e} + \frac{\epsilon P_T}{M-1} X_{4,4}}{\beta d^\alpha_{AB_n}} \right) \mathrm{d}x \\
&= \prod_{e\in\Phi_E} \int_0^\infty f_{X_{4,4}}(x) \left[1 - \left(1 + \frac{d^\alpha_{AE_e} + \frac{\epsilon P_T}{M-1} X_{4,4}}{\beta d^\alpha_{AB_n}} \right)^{-M} \right] \mathrm{d}x \\
&= \prod_{e\in\Phi_E} \left(1 - \int_0^\infty f_{X_{4,4}}(x) \left(1 + \frac{d^\alpha_{AE_e} + \frac{\epsilon P_T}{M-1} x}{\beta d^\alpha_{AB_n}} \right)^{-M} \right) \\
&= \prod_{e\in\Phi_E} \big(1 - \frac{1}{(\frac{\epsilon P_T}{(M-1)\beta d^\alpha_{AB_n}})^M} U(M, 2, \frac{(M-1)\beta d^\alpha_{AB_n}}{\epsilon P_T} \\
&\qquad + \frac{(M-1) d^\alpha_{AE_e}}{\epsilon P_T}) \big), \qquad (.22)
\end{aligned}
$$

where U denotes the confluent hypergeometric function of the second kind [42]. After applying Campbell's theorem [38] and setting $d_{AE_e} = r$, we have

$$P[S_{AB} > R_s | d_{AB_n}] = \exp\big(- 2\pi\rho_E (\frac{(M-1)\beta d_{AB_n}^{\alpha}}{\epsilon P_T})^M \times \int_0^{\infty} U(M, 2, \frac{(M-1)\beta d_{AB_n}^{\alpha}}{\epsilon P_T} + \frac{(M-1)r^{\alpha}}{\epsilon P_T}) r \mathrm{d}r \big). \tag{.23}$$

Further simplification can be done by using proof as shown in subsection .8.1:

$$\begin{aligned} &\left(\frac{(M-1)\beta d_{AB_n}^{\alpha}}{\epsilon P_T}\right)^M \int_0^{\infty} U(M, 2, \frac{(M-1)\beta d_{AB_n}^{\alpha}}{\epsilon P_T} + \\ &\quad \frac{(M-1)r^{\alpha}}{\epsilon P_T}) r \mathrm{d}r \\ &= \frac{1}{\alpha} \frac{(\beta d_{AB_n}^{\alpha})^M B(M - \frac{2}{\alpha}, \frac{2}{\alpha})}{(\frac{\epsilon P_T}{M-1})^{M-\frac{2}{\alpha}}} U(M - \frac{2}{\alpha}, 2 - \frac{2}{\alpha}, \\ &\quad \frac{(M-1)\beta d_{AB_n}^{\alpha}}{\epsilon P_T}). \end{aligned} \tag{.24}$$

.8.1 Proof of (.24)

Using the change of variables $c = \frac{(M-1)\beta d_{AB_n}^{\alpha}}{\epsilon P_T}$, we can write

$$\begin{aligned} &(\frac{(M-1)\beta d_{AB_n}^{\alpha}}{\epsilon P_T})^M \int_0^{\infty} U(M, 2, \frac{(M-1)\beta d_{AB_n}^{\alpha}}{\epsilon P_T} \\ &\quad + \frac{(M-1)r^{\alpha}}{\epsilon P_T}) r \mathrm{d}r \\ &= \frac{c^M}{\Gamma(M)} \int_{r=0}^{\infty} \int_{t=0}^{\infty} e^{-(c + \frac{(M-1)r^{\alpha}}{\epsilon P_T})t} t^{M-1} (1+t)^{2-M-1} \mathrm{d}t r \mathrm{d}r \\ &= \frac{c^M}{\Gamma(M)} \int_{t=0}^{\infty} \left(e^{-ct} t^{M-1} (1+t)^{1-M} \int_{r=0}^{\infty} e^{-\frac{(M-1)r^{\alpha}}{\epsilon P_T} t} r \mathrm{d}r \right) \mathrm{d}t. \end{aligned}$$

Using another change of variables $x = \frac{(M-1)r^\alpha}{\epsilon P_T}t$, the above becomes

$$\begin{aligned}
&\frac{(\frac{\epsilon P_T}{M-1})^{\frac{2}{\alpha}}c^M\Gamma(\frac{2}{\alpha})}{\alpha\Gamma(M)}\int_0^\infty e^{-ct}t^{M-\frac{2}{\alpha}-1} \\
&\qquad \times (1+t)^{2-\frac{2}{\alpha}-M+\frac{2}{\alpha}-1}\mathrm{d}t \\
&= \frac{(\frac{\epsilon P_T}{M-1})^{\frac{2}{\alpha}}c^M\Gamma(\frac{2}{\alpha})\Gamma(M-\frac{2}{\alpha})}{\alpha\Gamma(M)}\frac{1}{\Gamma(M-\frac{2}{\alpha})} \\
&\qquad \times \int_0^\infty e^{-ct}t^{M-\frac{2}{\alpha}-1}(1+t)^{2-\frac{2}{\alpha}-M+\frac{2}{\alpha}-1}\mathrm{d}t \\
&= \frac{(\frac{\epsilon P_T}{M-1})^{\frac{2}{\alpha}}c^M B(M-\frac{2}{\alpha},\frac{2}{\alpha})}{\alpha} \\
&\qquad \times U(M-\frac{2}{\alpha}, 2-\frac{2}{\alpha}, \frac{(M-1)\beta d_{AB_n}^\alpha}{\epsilon P_T}). \qquad (.25)
\end{aligned}$$

.9 Proof of (2.31)

When $\epsilon = 0$, we have

$$\begin{aligned}
& P[S_{AB_n} > R_s | d_{AB_n}, \Phi_E] \\
= \;& P[\max_{e\in\Phi_E}\frac{P_T X_4}{d_{AE_e}^\alpha} < \frac{P_T X_{2,n}}{\beta d_{AB_n}^\alpha} + \frac{1}{\beta} - 1] \\
\approx \;& P[\max_{e\in\Phi_E}\frac{X_4}{d_{AE_e}^\alpha} < \frac{X_{2,n}}{\beta d_{AB_n}^\alpha}] \quad \text{(for large } P_T\text{)} \\
= \;& \prod_{e\in\Phi_E} P[\frac{X_4}{X_{2,n}} < \frac{d_{AE_e}^\alpha}{\beta d_{AB_n}^\alpha}], \qquad (.26)
\end{aligned}$$

where $\frac{X_4}{X_{2,n}}$ follows an F-distribution, i.e., $f_{\frac{X_4}{X_{2,n}}}(x) = M(1+x)^{-(M+1)}$ and $F_{\frac{X_4}{X_{2,n}}}(x) = 1-(1+x)^{-M}$. Then,

$$P[S_{AB_n} > R_s | d_{AB_n}, \Phi_E] = \prod_{e\in\Phi_E}\big(1-(1+\frac{d_{AE_e}^\alpha}{\beta d_{AB_n}^\alpha})^{-M}\big). \qquad (.27)$$

After applying the Campbell's theorem [38] and setting $d_{AE_e} = r$ and $d_{AB_n} = x$, we have

$$P[S_{AB_n} > R_s | d_{AB_n}] = \exp\Big(- \frac{2}{\alpha}\pi\rho_E\beta^{\frac{2}{\alpha}} d_{AB_n}^2 \times B(M - \frac{2}{\alpha}, \frac{2}{\alpha})\Big). \quad (.28)$$

The computation of averaged SOP requires the PDF of the distance of the nth nearest user. The following lemma is known [35]:

Lemma 7 *The PDF of* d_{AB_n} *is*

$$f_{d_{AB_n}}(x) = \exp(-\rho_U\pi x^2)\frac{2\rho_U^n\pi^n x^{2n-1}}{\Gamma(n)}. \quad (.29)$$

It now follows from this lemma and (.28) that

$$\begin{aligned} P[S_{AB} > R_s] &= \int_0^\infty \exp\Big(- \frac{2}{\alpha}\pi\rho_E\beta^{\frac{2}{\alpha}} x^2 B(M - \frac{2}{\alpha}, \frac{2}{\alpha})\Big) \\ &\quad \times \exp(-\rho_U\pi x^2)\frac{2\rho_U^n\pi^n x^{2n-1}}{\Gamma(n)}\mathrm{d}x \\ &= \frac{1}{\Big(1 + \frac{\rho_E}{\rho_U}\frac{2}{\alpha}\beta^{\frac{2}{\alpha}} B(M - \frac{2}{\alpha}, \frac{2}{\alpha})\Big)^n}. \end{aligned}$$

.10 Proof of (3.2)

By definition, we have

$$\begin{aligned} \mathcal{L}_{I_e}(s) &= E_\Phi E_{I_e}\big[\exp(-s\sum_{e\in\Phi}\frac{|h_{A_{i^*}E_e}|^2}{\frac{d_{AE_e}^\alpha}{P_T} + \frac{d_{AE_e}^\alpha}{d_{BE_e}^\alpha} m X_2})\big] \\ &= E_\Phi\big[\prod_{e\in\Phi} E[\exp(-sH_e)]\big], \end{aligned} \quad (.30)$$

where $H_e = \frac{1}{f_e}\frac{|h_{A_{i^*}E_e}|^2}{\frac{d^\alpha_{BE_e}}{P_J}+X_2} = \frac{1}{f_e}\mathcal{X}_e$. From Lemma 2 or (2.18) with $M=1$, we know $f_{\mathcal{X}_e}(x_e) = e^{-\frac{d^\alpha_{BE_e}}{P_J}x_e}\left(\frac{1}{(1+x_e)^2}+\frac{\frac{d^\alpha_{BE_e}}{P_J}}{1+x_e}\right)$. Then,

$$
\begin{aligned}
E[e^{-sH_e}] &= \int_0^\infty e^{-sh_e} f_{H_e}(h_e)dh_e = \int_0^\infty e^{-s\frac{x_e}{f_e}} f_{\mathcal{X}_e}(x_e)\mathrm{d}x_e \\
&= \int_0^\infty e^{-\frac{(s+\frac{d^\alpha_{AE_e}}{P_T})}{f_e}x_e}\left(\frac{1}{(1+x_e)^2}+\frac{d^\alpha_{BE_e}}{P_J}\frac{1}{(1+x_e)}\right)\mathrm{d}x_e \\
&= \int_0^\infty e^{-K(s)x_e}\left(\frac{1}{(1+x_e)^2}+(K(s)-\frac{s}{f_e})\frac{1}{(1+x_e)}\right)\mathrm{d}x_e \\
&= \int_0^\infty \frac{e^{-K(s)x_e}}{(1+x_e)^2}\mathrm{d}x_e + (K(s)-\frac{s}{f_e})\int_0^\infty \frac{e^{-K(s)x_e}}{(1+x_e)}\mathrm{d}x_e \\
&= 1 - e^{K(s)}K(s)\mathbf{E_1}(K(s)) + (K(s)-\frac{s}{f_e})e^{K(s)}\mathbf{E_1}(K(s)) \\
&= 1 - \frac{s}{f_e}\mathbf{E_1}(K(s))e^{K(s)}, \qquad (.31)
\end{aligned}
$$

where $\mathbf{E_1}(a) = \int_0^\infty \frac{e^{-ax}}{1+x}\mathrm{d}x$ and $K(s) = \frac{s+\frac{d^\alpha_{AE_e}}{P_T}}{f_e}$. So we get:

$$
\begin{aligned}
\mathcal{L}_{I_e}(s) &= E_\Phi\big[\prod_{e\in\Phi} E[\exp(-sH_e)]\big] \\
&= E_\Phi\big[\prod_{e\in\Phi} 1 - \frac{s}{f_e}\mathbf{E_1}(K(s))e^{K(s)}\big] \\
&= \exp\left[-\rho_E\int_0^R\int_0^{2\pi}\frac{s}{f_e}\mathbf{E_1}(K(s))e^{K(s)}\mathrm{d}\theta r\mathrm{d}r\right]. \qquad (.32)
\end{aligned}
$$

.11 Properties of $\beta_{i,l}$ and $\beta_{E,i}$

Let the eigenvalue decomposition (EVD) of $\mathbf{\Sigma}_{(i)}\mathbf{P}^*_{(i)}\mathbf{P}^T_{(i)}\mathbf{\Sigma}_{(i)}$ with descending eigenvalues be $\sum_{k=1}^{N-1}\lambda_{i,k}\mathbf{u}_{i,k}\mathbf{u}^H_{i,k} = \mathbf{U}_i\mathbf{\Lambda}_i\mathbf{U}_i^H$. Also note that the $N-1$ diagonal entries of $\mathbf{\Sigma}_{(i)}\mathbf{P}^*_{(i)}\mathbf{P}^T_{(i)}\mathbf{\Sigma}_{(i)}$ are $\sigma^2_{i,j_k}n_1P_1$ with $k=1,\cdots,N-1$, $j_k\in\{1,\cdots,N\}$ and $j_k\neq i$. It follows

from (5.7) that

$$\mathbf{K}_{\Delta\mathbf{h}_{(i)}} = \mathbf{\Sigma}_{(i)}\mathbf{U}_i(\mathbf{I}+\mathbf{\Sigma}_i)^{-1}\mathbf{U}_i^H\mathbf{\Sigma}_{(i)} = \sum_{k=1}^{N-1}\frac{\mathbf{v}_{i,k}\mathbf{v}_{i,k}^H}{1+\lambda_{i,k}}, \tag{.33}$$

where $\mathbf{v}_{i,k} = \mathbf{\Sigma}_{(i)}\mathbf{u}_{i,k}$. From (.33) we get

$$\beta_{i,l} = (\mathbf{K}_{\Delta\mathbf{h}_{(i)}})_{l,l} = \sum_{k=1}^{N-1}\frac{(\mathbf{v}_{i,k}\mathbf{v}_{i,k}^H)_{l,l}}{1+\lambda_{i,k}}. \tag{.34}$$

Clearly, $\beta_{i,l} \to 0$ if $\min_k \lambda_{i,k} = \lambda_{i,N-1} \to \infty$.

To show that $\lambda_{i,N-1} \to \infty$ as $n_1P_1 \to \infty$, we first consider the case of $n_1 = N-1$. Then $\mathbf{P}_{(i)} = \sqrt{P_1}\mathbf{Q}_i$ where $\mathbf{Q}_i$ is an $(N-1)\times(N-1)$ submatrix of the $N\times N$ DFT matrix (with unit amplitude for each element). By the interlacing property of eigenvalues, we know that $N-2$ of the $N-1$ eigenvalues of $\mathbf{Q}_i\mathbf{Q}_i^H$ are equal to N, and the smallest eigenvalue η_i of $\mathbf{Q}_i\mathbf{Q}_i^H$ is between zero and N. More specifically, $\eta_i = \min_{\|\mathbf{v}\|=1}\mathbf{v}^H\mathbf{Q}_i\mathbf{Q}_i^H\mathbf{v} = N - \max_{\|\mathbf{v}\|=1}\|\mathbf{v}^H\mathbf{q}_i\|^2 = 1-\|\mathbf{q}_i\|^2 = 1$ where $\mathbf{q}_i$ is an $(N-1)\times 1$ subcolumn of the $N\times N$ DFT matrix. For any $n_1 \geq N-1$, we also know that $\eta_i > 0$ which is invariant to P_1. Therefore, as $n_1P_1 \to \infty$, we have $\lambda_{i,N-1}\to\infty$ and hence $\beta_{i,l}\to 0$ for all $i = 1,\cdots,N$ and $l = 1,\cdots,N-1$.

Similarly, let the EVD of the $N\times N$ matrix $\mathbf{\Sigma}_E\mathbf{P}^*\mathbf{P}^T\mathbf{\Sigma}_E$ with descending eigenvalues be $\sum_{k=1}^N \lambda_{E,k}\mathbf{u}_{E,k}\mathbf{u}_{E,k}^H = \mathbf{U}_E\mathbf{\Lambda}_E\mathbf{U}_E^H$ where $\lambda_{E,N} = 0$. Let $\mathbf{v}_{E,k} = \mathbf{\Sigma}_E\mathbf{u}_{E,k}$. Then, it follows from (5.9) that

$$\begin{aligned}\mathbf{K}_{\Delta\mathbf{h}_E} &= \left(\sum_{k=1}^{N-1}\frac{\mathbf{v}_{E,k}\mathbf{v}_{E,k}^H}{1+\lambda_{E,k}} + \mathbf{v}_{E,N}\mathbf{v}_{E,N}^H\right)\otimes\mathbf{I}_{N_E}\\ &\geq (\mathbf{v}_{E,N}\mathbf{v}_{E,N}^H)\otimes\mathbf{I}_{N_E},\end{aligned} \tag{.35}$$

where the lower bound is achieved when $n_1P_1\to\infty$. Consequently, $\beta_{E,i} = (\sum_{j=1}^{N-1}\frac{\mathbf{v}_{E,j}\mathbf{v}_{E,j}^H}{1+\lambda_{E,j}} + \mathbf{v}_{E,N}\mathbf{v}_{E,N}^H)_{i,i} \geq (\mathbf{v}_{E,N}\mathbf{v}_{E,N}^H)_{i,i} \triangleq c_i$.

.12 CDFs and PDFs of γ_e and γ_b

A generalized form of γ_e and γ_b can be written as

$$\gamma_x = \frac{a_x X_2}{b_x + X_1}, \tag{.36}$$

where X_1 and X_2 are independent, X_1 is exponentially distributed with unit mean, and X_2 is Chi-square distributed with DoF equal to $2N_x$. For γ_e, we let $N_x = N_E$ and replace a_x and b_x respectively by $a_e = \frac{\sigma_{E,i}^2}{\beta_{E,i}} - 1$ and $b_e = \frac{1}{\beta_{E,i} P_2}$. For γ_b, we let $N_x = 1$ and replace a_x and b_x respectively by $a_j = \frac{\sigma_{j,i}^2}{\beta_{j,i}} - 1$ and $b_j = \frac{1}{\beta_{j,i} P_2}$. Then the CDF of γ_x is

$$\begin{aligned}
F_{\gamma_x}(z) &= P\big[X_1 > \frac{a_x X_2}{z} - b_x\big] = 1 - P\left[X_1 < \frac{a_x X_2}{z} - b_x\right] \\
&= 1 - \int_{x=\frac{b_x}{a_x} z}^{\infty} \big(1 - e^{-(\frac{a_x}{z} x - b_x)}\big) f_{X_2}(x) \mathrm{d}x \\
&= F_{X_2}(\frac{b_x}{a_x} z) + \frac{e^{b_x}}{\Gamma(N_x)} \int_{x=\frac{b_x}{a_x} z}^{\infty} e^{-x(\frac{a_x}{z}+1)} x^{N_x - 1} \mathrm{d}x \\
&= F_{X_2}(\frac{b_x}{a_x} z) + \frac{e^{b_x} \int_{y=\frac{b_x}{a_x} z + b_x}^{\infty} e^{-y} y^{N_x - 1} \mathrm{d}y}{(\frac{a_x}{z} + 1)^{N_x} \Gamma(N_x)} \\
&= F_{X_2}(\frac{b_x}{a_x} z) + \frac{e^{b_x} \big(1 - F_{X_2}(\frac{b_x}{a_x} z + b_x)\big)}{(\frac{a_x}{z} + 1)^{N_x}},
\end{aligned} \tag{.37}$$

where $F_{X_2}(\frac{b_x}{a_x} z) = 1 - \frac{\Gamma(N_x, \frac{b_x}{a_x} z)}{\Gamma(N_x)}$, and the second term in the last expression of (.37) is zero if $b_x \to \infty$. Then the PDF of γ_x is

$$\begin{aligned}
f_{\gamma_x}(z) &= \frac{b_x}{a_x} f_{X_2}(\frac{b_x}{a_x} z) + \frac{e^{b_x}}{\Gamma(N_x)} \big[0 - \frac{b_x}{a_x} e^{-(\frac{b_x}{a_x} z)(\frac{a_x}{z}+1)} \\
&\quad \times (\frac{b_x}{a_x} z)^{N_x - 1} + \frac{a_x}{z^2} \int_{x=\frac{b_x}{a_x} z}^{\infty} e^{-x(\frac{a_x}{z}+1)} x^{N_x} dx\big] \\
&= \frac{a_x e^{b_x}}{\Gamma(N_x)} \frac{z^{N_x - 1}}{(z + a_x)^{N_x + 1}} \Gamma(N_x + 1, \frac{b_x}{a_x} z + b_x).
\end{aligned} \tag{.38}$$

.13 Proof of (4.23)

$$
\begin{aligned}
T_2 &= a_j \frac{n_b}{n_2} \frac{(\frac{b_e}{a_e})^{N_E} e^{-\frac{b_j}{a_j}(\alpha-1)}}{\Gamma(N_E)} \int_{y=\gamma_1}^{\infty} \frac{e^{-\frac{b_j}{a_j}\alpha y - \frac{b_e}{a_e} y} y^{N_E-1}}{\alpha y + \alpha - 1 + a_j} \mathrm{d}y \\
&\overset{(a)}{=} a_j \frac{n_b}{n_2} \frac{(\frac{b_e}{\alpha a_e})^{N_E} e^{-\frac{b_j}{a_j}\gamma - \frac{b_e}{a_e}\gamma_1}}{\Gamma(N_E)} \\
&\quad \times \int_{z=0}^{\infty} \frac{(\alpha\gamma_1 + z)^{N_E-1}}{z + \gamma + a_j} e^{-(\frac{b_j}{a_j} + \frac{b_e}{\alpha a_e})z} \mathrm{d}z \\
&= a_j \frac{n_b}{n_2} \frac{(\frac{b_e}{\alpha a_e})^{N_E} e^{-\frac{b_j}{a_j}\gamma - \frac{b_e}{a_e}\gamma_1}}{\Gamma(N_E)} \sum_{n=0}^{N_E-1} \binom{N_E-1}{n} \\
&\quad \times (\alpha\gamma_1)^{N_E-1-n} \int_{z=0}^{\infty} \frac{z^n}{z + \gamma + a_j} e^{-(\frac{b_j}{a_j} + \frac{b_e}{\alpha a_e})z} \mathrm{d}z \\
&\overset{(b)}{=} a_j \frac{n_b}{n_2} \frac{(\frac{b_e}{\alpha a_e})^{N_E} e^{-\frac{b_j}{a_j}\gamma - \frac{b_e}{a_e}\gamma_1}}{\Gamma(N_E)} \sum_{n=0}^{N_E-1} \binom{N_E-1}{n} \\
&\quad \times (\alpha\gamma_1)^{N_E-1-n} (\gamma + a_j)^n e^{(\frac{b_j}{a_j} + \frac{b_e}{\alpha a_e})(\gamma + a_j)} \\
&\quad \times \Gamma(n+1) \Gamma\big(-n, (\frac{b_j}{a_j} + \frac{b_e}{\alpha a_e})(\gamma + a_j)\big) \\
&= a_j \frac{n_b}{n_2} (\frac{b_e}{\alpha a_e})^{N_E} e^{b_j + \frac{b_e}{\alpha a_e}(\alpha - 1 + a_j)} \sum_{n=0}^{N_E-1} \frac{(\gamma + a_j)^n}{\Gamma(N_E - n)} \\
&\quad \times (\alpha\gamma_1)^{N_E-1-n} \Gamma\big(-n, (\frac{b_j}{a_j} + \frac{b_e}{\alpha a_e})(\gamma + a_j)\big), \qquad (.39)
\end{aligned}
$$

where step $\overset{(a)}{=}$ follows from the variable change $z = \alpha(y - \gamma_1)$, and step $\overset{(b)}{=}$ follows from the equation (3.383.10) in [64].

.14 Proof of (4.27)

$$\begin{aligned}
\Omega(\gamma_1) &= \int_{y=\gamma_1}^{\infty} \frac{e^{-\frac{b_j}{a_j}\alpha y} y^{N_E-1}}{(a_e+y)^{N_E+1}} \mathrm{d}y \\
&\overset{(a)}{=} \int_{x=0}^{\infty} \frac{e^{-\frac{b_j}{a_j}\alpha(\gamma_1+x)} (\gamma_1+x)^{N_E-1}}{(a_e+\gamma_1+x)^{N_E+1}} \mathrm{d}x \\
&= \frac{\gamma_1^{N_E-1} e^{-\frac{b_j}{a_j}\alpha\gamma_1}}{(a_e+\gamma_1)^{N_E+1}} \int_{x=0}^{\infty} \frac{e^{-\frac{b_j}{a_j}\alpha x} (1+\frac{x}{\gamma_1})^{N_E-1}}{(1+\frac{x}{a_e+\gamma_1})^{N_E+1}} \mathrm{d}x \\
&\overset{(b)}{=} \frac{\gamma_1^{N_E-1} e^{-\frac{b_j}{a_j}\alpha\gamma_1}}{(a_e+\gamma_1)^{N_E}} \sum_{n=0}^{N_E-1} \binom{N_E-1}{n} \frac{(a_e+\gamma_1)^n}{\gamma_1^n} \\
&\quad \times \int_{z=0}^{\infty} \frac{e^{-\frac{b_j}{a_j}\alpha(a_e+\gamma_1)z} z^n}{(1+z)^{N_E+1}} \mathrm{d}z, \qquad (.40)
\end{aligned}$$

where steps $\overset{(a)}{=}$ and $\overset{(b)}{=}$ follow from the changes of variables $x = y - \gamma_1$ and $z = \frac{x}{a_e+\gamma_1}$ respectively. After applying $\int_{z=0}^{\infty} \frac{t^{a-1}e^{-zt}}{(1+t)^{a+1-b}} \mathrm{d}t = \Gamma(a)U(a,b,z)$ from [64] in (.40), we get

$$\begin{aligned}
\Omega(\gamma_1) &= e^{-\frac{b_j}{a_j}\alpha\gamma_1} \Gamma(N_E) \sum_{n=0}^{N_E-1} \frac{1}{\Gamma(N_E-n)} \frac{\gamma_1^{N_E-1-n}}{(a_e+\gamma_1)^{N_E-n}} \\
&\quad \times U(n+1, n+1-N_E, \frac{b_j}{a_j}\alpha(a_e+\gamma_1)). \qquad (.41)
\end{aligned}$$

.15 Proof of (5.27)

Using $x_0(y) = \alpha(1+y) - 1$, $T_{2,1}$ follows as

$$\begin{aligned} T_{2,1} &= \alpha a_a N_A \frac{n_b}{n_2} \int_{y=\gamma_1}^{\infty} (\alpha y + \alpha - 1)^{N_A - 1} e^{-\frac{b_a}{a_a}(\alpha y + \alpha - 1)} \\ &\quad \times \sum_{k=0}^{N_A} \frac{(\frac{b_a}{a_a})^k}{k!} \frac{\left[1 - e^{-\frac{b_e}{a_e} y} \sum_{m=1}^{N_E - 1} \frac{(\frac{b_e}{a_e} y)^{m-1}}{\Gamma(m)}\right]}{(\alpha y + \alpha - 1 + a_a)^{N_A + 1 - k}} \mathrm{d}y \\ &\overset{(a)}{=} \alpha a_a N_A \frac{n_b}{n_2} \int_{x=0}^{\infty} (\alpha x + \gamma)^{N_A - 1} e^{-\frac{b_a}{a_a}(\alpha x + \gamma)} \sum_{k=0}^{N_A} \frac{(\frac{b_a}{a_a})^k}{k!} \\ &\quad \times \frac{\left[1 - e^{-\frac{b_e}{a_e}(\gamma_1 + x)} \sum_{m=1}^{N_E - 1} \frac{\left(\frac{b_e}{a_e} \gamma_1 (1 + \frac{x}{\gamma_1})\right)^{m-1}}{\Gamma(m)}\right]}{(\alpha x + \gamma + a_a)^{N_A + 1 - k}} \mathrm{d}x, \end{aligned} \tag{.42}$$

where step (a) follows from the variable change $x = y - \gamma_1$ and defined a constant $\gamma \triangleq \alpha\gamma_1 + \alpha - 1$. Then, we apply $z = \frac{\alpha x}{\gamma + a_a}$ and (.42) follows as

$$
\begin{aligned}
T_{2,1} &= a_a N_A \frac{n_b}{n_2} \gamma^{N_A-1} e^{-\frac{b_a}{a_a}\gamma} \sum_{k=0}^{N_A} \frac{(\frac{b_a}{a_a})^k}{k!(\gamma + a_a)^{N_A-k}} \\
&\times \int_{z=0}^{\infty} \frac{(1 + \frac{\gamma+a_a}{\gamma} z)^{N_A-1} e^{-\frac{b_a}{a_a}(\gamma+a_a)z}}{(1+z)^{N_A+1-k}} \Bigg[1 - e^{-\frac{b_e}{a_e}\gamma_1} \\
&\times e^{-(\frac{1}{\alpha}\frac{b_e}{a_e})(\gamma+a_a)z} \sum_{m=1}^{N_E-1} \frac{\left(\frac{b_e}{a_e}\gamma_1(1 + \frac{\gamma+a_a}{\alpha\gamma_1} z)\right)^{m-1}}{\Gamma(m)} \Bigg] \mathrm{d}z \\
&= a_a N_A \frac{n_b}{n_2} e^{-\frac{b_a}{a_a}\gamma} \sum_{k=0}^{N_A} \frac{(\frac{b_a}{a_a})^k}{k!} \sum_{l=0}^{N_A-1} \binom{N_A - 1}{l} \\
&\times \frac{\gamma^{N_A-1-l}}{(\gamma + a_a)^{N_A-k-l}} \int_{z=0}^{\infty} \frac{z^l e^{-\frac{b_a}{a_a}(\gamma+a_a)z}}{(1+z)^{N_A+1-k}} \Bigg[1 - e^{-\frac{b_e}{a_e}\gamma_1} \\
&\times e^{-(\frac{1}{\alpha}\frac{b_e}{a_e})(\gamma+a_a)z} \sum_{m=1}^{N_E-1} \frac{\left(\frac{b_e}{a_e}\gamma_1(1 + \frac{\gamma+a_a}{\alpha\gamma_1} z)\right)^{m-1}}{\Gamma(m)} \Bigg] \mathrm{d}z \\
&= a_a \frac{n_b}{n_2} e^{-\frac{b_a}{a_a}\gamma} \sum_{k=0}^{N_A} \frac{(\frac{b_a}{a_a})^k}{k!} \sum_{l=0}^{N_A-1} \frac{\Gamma(N_A+1)}{\Gamma(N_A-l)\Gamma(l+1)} \\
&\times \frac{\gamma^{N_A-1-l}}{(\gamma + a_a)^{N_A-k-l}} \Bigg[\int_{z=0}^{\infty} \frac{z^l e^{-\frac{b_a}{a_a}(\gamma+a_a)z}}{(1+z)^{N_A+1-k}} \mathrm{d}z - e^{-\frac{b_e}{a_e}\gamma_1} \\
&\times \sum_{m=1}^{N_E-1} \frac{(\frac{b_e}{a_e}\gamma_1)^{m-1}}{\Gamma(m)} \sum_{n=0}^{m-1} \binom{m-1}{n} (\frac{\gamma + a_a}{\alpha\gamma_1})^n \\
&\times \int_{z=0}^{\infty} \frac{z^{l+n} e^{-(\frac{b_a}{a_a} + \frac{1}{\alpha}\frac{b_e}{a_e})(\gamma+a_a)z}}{(1+z)^{N_A+1-k}} \mathrm{d}z \Bigg]. \qquad (.43)
\end{aligned}
$$

Finally, we apply $\int_{z=0}^{\infty} \frac{t^{a-1}e^{-zt}}{(1+t)^{a+1-b}} \mathrm{d}t = \Gamma(a)U(a,b,z)$ from [64] to evaluate the inte-

gral in (.42) and (.42) follows as

$$
\begin{aligned}
T_{2,1} &= a_a \frac{n_b}{n_2} e^{-\frac{b_a}{a_a}\gamma} \sum_{k=0}^{N_A} \frac{(\frac{b_a}{a_a})^k}{k!} \sum_{l=0}^{N_A-1} \frac{\Gamma(N_A+1)}{\Gamma(N_A-l)\Gamma(l+1)} \\
&\times \frac{\gamma^{N_A-1-l}}{(\gamma+a_a)^{N_A-k-l}} \Big[\Gamma(l+1) U\big(l+1, l+1+k-N_A, \\
&\frac{b_a}{a_a}(\gamma+a_a)\big) - e^{-\frac{b_e}{a_e}\gamma_1} \sum_{m=1}^{N_E-1} (\frac{b_e}{a_e}\gamma_1)^{m-1} \sum_{n=0}^{m-1} \frac{(\frac{\gamma+a_a}{\alpha\gamma_1})^n}{\Gamma(m-n)} \\
&\times \frac{\Gamma(l+n+1)}{\Gamma(n+1)} U\big(l+n+1, l+n+1+k-N_A, \\
&(\frac{b_a}{a_a} + \frac{1}{\alpha}\frac{b_e}{a_e})(\gamma+a_a)\big) \Big] \\
&= a_a \Gamma(N_A+1) \frac{n_b}{n_2} e^{-\frac{b_a}{a_a}\gamma} \sum_{k=0}^{N_A} \frac{(\frac{b_a}{a_a})^k}{k!} \sum_{l=0}^{N_A-1} \frac{1}{\Gamma(N_A-l)} \\
&\times \frac{\gamma^{N_A-1-l}}{(\gamma+a_a)^{N_A-k-l}} \Xi(k, l, \gamma_1, N_E). \qquad (.44)
\end{aligned}
$$

Here, the second term $T_{2,2}$ does not yield any closed form expression. To evaluate $T_{2,2}$, we apply the change of variable $x = \frac{1}{y}$ and then approximate the function by leveraging Gaussian-Chebyshev quadrature described earlier.

$$
\begin{aligned}
T_{2,2} &= \alpha a_a \frac{N_A}{\Gamma(N_E)} \frac{n_b}{n_2} \int_{y=\gamma_1}^{\infty} \frac{(\frac{b_e}{a_e}y)^{N_E-1}(\alpha y+\alpha-1)^{N_A-1}}{1+\frac{y}{a_e}} \\
&\times e^{-\frac{b_a}{a_a}(\alpha y+\alpha-1)-\frac{b_e}{a_e}y} \sum_{k=0}^{N_A} \frac{(\frac{b_a}{a_a})^k}{k!(\alpha y+\alpha-1+a_a)^{N_A+1-k}} \mathrm{d}y \\
&\approx \frac{\alpha a_a N_A}{2\gamma_1 \Gamma(N_E)} \frac{n_b}{n_2} \sum_{n=1}^{M} \frac{\pi}{M} h\big(\frac{1}{2\gamma_1}(t_n+1)\big) \sqrt{1-t_n^2}, \qquad (.45)
\end{aligned}
$$

where

$$
\begin{aligned}
h(x) &\triangleq \frac{\frac{b_e}{a_e}^{N_E-1}(\frac{\alpha}{x}+\alpha-1)^{N_A-1}}{x^{N_E+1}(1+\frac{1}{xa_e})} e^{-\frac{b_a}{a_a}(\frac{\alpha}{x}+\alpha-1)-\frac{b_e}{a_e}\frac{1}{x}} \\
&\times \sum_{k=0}^{N_A} \frac{(\frac{b_a}{a_a})^k}{k!(\frac{\alpha}{x}+\alpha-1+a_a)^{N_A+1-k}}. \qquad (.46)
\end{aligned}
$$

.16 Proof of (5.35)

$$
\begin{aligned}
T_{2,1}^{(u)} &= \alpha \frac{n_b}{n_2} \frac{(\frac{b_a}{a_a})^{N_A-1}}{\Gamma(N_A)} \int_{y=\gamma_1}^{\infty} \frac{e^{-\frac{b_a}{a_a}(\alpha+\alpha y-1)}(\alpha+\alpha y-1)^{N_A-1}}{(\alpha+\alpha y-1+a_a)} \\
&\times (N_A-1+b_a+\frac{a_a}{a_a+\alpha+\alpha y-1}) \Big[1-e^{-\frac{b_e}{a_e}y} \\
&\times \sum_{m=1}^{N_E-1} \frac{(\frac{b_e}{a_e}y)^{m-1}}{(m-1)!}\Big] \mathrm{d}y \\
&\overset{(a)}{=} \alpha \frac{n_b}{n_2} \frac{e^{-\frac{b_a}{a_a}\gamma}(\frac{b_a}{a_a})^{N_A-1}}{\Gamma(N_A)} \int_{x=0}^{\infty} \frac{e^{-\frac{b_a}{a_a}\alpha x}(\gamma+\alpha x)^{N_A-1}}{(a_a+\gamma+\alpha x)} \\
&\times (N_A-1+b_a+\frac{a_a}{a_a+\gamma+\alpha x}) \Big[1-e^{-\frac{b_e}{a_e}(x+\gamma_1)} \\
&\times \sum_{m=1}^{N_E-1} \frac{(\frac{b_e}{a_e}(x+\gamma_1))^{m-1}}{(m-1)!}\Big] \mathrm{d}x \\
&\overset{(b)}{=} \frac{n_b}{n_2} \frac{e^{-\frac{b_a}{a_a}\gamma}(\frac{b_a}{a_a}\gamma)^{N_A-1}}{\Gamma(N_A)} \int_{z=0}^{\infty} \frac{e^{-\frac{b_a}{a_a}(a_a+\gamma)z}(1+\frac{a_a+\gamma}{\gamma}z)^{N_A-1}}{(1+z)} \\
&\times (N_A-1+b_a+\frac{a_a}{a_a+\gamma}\frac{1}{1+z}) \Big[1-e^{-\frac{b_e}{a_e}\gamma_1}e^{-\frac{b_e}{\alpha a_e}(a_a+\gamma)z} \\
&\times \sum_{m=1}^{N_E-1} \frac{(\frac{b_e}{a_e}\gamma_1)^{m-1}}{\Gamma(m)}(1+\frac{a_a+\gamma}{\alpha\gamma_1}z)^{m-1}\Big] \mathrm{d}z, \qquad (.47)
\end{aligned}
$$

where step (a) and step (b) follow from the variable change $x = y - \gamma_1$ and $z = \frac{\alpha x}{\gamma + a_a}$ respectively. Now, (.47) follows as

$$
\begin{aligned}
T_{2,1}^{(u)} &= \frac{n_b}{n_2} e^{-\frac{b_a}{a_a}\gamma} (\frac{b_a}{a_a}\gamma)^{N_A-1} \sum_{l=0}^{N_A-1} \frac{(\frac{a_a+\gamma}{\gamma})^l}{\Gamma(N_A-l)\Gamma(l+1)} \int_{z=0}^{\infty} \frac{z^l}{1+z} \\
&\times e^{-\frac{b_a}{a_a}(a_a+\gamma)z} (N_A - 1 + b_a + \frac{a_a}{a_a+\gamma}\frac{1}{1+z}) \Big[1 - e^{-\frac{b_e}{a_e}\gamma_1} \\
&\times e^{-\frac{b_e}{\alpha a_e}(a_a+\gamma)z} \sum_{m=1}^{N_E-1} \frac{(\frac{b_e}{a_e}\gamma_1)^{m-1}}{\Gamma(m)} (1 + \frac{a_a+\gamma}{\alpha\gamma_1} z)^{m-1} \Big] \mathrm{d}z \\
&= \frac{n_b}{n_2} e^{-\frac{b_a}{a_a}\gamma} (\frac{b_a}{a_a}\gamma)^{N_A-1} \sum_{l=0}^{N_A-1} \frac{(\frac{a_a+\gamma}{\gamma})^l}{\Gamma(N_A-l)\Gamma(l+1)} \int_{z=0}^{\infty} \frac{z^l}{1+z} \\
&\times e^{-\frac{b_a}{a_a}(a_a+\gamma)z} (N_A - 1 + b_a + \frac{a_a}{a_a+\gamma}\frac{1}{1+z}) \Big[1 - e^{-\frac{b_e}{a_e}\gamma_1} \\
&\times e^{-\frac{b_e}{\alpha a_e}(a_a+\gamma)z} \sum_{m=1}^{N_E-1} (\frac{b_e}{a_e}\gamma_1)^{m-1} \sum_{n=0}^{m-1} \frac{(\frac{a_a+\gamma}{\alpha\gamma_1})^n z^n}{(m-n-1)!n!} \Big] \mathrm{d}z.
\end{aligned}
\tag{.48}
$$

Now, we apply $\int_{z=0}^{\infty} \frac{t^{a-1}e^{-zt}}{(1+t)^{a+1-b}} \mathrm{d}t = \Gamma(a)U(a,b,z)$ to evaluate the integral in (.48) and (.48) follows as

$$
\begin{aligned}
T_{2,1}^{(u)} &= \frac{n_b}{n_2} e^{-\frac{b_a}{a_a}\gamma} (\frac{b_a}{a_a}\gamma)^{N_A-1} \sum_{l=0}^{N_A-1} \frac{(\frac{a_a+\gamma}{\gamma})^l}{\Gamma(N_A-l)} \Big[(N_A - 1 + b_a) \\
&\times U\big(l+1, l+1, \frac{b_a}{a_a}(\gamma + a_a)\big) + \frac{a_a}{a_a+\gamma} U\big(l+1, l, \frac{b_a}{a_a} \\
&\times (\gamma + a_a)\big) - e^{-\frac{b_e}{a_e}\gamma_1} \sum_{m=1}^{N_E-1} (\frac{b_e}{a_e}\gamma_1)^{m-1} \sum_{n=0}^{m-1} \frac{(\frac{a_a+\gamma}{\alpha\gamma_1})^n}{\Gamma(m-n)} \\
&\times \frac{\Gamma(l+n+1)}{\Gamma(l+1)\Gamma(n+1)} \Big((N_A - 1 + b_a) U\big(l+n+1, l+n \\
&+ 1, (\frac{b_a}{a_a} + \frac{b_e}{\alpha a_e})(\gamma + a_a)\big) + \frac{a_a}{a_a+\gamma} U\big(l+n+1, l+n, \\
&(\frac{b_a}{a_a} + \frac{b_e}{\alpha a_e})(\gamma + a_a)\big) \Big) \Big].
\end{aligned}
\tag{.49}
$$

Now, using the similar arithmetic manipulation the second term can be written as

follows

$$
\begin{aligned}
T_{2,2}^{(u)} &= \alpha \frac{n_b}{n_2} \frac{(\frac{b_a}{a_a})^{N_A-1}}{\Gamma(N_A)\Gamma(N_E)} \int_{y=\gamma_1}^{\infty} \frac{(\alpha+\alpha y-1)^{N_A-1}}{(\alpha+\alpha y-1+a_a)} \\
&\quad \times e^{-\frac{b_a}{a_a}(\alpha+\alpha y-1)-\frac{b_e}{a_e}y} (N_A-1+b_a+\frac{a_a}{a_a+\alpha+\alpha y-1}) \\
&\quad \times \frac{a_e}{a_e+y} (\frac{b_e}{a_e} y)^{N_E-1} \mathrm{d}y \\
&= \frac{n_b}{n_2} \frac{(\frac{b_a}{a_a})^{N_A-1} (\frac{b_e}{a_e}\gamma_1)^{N_E-1}}{\Gamma(N_A)} \frac{e^{-\frac{b_a}{a_a}\gamma-\frac{b_e}{a_e}\gamma_1} \alpha a_e}{\alpha(a_e-1)-a_a+1} \sum_{l=0}^{N_E-1} \\
&\quad \times \frac{(\frac{\gamma+a_a}{\alpha\gamma_1})^l}{\Gamma(N_E-l)} \Bigg[(N_A-1+b_a-\frac{a_a}{\alpha(a_e-1)-a_a+1}) \\
&\quad \times \Bigg(U\big(l+1, l+1, (\frac{b_a}{a_a}+\frac{b_e}{\alpha a_e})(\gamma+a_a)\big) + \alpha^l (\frac{a_e+\gamma_1}{\gamma+a_a})^l \\
&\quad \times U\big(l+1, l+1, (\frac{b_a}{a_a}+\frac{b_e}{\alpha a_e})\alpha(a_e+\gamma_1)\big) \Bigg) + \frac{a_a}{\gamma+a_a} \\
&\quad \times U\big(l+1, l, (\frac{b_a}{a_a}+\frac{b_e}{\alpha a_e})(\gamma+a_a)\big) \Bigg] \qquad (.50)
\end{aligned}
$$

Bibliography

[1] A. D. Wyner, "The wire-tap channel", Bell Syst. Tech. J., vol. 54, pp. 1355-1387, Jan. 1975.

[2] N. Yang, L. Wang, G. Geraci, M. Elkashlan, J. Yuan, and M. D. Renzo, "Safeguarding 5G wireless communication networks using physical layer security," IEEE Commun. Mag., vol. 53, no. 4, pp. 20-27, Apr. 2015.

[3] E. Tekin and A. Yener, "The general gaussian multiple access and twoway wire-tap channels: achievable rates and cooperative jamming," IEEE Trans. Inform. Theory, vol. 54, pp. 2735-2751, June 2008.

[4] H. Zhang, H. Xing, J. Cheng, A. Nallanathan, and V. Leung, "Secure resource allocation for OFDMA two-way relay wireless sensor networks without and with cooperative jamming," IEEE Trans. Ind. Informat., vol. 12, no. 5, pp. 1714-1725, Oct. 2016.

[5] J. Zhang and M. C. Gursoy, "Relay beamforming strategies for physicallayer security," in Proc. 44th Annu. Conf. Inf. Sci. Syst., Princeton, NJ, USA, Mar. 2010, pp. 1-6.

[6] H. Weingarten, T. Liu, S. Shamai, Y. Steinberg, and P. Viswanath, "The capacity region of the degraded multiple-input multiple-output compound broadcast channel," IEEE Trans. Inf. Theory, vol. 55, pp. 5011-5023, Nov. 2009.

[7] L. Chen, Q. Zhu, W. Meng and Y. Hua, "Fast Power Allocation for Secure Communication with Full-Duplex Radio", IEEE Trans. Signal Processing, Vol. 65, No. 14, pp. 3846-3861, July 2017.

[8] G. Chen, Y. Gong, P. Xiao, and J. A. Chambers, "Dual antenna selection in secure cognitive radio networks," IEEE Trans. Veh. Technol., vol. 65, no. 10, pp. 7993-8002, Oct. 2016.

[9] A. Khisti, G. Wornell, A. Wiesel, and Y. Eldar, "On the Gaussian MIMO wiretap channel," in Proc. IEEE Int. Symp. Information Theory, Nice, France, June 2007.

[10] S. Goel and R. Negi, "Guaranteeing secrecy using artificial noise," IEEE Trans. Wireless Commun., vol. 7, no. 6, pp. 2180-2189, June 2008.

[11] Y. Huang, J. Wang, C. Zhong, T. Q. Duong, and G. K. Karagiannidis, "Secure transmission in cooperative relaying networks with multiple antennas," IEEE Trans. Wireless Commun., vol. 15, no. 10, pp. 6843-6856, Oct. 2016.

[12] M. Yang, B. Zhang, Y. Huang, N. Yang, D. B. da Costa, and D. Guo, "Secrecy enhancement of multiuser MISO networks using OSTBC and artificial noise," IEEE Trans. Veh. Technol., vol. 66, no. 12, pp. 11394-11398, Dec. 2017.

[13] M. Haenggi, "The secrecy graph and some of its properties," in Proc. IEEE Int. Symp. Inf. Theory, Toronto, Canada, pp. 539-543, July 2008.

[14] H. Wang, X. Zhou, and M. C. Reed, "Physical layer security in cellular networks: A stochastic geometry approach," IEEE Trans. Wireless Commun., vol. 12, no. 6, pp. 2776-2787, Jun. 2013.

[15] X. Zhou, R. K. Ganti, and J. G. Andrews, "Secure wireless network connectivity with multi-antenna transmission," IEEE Trans. Wireless Commun., vol. 10, no. 2, pp. 425-430, Dec. 2011.

[16] X. Zhang, X. Zhou and M. R. McKay, "On the design of artificial-noise aided secure multi-antenna transmission in slow fading channels," IEEE Trans. Veh. Technol., vol. 62, no. 5, pp. 2170-2181, Jun. 2013.

[17] T. X. Zheng, H. M. Wang, J. Yuan, D. Towsley, and M. H. Lee, "Multi-Antenna transmission with artificial noise against randomly distributed eavesdroppers," IEEE Trans. Commun., vol. 63, pp. 4347-4362, Nov. 2015.

[18] L. Zhang, H. Zhang, D. Wu, and D. Yuan, "Improving physical layer security for MISO systems via using artificial noise," in 2015 IEEE Global Communications Conference (GLOBECOM), 2015, pp. 1-6.

[19] T. X. Zheng, H. M. Wang, "Optimal Power Allocation for Artificial Noise Under Imperfect CSI Against Spatially Random Eavesdroppers," IEEE Trans. Vehicular Technology, vol. 65, pp. 8812-8817, Oct. 2016.

[20] X. Zhang, X. Zhou, and M. R. McKay, "Enhancing secrecy with multiantenna transmission in wireless ad hoc networks," IEEE Trans. Inf. Forensics and Security, vol. 8, no. 11, pp. 1802-1814, Nov. 2013.

[21] M. Ghogho and A. Swami, "Physical-layer secrecy of MIMO communications in the presence of a poisson random field of eavesdroppers," in Proc. IEEE ICC, Kyoto, Japan, Jun. 2011, pp. 1-5.

[22] X. Zhou, R. Ganti, J. Andrews, and A. Hjørungnes, "On the throughput cost of physical layer security in decentralized wireless networks," IEEE Trans. Wireless Commun., vol. 10, no. 8, pp. 2764-2775, Aug. 2011.

[23] G. Geraci, S. Singh, J. G. Andrews, J. Yuan, and I. B. Collings, "Secrecy rates in broadcast channels with confidential messages and external eavesdroppers," IEEE Trans. Wireless Commun., vol. 13, pp. 2931-2943, May 2014.

[24] T. X. Zheng, H. M. Wang, and Q. Yin, "On transmission secrecy outage of a multi-antenna system with randomly located eavesdroppers," IEEE Commun. Lett., vol. 18, pp. 1299-1302, Aug. 2014.

[25] T. Riihonen, S. Werner, R. Wichman, "Mitigation of loopback self-interference in full-duplex MIMO relays", IEEE Trans. Signal Process., Vol. 59, Dec 2011, 5983-5993.

[26] Y. Hua, Y. Ma, A. Gholian, Y. Li, A. Cirik, P. Liang, "Radio Self-Interference Cancellation by Transmit Beamforming, All-Analog Cancellation and Blind Digital Tuning," Signal Processing, Vol. 108, pp. 322-340, 2015.

[27] T. X. Zheng, H. M. Wang, Q. Yang, and M. H. Lee, "Safeguarding decentralized wireless networks using full-duplex jamming receivers," IEEE Trans. Wireless Commun., vol. 16, no. 1, pp. 278-292, Jan. 2017.

[28] T. Zhang, Y. Cai, Y. Huang, T. Q. Duong, and W. Yang, "Secure full-duplex spectrum-sharing wiretap networks with different antenna reception schemes," IEEE Trans. Commun., vol. 65, no. 1, pp. 335-346, Jan. 2017.

[29] Y. Hua, Q. Zhu, and R. Sohrabi, "Fundamental Properties of Full-Duplex Radio for Secure Wireless Communications," http://arxiv.org/abs/1711.10001, 2017.

[30] Y. Hua, "Advanced Properties of Full-Duplex Radio for Securing Wireless Network," IEEE Trans. Signal Processing, Vol. 67, pp. 120-135, Jan. 2019.

[31] R. Sohrabi, Q. Zhu, Y. Hua, "Secrecy analyses of a full-duplex MIMOME network," IEEE Transactions on Signal Processing, Vol. 67, No. 23, pp. 5968-5982, Dec. 2019.

[32] M. Xie and T.-M. Lok, "Antenna Selection in RF-Chain-Limited MIMO Interference Networks Under Interference Alignment," IEEE Trans. on Vehicular Technology, vol. 66, no. 5, pp. 3856-3870,May 2017.

[33] G. Chen, J. P. Coon and M. D. Renzo, "Secrecy Outage Analysis for Downlink Transmissions in the Presence of Randomly Located Eavesdroppers,"IEEE Trans. Information Forensics and Security, Vol. 12, PP. 1195 - 1206, May 2017.

[34] I. Zabir, A. Maksud, B. Sadler and Y. Hua, "Secure Downlink Transmission to Full-Duplex User against Randomly Located Eavesdroppers," IEEE Global Communications Conference (GLOBECOM), Waikoloa, HI, USA, Dec. 2019.

[35] G. Chen and J. P. Coon, "Secrecy Outage Analysis in Random Wireless Networks With Antenna Selection and User Ordering," IEEE Wireless Commun. Letters, Vol. 6, No. , pp.334-337, June 2017.

[36] Y. Hua, P. Liang, Y. Ma, A. Cirik and Q. Gao, "A method for broadband full-duplex MIMO radio," IEEE Signal Processing Letters, Vol. 19, No. 12, pp. 793-796, Dec 2012.

[37] P. B. Patnaik, "The non-central χ^2- and F-distribution and their applications," Biometrika, vol. 36, no. 1/2, pp. 202-232, Jun. 1949.

[38] R. L. Streit, The Poisson Point Process, Springer, Boston, MA, 2010.

[39] Y. Ju, H. M. Wang, T. X. Zheng, Q. Yin, M. H. Lee, "Safeguarding Millimeter Wave Communications Against Randomly Located Eavesdroppers", IEEE Trans. Wireless Commun., Vol. 17, Issue: 4, pp. 2675 - 2689, April 2018.

[40] C. Wang, H. M. Wang, "Physical Layer Security in Millimeter Wave Cellular Networks," IEEE Trans. Wireless Commun., Vol. 15, Issue: 8, pp. 5569 - 5585, Aug. 2016.

[41] T. Bai, R. W. Heath, "Coverage and Rate Analysis for Millimeter-Wave Cellular Networks," IEEE Trans. Wireless Commun., Vol. 14 Issue: 2, pp. 1100 - 1114, 2, Feb. 2015.

[42] L. C. Andrews, "Special Functions of Mathematics for Engineers," SPIE Press, chapter 10, 1998.

[43] L. Bostock, S. Chandler, and F. S. Chandler, Pure Mathematics 2, Nelson Thornes, 1979.

[44] S. Sanayei and A. Nosratinia, "Antenna Selection in MIMO Systems," IEEE Communications Magazine, October 2004.

[45] L. Dritsoula, Z. Wang, H. R. Sadjadpour, J.J. Garcia-Luna-Aceves, "Antenna selection for opportunistic interference management in MIMO broadcast channels," IEEE Workshop on Signal Processing Advances in Wireless Communications (SPAWC), 2010.

[46] Y. Gao, and T. Kaiser, "Antenna Selection in Massive MIMO Systems: Full-array Selection or Subarray Selection?" IEEE Workshop on Sensor Array and Multichannel Signal Processing Workshop, 2016.

[47] H. Alves, R. D. Souza, M. Debbah, and M. Bennis, "Performance of Transmit Antenna Selection Physical Layer Security Schemes," IEEE Signal Processing Letters, June 2012.

[48] Q. Zhu, S. Wu, and Y. Hua, "Optimal pilots for anti-eavesdropping channel estimation," IEEE Trans. on Signal Processing, Vol. 68, pp. 2629-2644, 2020.

[49] G. Durisi, T. Koch, and P. Popovski, "Toward massive, ultrareliable, and low-latency wireless communication with short packets," Proc. IEEE, vol. 104, no. 9, pp. 1711-1726, Sep. 2016.

[50] R. Chen, C. Li, S. Yan, R. Malaney, and J. Yuan, "Physical layer security for ultra-reliable and low-latency communications," IEEE Trans. Wireless Commun., vol. 26, no. 5, pp. 6-11, 2019.

[51] T. Zheng, H. Wang, D. W. K. Ng and J. Yuan, "Physical-Layer Security in the Finite Blocklength Regime over Fading Channels," in IEEE Trans. on Wireless Commun., Vol. 19, No. 5, pp. 3405-3420, 2020.

[52] N. Ari, N. Thomos and L. Musavian, "Average Secrecy Throughput Analysis with Multiple Eavesdroppers in the Finite Blocklength," 2020 IEEE 31st Annual International Symposium on Personal, Indoor and Mobile Radio Communications, London, UK, pp. 1-5,2020.

[53] H. Wang, Q. Yang, Z. Ding, and H. V. Poor, "Secure short-packet communications for mission-critical IoT applications," IEEE Trans. Wireless Commun., vol. 18, no. 5, pp. 2565-2578, 2019.

[54] B. Makki, T. Svensson, and M. Zorzi, "Finite block-length analysis of the incremental redundancy HARQ," IEEE Wireless Commun. Lett., vol. 3, no. 5, pp. 529-532, 2014.

[55] B. Makki, T. Svensson, and M. Zorzi, "Wireless energy and information transmission using feedback: Infinite and finite block-length analysis," IEEE Trans. Commun., vol. 64, no. 12, pp. 5304-5318, Dec. 2016.

[56] W. Yang, R. F. Schaefer, and H. V. Poor, "Finite-blocklength bounds for wiretap channels," in Proc. IEEE Int. Symp. Inf. Theory (ISIT), Barcelona, Spain, Jul. 2016, pp. 3087-3091.

[57] Y. Polyanskiy, H. V. Poor, and S. Verdu, "Channel coding rate in the finite blocklength regime," IEEE Trans. Inf. Theory, vol. 56, no. 5, pp. 2307-2359, May 2010.

[58] P. Mary, J. Gorce, A. Unsal and H. V. Poor, "Finite Blocklength Information Theory: What Is the Practical Impact on Wireless Communications?," in Proc. IEEE Globecom Workshops, Washington, DC, pp. 1-6, 2016.

[59] F. B. Hildebrand, "Introduction to Numerical Analysis," 2nd ed. Mineola, NY, USA: Dover, 1987.

[60] L. Zhang and Y. Liang, "Average throughput analysis and optimization in cooperative IoT networks with short packet communication," IEEE Trans. Veh. Technol., vol. 67, no. 12, pp. 11 549-11 562, 2018.

[61] R. Chen, C. Li, S. Yan, R. Malaney, and J. Yuan, "Physical layer security for ultra-reliable and low-latency communications," IEEE Trans. Wireless Commun., vol. 26, no. 5, pp. 6-11, 2019.

[62] I. Zabir, A. Swami and Y. Hua,"Secrecy Throughput of ANECE Assisted Transmission of Information in Finite Blocklength,"submitted to 2022 IEEE Wireless Commun. and Networking Conference (WCNC).

[63] I. Zabir, A. Maksud, G Chen, B. Sadler and Y. Hua,"Secrecy of Multi-Antenna Transmission with Full-Duplex User in the Presence of Randomly Located Eavesdroppers," IEEE Trans. on Information Forensics and Security, vol. 16, pp. 2060-2075, Dec. 2020.

[64] I. S. Gradshteyn and I. M. Ryzhik, "Table of Integrals, Series, and Products," 7th ed. New York, NY, USA: Academic, 2007.

[65] H. Gao, P. J. Smith, and M. V. Clark, "Theoretical reliability of MMSE linear diversity combining in Releigh-fading additive interference channels," IEEE Trans. Commun., vol. 46, no. 5, pp. 666-672, May 1998.

[66] H. Lim and D. Yoon, "On the distribution of SINR for MMSE MIMO systems," IEEE Trans. Commun., vol. 67, no. 6, pp. 4035-4046, Jun. 2019.

[67] `https://en.wikipedia.org/wiki/Schur_complement`